

INFORMATION TO USERS

This reproduction was made from a copy of a document sent to us for microfilming. While the most advanced technology has been used to photograph and reproduce this document, the quality of the reproduction is heavily dependent upon the quality of the material submitted.

The following explanation of techniques is provided to help clarify markings or notations which may appear on this reproduction.

1. The sign or "target" for pages apparently lacking from the document photographed is "Missing Page(s)". If it was possible to obtain the missing page(s) or section, they are spliced into the film along with adjacent pages. This may have necessitated cutting through an image and duplicating adjacent pages to assure complete continuity.
2. When an image on the film is obliterated with a round black mark, it is an indication of either blurred copy because of movement during exposure, duplicate copy, or copyrighted materials that should not have been filmed. For blurred pages, a good image of the page can be found in the adjacent frame. If copyrighted materials were deleted, a target note will appear listing the pages in the adjacent frame.
3. When a map, drawing or chart, etc., is part of the material being photographed, a definite method of "sectioning" the material has been followed. It is customary to begin filming at the upper left hand corner of a large sheet and to continue from left to right in equal sections with small overlaps. If necessary, sectioning is continued again—beginning below the first row and continuing on until complete.
4. For illustrations that cannot be satisfactorily reproduced by xerographic means, photographic prints can be purchased at additional cost and inserted into your xerographic copy. These prints are available upon request from the Dissertations Customer Services Department.
5. Some pages in any document may have indistinct print. In all cases the best available copy has been filmed.

**University
Microfilms
International**

300 N. Zeeb Road
Ann Arbor, MI 48106



8407037

Unkulvasapaul, Yothin

**MODELING OF WATER QUALITY IN ESTUARIES AND ESTUARINE
NETWORKS**

The College of William and Mary in Virginia

PH.D. 1983

**University
Microfilms
International** 300 N. Zeeb Road, Ann Arbor, MI 48106

PLEASE NOTE:

In all cases this material has been filmed in the best possible way from the available copy. Problems encountered with this document have been identified here with a check mark .

1. Glossy photographs or pages _____
2. Colored illustrations, paper or print _____
3. Photographs with dark background _____
4. Illustrations are poor copy _____
5. Pages with black marks, not original copy _____
6. Print shows through as there is text on both sides of page _____
7. Indistinct, broken or small print on several pages
8. Print exceeds margin requirements _____
9. Tightly bound copy with print lost in spine _____
10. Computer printout pages with indistinct print _____
11. Page(s) _____ lacking when material received, and not available from school or author.
12. Page(s) _____ seem to be missing in numbering only as text follows.
13. Two pages numbered _____. Text follows.
14. Curling and wrinkled pages _____
15. Other _____

University
Microfilms
International

MODELING OF WATER QUALITY IN ESTUARIES AND ESTUARINE NETWORKS

A Dissertation

Presented to

The Faculty of the School of Marine Science
The College of William and Mary in Virginia

In Partial Fulfillment

Of the Requirements for the Degree of
Doctor of Philosophy

by

Yothin Unkulvasapaul

1983

APPROVAL SHEET

This dissertation is submitted in partial fulfillment of
the requirements for the degree of
Doctor of Philosophy

Yothin Unkulvasapaul

Yothin Unkulvasapaul

Approved, October 1983

Bruce Neilson

Bruce J. Neilson

C.S. Fang

C.S. Fang

Charles S. Welch

C.S. Welch

Robert J. Diaz

Robert J. Diaz

H. S. Chen

H.S. Chen, Coastal Engineering
Research Center, Vicksburg, Miss.

TABLE OF CONTENTS

	PAGE
ACKNOWLEDGEMENTS.....	iv
LIST OF TABLES.....	v
LIST OF FIGURES.....	vi
LIST OF SYMBOLS.....	x
ABSTRACT.....	xx
CHAPTER 1 INTRODUCTION.....	2
CHAPTER 2 LITERATURE REVIEW.....	8
CHAPTER 3 MATHEMATICAL FORMULATION.....	18
CHAPTER 4 FINITE ELEMENT FORMULATION.....	42
CHAPTER 5 VERIFICATION.....	52
CHAPTER 6 APPLICATION TO THE JAMES RIVER.....	62
CHAPTER 7 NETWORK FORMULATION.....	121
CHAPTER 8 APPLICATION TO THE APPOMATOX RIVER.....	125
CHAPTER 9 EXPLICIT INTEGRATION.....	146
CHAPTER 10 CONCLUDING REMARKS.....	151
APPENDIX EVALUATION OF THE ELEMENT INTEGRALS.....	154
REFERENCES.....	160
VITA.....	164

ACKNOWLEDGEMENTS

I am especially grateful to Dr. H.S. Chen who provided many of the fundamental ideas upon which this study is based. His constant encouragement, support, and guidance throughout this study are sincerely appreciated.

I am also very grateful to Dr. C.S. Fang for his general guidance and for making the resources available for this research. Special thanks are due to Dr. Bruce J. Neilson who served as the Chairman of the committee after Dr. Chen's departure from VIMS, and to the rest of the committee members for their careful review and comments on the manuscript.

Special appreciation is extended to Dr. C. John Klein of the EPA Chesapeake Bay Program, Annapolis, for providing the water quality data for the James River study; and to the field crew of the Department of Physical Oceanography for collecting the data for the Appomatox River.

Computer work was done at the Computer Center of the College of William and Mary and at the Computer Center of the Virginia Institute of Marine Science. Thanks are due to Mr. Robert J. Lukens and Mr. Williams P. Blystone for their frequent assistance in computer programming.

And lastly many thanks to my wife Manida who patiently typed the manuscript on the word processor, and for her support throughout the study.

LIST OF TABLES

Table	Page
6.1 Point Source Loadings for the James River (kg/day).....	90
6.2 Benthic Releases for Spring (kg/day).....	91
6.3 Benthic Releases for Early Summer (kg/day).....	91
6.4 Benthic Releases for Late Summer (kg/day).....	92
6.5 Benthic Releases for Fall (kg/day).....	92
6.6 Calibration Parameters for the James River.....	120
7.1 Connectivity Matrix.....	122
8.1 Point Source Loadings for the Appomatox River.....	130
8.2 Nutrient Export from Glebe Gut. After Sweeny (1978).....	131
8.3 Estimated Nutrient Loadings from Marshes (kg/day).....	132
8.4 Estimated Nutrient Loadings from Urban Runoff (kg/ha/day)...	132
8.5 Estimated Nutrient Loadings from Urban Runoff (kg/day).....	133
8.6 Estimated Total Non-point Source Loadings.....	134
8.7 Boundary Concentrations.....	135
8.8 Mean Tidal Amplitudes.....	136
8.9 Mean Current Amplitudes.....	137
8.10 Calibration Parameters for the Appomatox River.....	145

LIST OF FIGURES

Figure	Page
3.1 Schematic diagram showing the interactions of the nine constituents in the water quality model.....	29
4.1 Finite element approximation to the exact solution.....	45
5.1 Comparison of numerical solution and analytical solution of surface elevation at $x = L$	55
5.2 Comparison of numerical solution and analytical solution of velocity at $x = 0$	56
5.3 Comparison of numerical solutions to analytical solutions of concentration propagation using no decay rate.....	59
5.4 Comparison of numerical solutions to analytical solutions of concentration propagation using decay rate = 0.5 per hour...	61
6.1 Fresh water inflows to the James River model.....	64
6.2 Model segments for the James River estuary.....	66
6.3 Schematic cross-section of the river.....	67
6.4 (a) Observed tidal elevation at Sandy Point, (b) Computed tidal elevation at node 18 (Sandy Point).....	71
6.5 (a) Observed tidal elevation at Jordan Point, (b) Computed tidal elevation at node 26 (Jordan Point).....	72
6.6 (a) Observed tidal elevation at Dutch Gap, (b) Computed tidal elevation at node 31 (Dutch Gap).....	73
6.7 (a) Observed tidal elevation at Richmond, (b) Computed tidal elevation at node 40 (Richmond).....	74
6.8 Computed current at node 18 (Sandy Point).....	76
6.9 Computed current at node 26 (Jordan Point).....	76

Figure	Page
6.10 Computed current at node 31 (Dutch Gap).....	77
6.11 Computed current at node 40 (Richmond).....	77
6.12 Computed vs observed salinity at node 1 (River mouth).....	78
6.13 Computed vs observed salinity at node 4 (Newport News).....	78
6.14 Computed vs observed salinity at node 7 (Jail Point).....	79
6.15 Computed vs observed salinity at node 11 (Hog Point).....	79
6.16 Computed vs observed salinity at node 15 (Swanns Point).....	80
6.17 Computed vs observed salinity at node 18 (Sandy Point).....	80
6.18 Chlorophyll nonpoint source loadings to the James River model.....	82
6.19 Organic-N nonpoint source loadings to the James River model.....	83
6.20 Ammonia-N nonpoint source loadings to the James River model.....	84
6.21 NO ₂ -NO ₃ -N nonpoint source loadings to the James River model.....	85
6.22 Organic-P nonpoint source loadings to the James River model.....	86
6.23 Inorganic-P nonpoint source loadings to the James River model.....	87
6.24 CBOD nonpoint source loadings to the James River model.....	88
6.25 DO Deficit nonpoint source loadings to the James River model.....	89
6.26 James River solar radiation from March 1, 1971 to October 31, 1971, (a) Upper James River, (b) Lower James River.....	93
6.27 Water temperature variations from March 1, 1971 to October 31, 1971.....	94
6.28 Computed and observed water quality constituents at node 4 in The James River.....	96

Figure	Page
6.29 Computed and observed water quality constituents at node 9 in The James River.....	99
6.30 Computed and observed water quality constituents at node 17 in The James River.....	102
6.31 Computed and observed water quality constituents at node 16 in The James River.....	105
6.32 Computed and observed water quality constituents at node 19 in The James River.....	108
6.33 Computed and observed water quality constituents at node 26 in The James River.....	111
6.34 Computed and observed water quality constituents at node 32 in The James River.....	114
6.35 Computed and observed water quality constituents at node 40 in The James River.....	117
7.1 An arbitrary channel network.....	122
7.2 Two example channel networks used in the model.....	124
8.1 Location of sampling stations in the Appomatox River.....	126
8.2 Model segments for the Appomatox River.....	128
8.3 Computed vs observed Chlorophyll 'a' concentrations, (a) North branch, (b) South branch.....	139
8.4 Computed vs observed Organic-N concentrations, (a) North branch, (b) South branch.....	140
8.5 Computed vs observed Ammonia-N concentrations, (a) North branch, (b) South branch.....	141
8.6 Computed vs observed NO ₂ -NO ₃ -N concentrations, (a) North branch, (b) South branch.....	142
8.7 Computed vs observed CBOD concentrations, (a) North branch, (b) South branch.....	143
8.8 Computed vs observed DO concentrations, (a) North branch, (b) South branch.....	144
9.1 Comparison of explicit solutions to analytical solutions using no decay rate.....	148

Figure

Page

9.2 Comparison of explicit solutions to analytical solutions using decay rate = 0.5 per hour.....	149
--	-----

LIST OF SYMBOLS

A	cross-sectional area
A_c	core area (Equation 6.3)
A_s	storage area (Equation 6.3)
[A]	an $n \times n$ matrix of transport and dispersion effects (Equation 2.6)
a	a constant division rate of phytoplankton (Equation 2.1)
a	amplitude of forcing sine wave (Equation 5.3)
a_i	amplitude of the i th tidal constituent (Equation 6.3)
a	fitted constant for temperature (Equation 6.6)
a_i	velocity amplitude of node i (m/hr) (Equation 8.2)
a_p	rate of oxygen production from photosynthesis (1/day)
a_r	rate of oxygen depletion by respiration (1/day)
B	channel top width
B	wL/c (Equations 5.5 and 5.6)
B_c	core width (Equation 6.1)
B_s	storage width (Equation 6.1)
b	initial grazing rate (Equation 2.1)
b	nitrogen-chlorophyll ratio (Equation 2.5)
b	0.5 is an arbitrary weighting factor (Equation 6.5)
b	fitted constant for temperature (Equation 6.6)

b_i	tidal amplitude at node i (Equation 8.1)
b'_8	benthic oxygen demand at 20°C
b_8	benthic oxygen demand ($\text{gm-O}_2/\text{m}^2/\text{day}$)
C	cross-sectional average concentration
\hat{C}	approximate solution of C in an element
C_1, C_2	local nodal concentration values at the two ends of an element
C_0	given initial concentrations
C_0	coliform bacteria (number/100 ml)
C_1	chlorophyll 'a' ($\mu\text{g}/\text{l}$)
C_2	organic nitrogen (mg/l)
C_3	ammonia nitrogen (mg/l)
C_4	nitrite-nitrate nitrogen (mg/l)
C_5	nitrate nitrogen (Equation 2.9)
C_5	organic phosphorous (mg/l)
C_6	inorganic phosphorous (mg/l)
C_7	CBOD (mg/l)
C_8	dissolved oxygen deficit (mg/l)
C_9	salinity (ppt)
C_c	Chezy coefficient
C_i	concentration of the i th water quality constituent (Equation 3.13)
C_j	concentration at junction j (Equation 7.1)

C_j^n	concentration of node n entering into junction j (Equation 7.1)
c	an arbitrary rate of increase of grazing rate (Equation 2.1)
c	concentration of a water quality constituent (Equation 3.5)
c	wave speed (Equations 5.5 and 5.6)
c	fitted constant for temperature (Equation 6.6)
c''	spatial deviation from the average concentration.
D	endogenous respiration rate of phytoplankton (1/day)
D_p	death rate of phytoplankton due to zooplankton grazing (Equation 2.3)
D_s	Secchi disk visibility reading
D_x	molecular diffusivities in the x direction
D_y	molecular diffusivities in the y direction
D_z	molecular diffusivities in the z direction
D_z	zooplankton death rate (Equation 2.4)
E_2	spatially varying dispersion coefficient (Equation 3.12)
E_L	longitudinal dispersion coefficient (Equation 3.9)
E_T	Taylor's dispersion coefficient (Equation 3.11)
d_c	distance from water surface to centroid of cross-section
e	2.1718
erfc	complementary error function
F	attenuation of growth due to non-optimal light (Equation 3.15)
F_x^*	prescribed dispersive flux boundary condition at x
f	photoperiod (Equation 3.19)

f_z	assimilation efficiency value ranges from 0.4 to 0.8
G	zooplankton grazing rate (Equation 2.2)
G	growth rate of phytoplankton (1/day)
G_{It}	functional relationship of the growth rate (Equation 2.7)
G_p	phytoplankton growth rate (Equation 2.3)
G_{pj}	growth rate (Equation 2.7)
G_z	zooplankton growth rate (Equation 2.4)
g	gravitational acceleration
H	water depth
I	solar radiation (Equation 2.3)
I	light intensity in the water column (langleys)
I_0	surface light intensity
I_a	mean daily light intensity (Equation 3.19)
I_j	average surface light intensity j days earlier, $j = 1, 2$ and 3 (Equation 3.21a)
I_m	total daily solar radiation (langleys) (Equation 3.20)
I_s	saturating or optimal light intensity (langleys)
k	decay rate (Equation 5.7)
k'_0	coliform bacteria die off rate at 20°C.
k_0	coliform bacteria die off rate (1/day)
k'_2	organic nitrogen to ammonia nitrogen hydrolysis coefficient
k_2	organic nitrogen to ammonia nitrogen hydrolysis rate (1/day)
k'_3	ammonia to nitrate nitrification coefficient (1/day/°C)

k_3	ammonia to nitrate nitrification rate (1/day)
k_5'	organic phosphorous to inorganic phosphorus conversion coefficient
k_5	organic phosphorous to inorganic phosphorous conversion rate
k_7'	CBOD oxidation rate at 20°C
k_7	CBOD oxidation rate (1/day)
k_8'	reaeration coefficient at 20°C
k_8	reaeration rate (1/day)
k_e'	light extinction coefficient at zero chlorophyll concentration
k_e	light extinction coefficient
k_g	optimum growth rate coefficient (1/day/°C)
k_{mn}	Michaelis-Menton constant for total inorganic nitrogen (Equation 2.7)
k_{mn}	Michaelis-Menton constant for inorganic nitrogen (mg/l)
k_{mp}	Michaelis-Menton constant for orthophosphate concentration (Equation 2.7)
k_{mp}	Michaelis-Menton constant for inorganic phosphorous (mg/l)
k_{op}	photosynthetic quotient
k_{or}	respiration ratio
k_r	endogenous respiration coefficient (1/day/°C)
k_s	loss rate (Equation 3.13)
k_z	zooplankton grazing coefficient (1/day/°C).
L	length scale

L_d	day length (hours) (Equation 3.20)
l_j	distance to the neighbouring node j (Equation 6.5)
M	mass scale
m	a factor to account for channel irregularities (Equation 3.12)
N	inorganic nitrogen (Equation 2.3)
N	attenuation of growth due to nutrient limitation (Equation 3.15)
N_{In}	total inorganic nitrogen (Equation 2.7)
N_{p2}	orthophosphate concentration (Equation 2.7)
N_s	influent concentrations of inorganic nitrogen (Equation 2.5)
N_2	ammonia nitrogen concentration (Equation 2.8)
$\{N\}^T$	a row vector of the interpolation function
n	number of segments (Equation 2.6)
P	biomass of phytoplankton (Equation 2.1)
P	phytoplankton population (Equation 2.2)
P	phytoplankton chlorophyll 'a' in mg/l dry weight (Equation 2.3)
P	nitrate or ammonia nitrogen preference
\bar{P}_h	depth averaged photosynthesis rate (Equation 2.2)
P_s	influent concentrations of phytoplankton (Equation 2.3)
$\{P\}$	an $n \times 1$ phytoplankton chlorophyll 'a' vector (Equation 2.6)
Q	cross-sectionally averaged discharge
\hat{Q}	approximate solution of Q in an element
Q_j^n	flow of node n into junction j (Equation 7.2)
Q_{fi}	fresh water inflow from the drainage area upstream of node i (Equation 8.2)

q	fresh water inflow per unit length
R	endogenous respiration rate of phytoplankton (Equation 2.2)
R_i	time rate of sources or sinks due to biochemical reactions (Equation 3.13)
R_h	hydraulic radius of the channel
r_c	carbon-chlorophyll ratio (mg-C/ μ g-chlorophyll)
r_n	nitrogen-chlorophyll ratio (mg-N/ μ g-chlorophyll)
r_p	phosphorus-chlorophyll ratio (mg-P/ μ g-chlorophyll).
S	inorganic nitrogen from death of zooplankton and phytoplankton (Equation 2.5)
S	time rate of addition or removal of substance per unit volume
S_s	average side slope of the channel (Equation 6.2)
$\{S_p\}$	an $n \times 1$ vector of source terms (Equation 2.6)
s	average salinity (ppt) (Equation 3.3)
T	temperature (Equation 2.3)
T	time scale
T	temperature ($^{\circ}$ C)
T	period of forcing sine wave (Equation 5.3)
T	tidal period, 12.42 hr (Equation 8.1)
t_0	detention time equal to volume divided by flow (Equations 2.3 to 2.5)
t	time
t_d	time of day (hours) (Equation 3.20)
t_s	sunrise time (hours) (Equation 3.20)
t_y	days since January 1st (Equation 3.20)

U	cross-sectionally averaged velocity
U_i	velocity at node i (Equation 6.5)
U_0	initial velocity
U_j	velocity at the neighbouring node j (Equation 6.5)
U_s	smoothed value of velocity (Equation 6.5)
u	instantaneous velocity in the x direction (Equation 3.5)
\bar{u}	time average velocity in the x direction (Equation 3.6)
u''	spatial deviation from the average velocity in the x direction (Equation 3.7)
u'	temporal deviation from the average velocity in the x direction (Equation 3.6)
U_i	tidal velocity at node i (m/hr) (Equation 8.2)
V	segment volume (Equation 2.5)
$[V]$	an $n \times n$ diagonal matrix of segment volumes (Equation 2.6)
v	instantaneous velocity in the y direction (Equation 3.5)
\bar{v}	time average velocity in the y direction (Equation 3.6)
v''	spatial deviation from the average velocity in the y direction (Equation 3.7)
v'	temporal deviation from the average velocity in the y direction (Equation 3.6)
W	input inorganic nitrogen from waste discharge or runoff (Equation 2.5)
W_i	external waste input loads (Equation 3.13)
W_x	wind velocity along the channel
w	instantaneous velocity in the z direction (Equation 3.5)
\bar{w}	time average velocity in the z direction (Equation 3.6)
w	angular frequency (Equations 5.3 and 6.3)

w''	spatial deviation from the average velocity in the z direction (Equation 3.7)
w'	temporal deviation from the average velocity in the z direction (Equation 3.6)
x	distance along the channel
x_1, x_2	local coordinates of the two ends of an element
Z	zooplankton concentration (Equation 2.4)
Z	zooplankton grazing rate (1/day)
Z_s	influent concentrations of zooplankton (Equation 2.4)
z	depth (Equation 3.17)
β	wind shear stress coefficient
γ	phase difference between tidal current and tidal velocity (Equation 8.1)
ϵ_x	turbulent diffusivity in the x direction (Equation 3.6)
$\bar{\epsilon}_x$	spatial mean value of the turbulent diffusivity
ϵ_y	turbulent diffusivity in the y direction (Equation 3.6)
ϵ_z	turbulent diffusivity in the z direction (Equation 3.6)
η	elevation of water surface with respect to a horizontal datum
η_0	initial water surface elevation
η_a	astronomical tide.
$\hat{\eta}$	approximate solution of η in an element
Ω	$(U^2 + 4kE)^{1/2}$ (Equation 5.9)
ρ	water density
ρ_a	air density
ρ	water density (kg/m^3) (Equation 3.3)

π	3.14159
χ	$x/2E$ (Equation 5.9)
θ	tidal phase (Equation 6.3)
θ_i	phase difference between tide at the mouth and node i (Equation 8.1)
H	typical water depth (Equation 4.13)
Δt	size of the integration time step (Equation 4.13)
Δt_{cr}	critical time step for the onset of instability (Equation 4.13)
Δx	typical grid size (Equation 4.13)

ABSTRACT

A one dimensional finite element model for the prediction of transient water quality in an estuary is developed. Ten water quality constituents, salinity, coliform bacteria, organic nitrogen, ammonia nitrogen, nitrite-nitrate nitrogen, organic phosphorous, inorganic phosphorous, phytoplankton as measured by chlorophyll 'a', DO and CBOD are included in the model. The effects of temperature, solar radiation and zooplankton predation are incorporated into the model as external forcing functions. The concentration distributions are obtained by solving the conservation of mass equations successively. A compatible hydrodynamic model is also developed to provide the driving transport processes to the water quality model.

The finite element method is chosen in the numerical formulation because of its flexibility in grid layout. Linear interpolation functions are used for the spatial discretization. The time scale of the model is tidal time. The downstream boundary condition is related to the direction of tide. On flood tide the concentration of the inflowing water is prescribed. On ebb tide the dispersive flux is determined by the concentration distribution within the estuary.

Two time integration methods, trapezoidal and explicit method with split time scheme, are developed. The trapezoidal scheme is found to be very stable and the accuracy is adequate for most applications. The explicit version of the computer program is shorter and the execution time is faster, but the size of the integration time step is more restricted. Both versions are validated against known analytical solutions for a rectangular channel with constant upstream boundary concentrations and uniform velocities. The implicit model was used to simulate the water quality in the James River estuary from March to October 1971. The model has also been applied to the Potomac River in Virginia, and is being applied to the Chester River in Maryland.

A network version of the water quality model is also developed. The model is capable of simulating water quality in estuaries that have interconnecting channels or estuarine networks such as the lower portion of the Appomatox River. This model was used to simulate average water quality conditions in the Appomatox River.

MODELING OF WATER QUALITY IN ESTUARIES AND ESTUARINE NETWORKS

1 INTRODUCTION

The use of water quality models in the management of estuarine water quality is widely accepted. One of the major needs or requirements in estuarine water quality management is the ability to predict the effectiveness of various pollution control measures such as the construction of sewage treatment plants or the implementation of nonpoint source controls. Since the costs associated with providing these controls are very high, rational water quality management must be based on quantitative assessment of the costs and benefits of the controls. A water quality model is a predictive tool that can incorporate the complexity of the relevant natural processes and calculate the response of the estuary to the various control measures. This information can help the management to make decisions that are justified on a scientific basis. The models must be frequently updated as new information on the estuarine environment is acquired. The models must also be refined to give more accurate calculations when more advanced levels of treatment are required.

Water quality modeling begins by observing the natural processes in the estuary. From these observations, a conceptual model depicting the major features of the estuary can then be constructed. When a contaminant is introduced into an estuary, its dispersal is subjected to the combined effects of transport processes and biochemical reaction processes. The transport processes describe the hydrodynamic regimes

of the water which spread the contaminant by advection, mixing and turbulent diffusion. The reaction processes describe the degradation, production or transformation of the contaminant by various biochemical reactions. A conservation of mass equation which takes into account these factors is then developed for each of the water quality constituents that we wish to simulate. The question of how many constituents to simulate very much depends on how much detail is required for the system under investigation. The simplest model will simulate only one conservative substance such as salinity or suspended solids. A more complicated model will incorporate several biochemically interacting substances.

Najarian and Harleman (1975) classified models of aquatic ecosystems based on the method of structuring of the models into three categories : (1) Biodemographic Models. These models are formulated based upon the principle of conservation of species. They are concerned with the simulation of life cycles of species or individual numbers. These models are used in fishery management studies. (2) Bioenergetic Models. These models are based on the principle of conservation of energy, they simulate energy flow, energy storage and energy dissipation processes. (3) Biogeochemical Models. These models are based on the principle of conservation of mass. They simulate the transport and biochemical processes of the substances that we are interested in. Most engineering models that are used to simulate the distribution of water quality fall into this class. These models usually are not taxon specific. Some of the water quality constituents simulated are aggregated variables, for example the total phytoplankton biomass is represented by the concentration of chlorophyll 'a'.

Biogeochemical models can be further classified according to the simplifying assumptions made in the space and time domain. The most exact model would solve the equations in three dimensions in space and real time. But the common approach is to use one dimension or two dimensions spatially. Although the assumption of one dimensionality is not always met in real estuaries, such models have been used with good results, however. For most tidal estuaries in Virginia, a one dimensional model has been found to be sufficient for water quality analysis (Kuo et al., 1979). Averaging in the time domain can be done over a time scale either longer than or shorter than a tidal cycle. When the averaging time scale is a tidal cycle, it is known as a tidal average or a steady state model. When the time scale used is much shorter than a tidal cycle, it is known as a tidal time or real time model. The main objection against the use of steady state models is that they are not capable of simulating true mass transport; this makes it difficult to derive reliable steady state dispersion coefficients. In an ecosystem model where it is important to accurately compute the diurnal dissolved oxygen (DO) and phytoplankton concentrations and the nutrient fluxes in and out of a reach of estuary, the use of real time models is imperative.

A large number of water quality models has been developed in the past. This is the direct result of the tremendous diversity in scope, purpose and mathematical details being sought by the modellers. The estuaries themselves differ greatly in their geomorphological structure and hydrologic regime. A particular model is therefore limited to certain applications only. A universal model that can cover all conditions is not likely to be developed. Traco (1971) presented an

excellent review of many earlier water quality models. Historically, water quality models have emphasized the importance of dissolved oxygen (DO) as the primary indicator of water quality (Daily and Harleman, 1972; O'Connor 1966; Thomann, 1963) These models used the concept of carbonaceous biochemical oxygen demand (CBOD) to represent organic materials that consume DO as they are degraded by bacteria. Recently there has been a growing concern about nutrient enrichment in the estuaries which leads to the excessive algae population and which in turn affects DO level (Neilson and Cronin, 1981). Therefore the use of a DO model is not adequate to describe water quality in the estuaries. We need models that can simulate nutrient-phytoplankton-DO dynamics in order to assess the impact of nutrient enrichment on the trophic level of the estuaries. These models can be used to identify the nutrients that enhance eutrophication, and to estimate the amount of removal required to reduce the eutrophication. Phytoplankton dynamic models are often called phytoplankton models or ecosystem models. At present there are a few phytoplankton dynamic models available, but most are either steady state models or lack a compatible hydrodynamic model to couple to. As we are going into higher levels of waste treatment, it is clear that we need models that also have accurate hydrodynamics.

Chen (1979) developed a two-dimensional phytoplankton model that simulated ten water quality constituents. The model is a real time, vertically integrated model coupled to a compatible hydrodynamic model. This model is considered to be one of the most sophisticated phytoplankton models at present. The intent of this study is to develop a one dimensional counterpart. One-dimensional models are needed when the geometry of the estuary does not warrant the use of a two-dimensional

model, when there is lack of consistent and detailed water quality data needed for calibration, or when the computation cost must be kept low.

The objective of this study is to develop a one dimensional water quality model to simulate phytoplankton dynamics in a natural estuary of network waterways and to develop a compatible hydrodynamic model to couple to the water quality model.

Ten water quality constituents; namely, salinity, coliform bacteria, chlorophyll 'a', organic nitrogen, ammonia nitrogen, nitrite-nitrate nitrogen, organic phosphorus, inorganic phosphorus, CBOD, and DO are simulated in the model. These constituents are commonly considered important in current engineering practices. Except for salinity and coliform bacteria, all other components are coupled.

The time scale used for the model is real time; this permits the specification of time varying boundary conditions, temperature, waste inputs and other external inputs. The numerical method used to solve the set of equations is the finite element method (FEM). The advantages of the FEM are quite well known, especially the variable mesh capability of the FEM is very useful in the vicinity of high concentration gradients where a local fine mesh can be used.

The one-dimensional network model has not received much attention in the past. The complicated condition at the junctions makes analysis difficult. But network models are useful for simulating geometrically complex estuaries. A network estuary is defined as an estuary which consists of several channels connected in an arbitrary manner. An examples of this type of estuary is the Appomatox River which has a complicated network of channels above Point of Rocks. A model for the Appomatox River has not been previously developed. A network model

apart from being able to simulate water quality in geometrically complex estuaries, can also be used to simulate estuaries with channels and embayments.

The water quality model developed in this study has been applied to the James River and the Potomac River in Virginia. The model is also being applied to the Chester River in Maryland. The network version of the model has been applied to the Appomatox River in Virginia.

2 LITERATURE REVIEW

A large number of estuarine water quality models has been developed in the past. The models developed prior to 1971 have been well summarized by Tracor (1971). Most of these early models used simplified forms of equations and had only one or two water quality constituents. Many of these models evolved from the work of Streeter and Phelps (O'Connor, 1960; Thomann, 1963). In these models the concentrations of dissolved oxygen (DO) were assumed to be the result of two processes: namely, reaeration from the atmosphere and the consumption of DO in the oxidation of biochemical oxygen demand (BOD). Dobbins (1964) improved this scheme by adding source and sink terms for DO due to photosynthesis, respiration and benthic oxygen demands. O'Connor (1967) improved the model by incorporating the time variability and spatial distribution into his model. O'Connor and Di Toro (1970) took a further step by separating BOD into carbonaceous and nitrogenous components (CBOD and NBOD). The two forms of BOD were associated with different types of sewage loadings and different types of bacteria.

For marine ecosystem models, Kremer and Nixon (1978) presented a review of some of the earlier studies. The early studies are of historical interest because all of the present day models are based on the same concepts used in these pioneering developments. Fleming (1939), as described by Kremer and Nixon (1978), studied seasonal changes in phytoplankton population levels in the English channel using

the differential equation

$$\frac{dP}{dt} = P[a - (b + ct)] \quad (2.1)$$

where

P = biomass of phytoplankton,

t = time,

a = a constant division rate of phytoplankton,

b = initial grazing rate and

c = an arbitrary rate of increase of grazing rate.

This simple differential equation relates the rate of change of phytoplankton populations to the biomass of phytoplankton P, to the constant division rate a, and to a grazing rate with an initial value b and an arbitrary rate of increase c. This formula assumes a homogeneous region and no advective processes. Except for the additional term c, Fleming's description was essentially identical to the formulations given earlier by Lotka (1925), Volterra (1926), and others.

Also as described by Kremer and Nixon (1978), Riley (1946) proposed a model to study the annual phytoplankton dynamics on Georges Bank based on the equation

$$\frac{dP}{dt} = P(\bar{P}_h - R - G) \quad (2.2)$$

where

P = phytoplankton population,

t = time,

\bar{P}_h = depth averaged photosynthesis rate,

R = endogenous respiration rate of phytoplankton and
 G = zooplankton grazing rate.

The phytoplankton and zooplankton concentrations are expressed as grams of carbon per unit area to represent the depth-averaged concentrations over the euphotic zone. A major improvement in Riley's formulation is that it attempted to relate the growth, respiration and grazing rates to other environmental variables such as light and temperature.

Further progress in the phytoplankton model structure has been made by the introduction of Michaelis-Menton reaction kinetics. The Michaelis-Menton kinetics were used by Chen (1970) and by Di Toro et al. (1970) who presented an early version of a dynamic phytoplankton model. The model consisted of the following equations

$$\frac{dP}{dt} = \frac{P_s}{t_o} + G_p(N, I, T)P - D_p(Z, T)P - \frac{P}{t_o} \quad (2.3)$$

$$\frac{dZ}{dt} = \frac{Z_s}{t_o} + G_z(P)Z - D_z(T)Z - \frac{Z}{t_o} \quad (2.4)$$

$$\frac{dN}{dt} = \frac{N_s}{t_o} - bG_p(N, I, T)P + S(P, Z, T) - \frac{N}{t_o} + \frac{W}{V} \quad (2.5)$$

where

P = phytoplankton chlorophyll 'a' in mg/l dry weight,

G_p = phytoplankton growth rate,

N = inorganic nitrogen,

I = solar radiation,

T = temperature,

S = inorganic nitrogen from death of zooplankton and phytoplankton,

- V = segment volume,
 D_P = death rate of phytoplankton due to zooplankton grazing and endogenous respiration rate,
 Z = zooplankton concentration,
 G_Z = zooplankton growth rate,
 D_Z = zooplankton death rate,
 b = nitrogen-chlorophyll ratio,
 W = input inorganic nitrogen from waste discharge or runoff,
 t_0 = detention time equal to volume divided by flow and
 P_s, Z_s, N_s = the respective influent concentrations of phytoplankton, zooplankton and inorganic nitrogen.

This form of equation represents a completely mixed system in a volume segment, therefore spatial distributions within a segment and intertidal variability can not be simulated.

Later, Thomann et al. (1974) and Di Toro et al. (1977) presented a sequence of progressively more complex versions which were more detailed in both their spatial and kinetic structures. The version presented by Thomann et al. (1974) was the Preliminary Potomac Estuary Phytoplankton Model. This model included nine interacting variables. The general matrix equation for the phytoplankton system under a finite difference approximation was given by

$$[V] \frac{d\{P\}}{dt} = [A]\{P\} + [V]\{S_p\} \quad (2.6)$$

where

- $\{P\}$ = an $n \times 1$ phytoplankton chlorophyll 'a' vector,
 $[A]$ = an $n \times n$ matrix of transport and dispersion effects,

$[V]$ = an $n \times n$ diagonal matrix of segment volumes,

$\{S_p\}$ = an $n \times 1$ vector of source terms and

n = number of segments.

The spatial distribution was achieved by dividing the water body into a number of segments, with each segment volume treated as completely mixed and the transport and dispersion between adjacent segments given by the matrix $[A]$; but no details about this matrix were given in the paper. The phytoplankton growth rate in each segment j was calculated by

$$G_{pj} = G_{It}(I, T, f, H, k) \frac{N_{In}}{k_{mn} + N_{In}} \frac{N_{p2}}{k_{mp} + N_{p2}} \quad (2.7)$$

where

G_{pj} = growth rate,

G_{It} = the functional relationship of the growth rate and solar radiation I , photoperiod f , water temperature T , depth H , and light extinction coefficient k ,

N_{In} = the total inorganic nitrogen,

k_{mn} = Michaelis-Menton constant for total inorganic nitrogen,

N_{p2} = orthophosphate concentration and

k_{mp} = Michaelis-Menton constant for orthophosphate concentration.

The model incorporated the ammonia nitrogen preference of phytoplankton uptake by multiplying the ammonia nitrogen uptake rate by a preference factor P , and the uptake of nitrate nitrogen by the factor $(1 - P)$, where

$$P = \frac{N_2}{N_2 + k_{mn}} \quad (2.8)$$

and

N_2 = ammonia nitrogen concentration.

The use of ammonia nitrogen preference in this form has raised some objections by Najarian et al. (1975), who had shown that in multi-nutrient environments, if a particular nutrient such as nitrate nitrogen were depleted, there was still uptake of nitrate by phytoplankton, hence the principle of conservation of mass was violated.

Di Toro et al. (1977) modified the preference factor to

$$P = \left(\frac{C_5}{k_{mn} + C_5} \right) \left(\frac{C_4}{k_{mn} + C_4} \right) + \left(\frac{k_{mn}}{k_{mn} + C_5} \right) \left(\frac{C_4}{C_4 + C_5} \right)$$

where

C_4 = ammonia nitrogen and

C_5 = nitrate nitrogen.

In this expression, the preference is determined in proportion to the abundance of ammonia nitrogen or nitrate nitrogen concentrations. If $P \rightarrow 1$ ammonia nitrogen is used. If $P \rightarrow 0$ nitrate nitrogen is used. This factor avoids the pitfall mentioned above, but it is quite arbitrary. At present, because the uptake in an multi-nutrient environment is still largely unknown, it is difficult to have an a priori decision as to which formula is the most appropriate.

Another aspect of model development is the coupling of water quality models with real time hydrodynamic models. Feigner and Harris (1970) presented the Dynamic Estuary Model (DEM). The term dynamic

refers to the fact that the model includes the effects of tidal motion as opposed to the non-tidal models which neglect them. The primary intent of the model was to provide the capability for handling a network of channels. The formulation of the model was based on the so called link and node method, in which the network was represented by a series of uniform channels connected to junctions. The junctions act as completely mixed reservoirs to store the mass in the system, and the channels serve to convey mass between the junctions. A disadvantage of node-link approach to solve the mass balance equation is that it cannot describe the mass center accurately, and therefore it often requires the use of unrealistic dispersion coefficients in the links.

Gunaratnum and Perkins (1970) developed a hydrodynamic model using a high accuracy numerical scheme for the solution of unsteady flow in open channels. The model was formulated using the Galerkin weighted residual method. They also proposed a framework for the solution to a network of open channels.

Dailey and Harleman (1972) developed a numerical model for unsteady water quality transport also using Galerkin weighted residual method. This model was combined with the hydrodynamic model of Gunaratnum and Perkins. The resulting model also incorporated the network formulation. The Dailey and Harleman network model provided for the solution of four water quality constituents; namely salinity, temperature, BOD and DO. The reaction processes were assumed to be first order. The momentum equation was cast in linearized characteristic form. The technique for the network solution was by the method of superposition, which is similar to the influence functions commonly used in structural analysis.

Najarian et al. (1975) presented a dynamic estuarine nitrogen cycle

model consisted of closed matter-flow loop having seven nitrogen storage variables and twelve transformations of the element nitrogen. The seven storage variables are : (1) ammonia nitrogen, (2) nitrite nitrogen, (3) nitrate nitrogen, (4) phytoplankton nitrogen, (5) zooplankton nitrogen, (6) particulate nitrogen and (7) dissolved organic nitrogen. These storage variables represent the physical states, chemical states and biological states of the element nitrogen. The biochemical and ecological transformations include nitrification, uptake of inorganic nutrients by autotrophs, grazing of heterotrophs, ammonia regeneration by living cells, lysis and leakage of organic matter through cell walls, natural death of microorganisms and ammonification. The transformation rates are functions of nutrient concentrations and available energy in the forms of heat and light. As a consequence, the model contains a large number of rate parameters many of which are not well known. They had to be carefully synthesized from information available in the literature. Implementation of this model tends to be very difficult, because field data are not normally available in the form used by the model; some arbitrary conversion factors must be used to convert field data into the form required by the model. Moreover, phosphorous nutrients are not simulated in the model, therefore the model is strictly for nitrogen limited systems only.

Hyer, Kuo, and Neilson (1977) presented an ecosystem model for the Back and the Poquoson Rivers. The conceptual framework of this model is similar to Di Toro (1977), but Hyer's formulation is a real time model, the solution is by the finite difference method. Nitrate nitrogen and nitrite nitrogen are combined into one variable. The velocity input to the model is calculated by the kinematic tide method, however. A

version of this model is also available for branched estuarine systems. In the branched version, each branch is treated independently except at the points of conjunction. This model was calibrated for the Back and the Poquoson Rivers, and later was also successfully applied to the Pagen river and the Elizabeth river.

Perhaps the most sophisticated phytoplankton model developed to date is the model presented by Chen (1979). This model is a two dimensional real time model based on the depth integrated mass balance equation. It contains ten water quality constituents. The Galerkin weighted residual method with linear triangular element was used in the finite element formulation. The reactions rates are either of the first order or of the Michaelis-Menton type. The model is coupled to a two dimensional depth integrated hydrodynamic model and has been applied to the lower James River estuary (Hampton Roads).

In summary, the use of numerical models for the study of water quality has been recognized for almost 60 years. The literature on water quality modeling is therefore very exhaustive. In this review only a few significant recent works were discussed. The early models were generally single component, steady state and non-spatially varying models. The more complex models did not begin until the 1960's when digital computers became widely available. The majority of the models are based on the principle of conservation of mass. Models based on other principles such as energy flow and stochastic processes have also been attempted, but are not included in this review. As the water quality requirements became more stringent, the models also became more complex, capable of simulating several nutrient-components. There is a trend at present towards using real time models because large temporal

variations of water quality concentrations have been known to occur within a tidal cycle. The use of steady state models for complex systems can lead to serious misunderstandings. Spatial distributions of water quality concentrations can be simulated by using powerful numerical techniques such as the finite difference method or the finite element method. The use of the finite element method is more advantageous because it can represent the natural geometry more accurately. The knowledge of the reaction kinetics, however, is lagging, mainly due to the enormous complexity of the natural processes. The reaction kinetics commonly used are mainly of the first order type or the Michaelis-Menton type. The collection of field data is in general lagging due to the expenses involved; the lack of field data in kind and in quantity has limited the extent to which models can be calibrated or verified. The use of hydrodynamic model to provide flow inputs into water quality models is desirable for economic reasons. The state of the art in hydrodynamic modeling in general is considered to be much more advanced than the water quality models, although both kinds of models use the same basic principle of conservation of mass, but the mathematical relationships which describe the hydrodynamics of a system are scientifically more valid than those describing the biochemical reactions. In this respect, the use of a very advanced hydrodynamic model to couple to a water quality model may not be always necessary, because the uncertainties in the biochemical processes far outweigh the hydrodynamic effects, but the hydrodynamic effects should be incorporated at least to a level significant with respect to the water quality model.

3 MATHEMATICAL FORMULATION

3.1 Hydrodynamic Model

A complete set of field measurements of water elevation and current to provide input to water quality models is rarely available; ideally a hydrodynamic model should be developed to provide the driving transport processes to water quality models. Water movement in shallow water estuaries can be successfully modeled using the cross-sectional area-integrated continuity and momentum equations. These equations have been previously derived by several authors such as Harleman and Lee (1969). The governing equations for the one-dimensional unsteady flow in variable area tidal channels are the continuity equation,

$$B \frac{\partial \eta}{\partial t} + \frac{\partial Q}{\partial x} = q \quad (3.1)$$

and the momentum equation,

$$\frac{\partial Q}{\partial t} + \frac{\partial QU}{\partial x} + gA \frac{\partial \eta}{\partial x} + \frac{gQ|Q|}{AC^2R_h} + \frac{\beta W_x |W_x| B}{\rho} + \frac{gAd_c}{\rho} \frac{\partial \rho}{\partial x} = 0 \quad (3.2)$$

where

η = elevation of water surface with respect to a horizontal datum,

Q = cross-sectionally averaged discharge, $Q = AU$,

A = cross-sectional area,

- U = cross-sectionally averaged velocity,
 x = distance along the channel,
 t = time,
 B = channel top width,
 q = fresh water inflow per unit length,
 g = gravitational acceleration,
 C_c = Chezy coefficient,
 d_c = distance from water surface to centroid of cross-section,
 ρ = water density,
 ρ_a = air density,
 β = wind shear stress coefficient,
 W_x = wind velocity along the channel and
 R_h = hydraulic radius of the channel.

The last term in equation (3.2) represents the effects of a longitudinal density gradient. The relationship between density of water and salinity is approximated by

$$\rho = 1000 + 0.75s \quad (3.3)$$

where

- s = average salinity (ppt) and
 ρ = water density (kg/m^3).

3.1.1 Initial and Boundary Conditions

The solution of equations (3.1) and (3.2) requires the specification of initial and boundary conditions. Initial conditions are specified for water surface elevation, η_0 , and velocity, U_0 , at the start time, say, $t = 0$

$$\eta(x,0) = \eta_0 \quad (3.4a)$$

$$U(x,0) = U_0 \quad (3.4b)$$

There are normally two types of boundary conditions; one specifies flow velocity and the other specifies elevation. At the ocean boundary, $x = x_a$, where most tide measurements exist, the surface elevation is prescribed

$$\eta(x_a,t) = \eta_a \quad (3.4c)$$

where

η_a = the astronomical tide.

At the upstream end, $x = x_g$, either a free surface or velocity can be prescribed. In case of a land boundary the velocity is normally assumed to be zero.

$$U(x_g,t) = 0 \quad (3.4d)$$

Equations (3.1), (3.2) and (3.4) constitute the hydrodynamic model. These will be solved using the finite element method described in the next chapter.

3.2 Biochemical Water Quality Model

The biochemical water quality model is based on the conservation of mass equation. The one-dimensional conservation of mass equation has been previously derived by several authors such as Harleman (1971). In order to emphasize the important assumptions, a brief description of the derivation is repeated here for reference. The general three dimensional conservation of mass equation in Cartesian coordinates is

$$\frac{\partial c}{\partial t} + \frac{\partial uc}{\partial x} + \frac{\partial vc}{\partial y} + \frac{\partial wc}{\partial z} = \frac{\partial}{\partial x} \left(D_x \frac{\partial c}{\partial x} \right) + \frac{\partial}{\partial y} \left(D_y \frac{\partial c}{\partial y} \right) + \frac{\partial}{\partial z} \left(D_z \frac{\partial c}{\partial z} \right) \quad (3.5)$$

where

- c = concentration of a water quality constituent (M/L³),
- u, v, w = instantaneous velocities in the x, y, and z directions (L/T),
- D_x, D_y, D_z = molecular diffusivities in the x, y, and z directions (L²/T),
- S = time rate of addition or removal of substance per unit volume (M/TL³) and
- M, L, T = mass, length and time scales.

The velocities and concentrations in equation (3.5) are instantaneous values. But it is more practical to smooth out the small time scale fluctuations. This is carried out by averaging the equation over a time scale long enough to smooth out the turbulence in the flow, yet short when compared to the temporal details we wish to resolve. In most applications where the intertidal quantities are of interest, the suitable time scale for such studies are generally in the order of minutes. Models using this magnitude of time scale are often called real time or tidal time models. There are a number of advantages in using a real time model: apart from being able to delineate intertidal

details, a real time model is less sensitive to the longitudinal dispersion coefficient than a tidally averaged model. Thus one can avoid expensive dye studies to determine the longitudinal dispersion coefficient. Using this time scale, the time averages of the fluctuation of the quantities associated with the fluid turbulence are obtained. The averaging is carried out following the approach used by Osborn Reynolds, where the quantities u , v , w , and c are separated into a mean part and a fluctuation part such that ; $u = \bar{u} + u'$, $v = \bar{v} + v'$, $w = \bar{w} + w'$ and $c = \bar{c} + c'$, where the overbar denotes the time average and the prime denotes the deviation from the time average. When these are substituted into equation (3.5) and the time averages are taken, we get

$$\frac{\partial \bar{c}}{\partial t} + \frac{\partial \bar{uc}}{\partial x} + \frac{\partial \bar{vc}}{\partial y} + \frac{\partial \bar{wc}}{\partial z} = \frac{\partial}{\partial x} \left(\epsilon_x \frac{\partial \bar{c}}{\partial x} \right) + \frac{\partial}{\partial y} \left(\epsilon_y \frac{\partial \bar{c}}{\partial y} \right) + \frac{\partial}{\partial z} \left(\epsilon_z \frac{\partial \bar{c}}{\partial z} \right)$$

where

ϵ_x , ϵ_y , ϵ_z = turbulent diffusivities which are defined such that

$$\frac{\partial \bar{c}}{\partial x} = D_x \frac{\partial c}{\partial x} \overline{u'c'}$$

and similarly for ϵ_x and ϵ_y .

The cross product terms such as $\overline{u'c'}$ represent the flux of mass due to turbulent fluctuations.

The one dimensional equation is derived by integrating equation (3.6) over the cross-sectional area, and by defining

$$\bar{u} = U + u'' \tag{3.7a}$$

$$\bar{v} = v'' \tag{3.7b}$$

$$\bar{w} = w'' \tag{3.7c}$$

$$\bar{c} = C + c'' \quad (3.7d)$$

such that

$$\int_A \bar{u} dA = AU$$

$$\int_A \bar{c} dA = AC$$

$$\int_A u'' dA = \int_A v'' dA = \int_A w'' dA = \int_A c'' dA = 0$$

where

- U = is the cross-sectional average velocity,
- u'', v'', w'' = spatial deviations from the average velocity,
- C = is the cross-sectional average concentration and
- c'' = spatial deviation from the average concentration.

When equations (3.7a to d) are substituted into equation (3.6) and integrated over the cross-sectional area, neglecting the cross product terms containing v''c'' and w''c'' yields

$$\frac{\partial AC}{\partial t} + \frac{\partial QC}{\partial x} + \frac{\partial}{\partial x} \int_A u'' c'' dA = \frac{\partial}{\partial x} \left(A \bar{\epsilon}_x \frac{\partial C}{\partial x} \right)$$

where

$\bar{\epsilon}_x$ = spatial mean value of the turbulent diffusivity.

Following Taylor (1954), the cross product term containing u''c'', which is due to the spatial deviations, can be represented in a form analogous to the turbulent diffusion coefficient; this term is called the longitudinal dispersion coefficient, E_L , and is defined such that

$$\int_A u''c''dA = -AE_L \frac{\partial C}{\partial x}$$

Thus the effects of shear and spatial averaging are accounted for. This is why a model which is not averaged over the tidal cycle is better and able to represent the mixing phenomena; it properly represents the advection. The negative sign indicates that transport due to dispersion is always in the direction of decreasing concentration. The coefficient E_L is always very much larger than $\bar{\epsilon}_x$, therefore it is convenient to combine the two coefficients and refer to the sum as the longitudinal dispersion coefficient, E , where

$$E = E_L + \bar{\epsilon}_x \quad (3.9)$$

It must be recalled that in the averaging process, the advective term will generate additional contributions, say, to the dispersion term, as long as fluctuations of flow and concentration are significant. Therefore it is an important consideration when transpositioning the values of the longitudinal dispersion coefficients. Equation (3.8) now becomes

$$\frac{\partial}{\partial t}(AC) + \frac{\partial}{\partial x}(QC) = \frac{\partial}{\partial x}(AE \frac{\partial C}{\partial x}) + AS \quad (3.10)$$

The first term in equation (3.10) represents the time rate of change of the concentration of a substance, the second and third terms are the mass flux of the substance due to advection and dispersion respectively. The fourth term is the source/sink term. The dispersion coefficient represents the mass transfer due to the non-uniform velocity distribution and the turbulent diffusion. The modified Taylor's dispersion formula

$$E_T = 63 n U R_h^{5/6} \quad (3.11)$$

(in MKS units) has been successfully used in the fresh water region of the estuary. However, in the salinity intrusion region it is well known that the presence of salinity enhances mixing by the longitudinal density gradients, therefore the dispersion coefficient is expected to be larger than in the non-saline region. Also at the downstream end of an estuary the water body is normally much wider than the upstream end and therefore more susceptible to wind wave action. In this study the following dispersion formula is used

$$E(x,t) = m(x)E_T + E_2(x) \quad (3.12)$$

Where E_T is the modified Taylor's expression and m is a coefficient to account for channel irregularities. The second term, E_2 , is a spatially varying constant which takes into account the increased dispersion towards the downstream end. Both m and E_2 have to be adjusted against field observations during model calibration.

The various biochemical reactions and waste load inputs are incorporated into the equation through the source/sink term S . Equation (3.10) is the basic equation used to describe the spatial and temporal concentration for each of the water quality constituents, ie. an equation must be applied to each constituent to ensure conservation of mass. For convenience the source/sink term is separated into three parts and the subscript i ($i = 1,2,3,\dots,0$) will be used to denote each of the water quality constituents being modeled. The conservation of mass

equation now becomes

$$\frac{\partial}{\partial t}(AC_i) + \frac{\partial}{\partial x}(QC_i) = \frac{\partial}{\partial x}(AE\frac{\partial C_i}{\partial x}) + AR_i - Ak_{si}C_i + W_i \quad (3.13)$$

where

C_i = concentration of the i th water quality constituent (M/L^3),

R_i = time rate of sources or sinks due to biochemical reactions (M/TL^3),

k_{si} = loss rate ($1/T$) and

W_i = external waste input loads (M/LT).

The loss rate k_{si} is the loss out of the system either by settling out or by other loss mechanisms which cannot be easily modeled; such as the exchange of nutrients between the water column and the river bottom. The magnitude of the loss rate has to be determined against observed data during model calibration. The term W_i represents external waste inputs into the model, this includes waste loads from point and nonpoint-sources.

3.2.1 Initial and Boundary Conditions

Equation (3.13) requires the specification of initial and boundary conditions. Initial conditions specify the water quality concentrations at the model start time, say at $t = 0$.

$$C_i(x,0) = C_i^0$$

where

C_i^0 = the given initial concentrations.

There are two types of boundary conditions (Christodoulou, 1976)

(i) Concentration boundary conditions and

(ii) Dispersive boundary conditions.

These correspond to the essential and the natural boundary conditions respectively. The concentration boundary conditions specify concentrations $C_i(x_B, t)$ at the boundaries $x = x_B$. The dispersive boundary conditions specifies $AE\partial C_i/\partial x$ at the boundaries $x = x_D$. The choice of boundary conditions depends on the behavior and the availability of field data for a specific problem

Finally, it must be emphasized that a one dimensional model limits the results to quantities which are averaged over a channel cross-section. This assumption may not be appropriate if the water body is wide, or if there is pronounced stratification. Also the waste discharge at a point is assumed to be completely mixed over the cross-section. This assumption may not be valid at the point of discharge, but will be reasonable at some distance away from the point of discharge.

3.3 Biochemical Processes

The various biochemical processes are incorporated into equation (3.13) through the term R_i . In the following section, the formulation of the term R_i for each of the water quality constituent will be described. In this study the following ten constituents are modeled

- (1) Chlorophyll 'a',
- (2) Organic nitrogen,
- (3) Ammonia nitrogen,
- (4) Nitrite-nitrate nitrogen,
- (5) Organic phosphorus,
- (6) Inorganic phosphorus,

- (7) CBOD,
- (8) Dissolved oxygen deficit,
- (9) Salinity and
- (10) Coliform bacteria.

The schematic diagram of the ten interacting constituents is shown in Figure 3.1. Each constituent in the model is represented by a box; the arrows between the boxes show the assumed relationships and the directions of transfer of material. The modeling domain is inscribed in the big circle. The external influences such as waste inputs and solar radiation are indicated outside the big circle. The notation for each constituent is represented by C_i , where the subscript i ($i = 1, 2, 3, \dots, 9, 0$) is used to represent the ten constituents in the orders as given above respectively.

The reactions occurring in estuarine waters are very complex and involve feed forward mechanisms which produce pronounced non-linearities. In general our knowledge of reactions in natural waters is not well advanced. Consequently reaction rates are commonly represented by simplified mathematical expressions. The reaction kinetics used in this study are of two types, namely; (1) First order reactions and (2) Michaelis-Menton reactions. These reaction forms are empirical, they have been usually adopted because of mathematical tractability. The kinetic term R_i in equation (3.13) for each constituent is formulated as follows

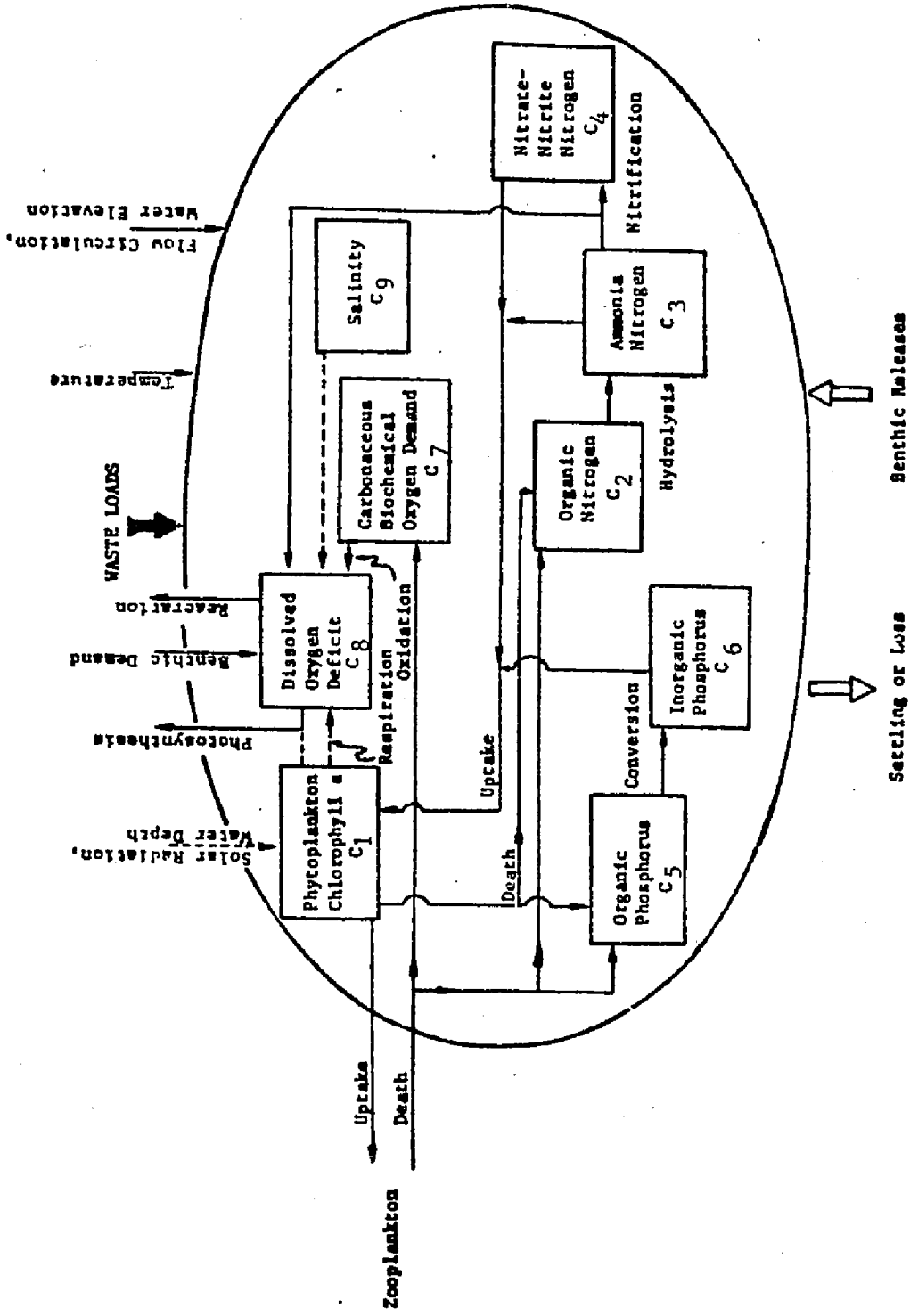


Figure 3.1 Schematic diagram showing the interactions of the nine constituents in the water quality model (Adapted from Chen 1979).

3.3.1 Chlorophyll 'a', C_1

The biomass of phytoplankton in the estuary is represented by the concentration of chlorophyll 'a'. A relatively homogeneous layer of phytoplankton is assumed, so that the growth and death rates are average values for the entire phytoplankton community. The basic kinetics governing the amount of chlorophyll 'a' in the water body is the growth, death and zooplankton predation as expressed by the equation

$$R_1 = (G - D - Z)C_1 \quad (3.14)$$

where

C_1 = chlorophyll 'a' ($\mu\text{g/l}$),

G = growth rate of phytoplankton (1/day),

D = endogenous respiration rate of phytoplankton (1/day) and

Z = zooplankton grazing rate (1/day).

Phytoplankton grow by assimilating inorganic nutrients in the presence of light. The growth rate is assumed to be a direct function of temperature when under optimal light and nutrient conditions; non-optimal light and nutrient conditions will reduce this growth rate. The equation for growth of phytoplankton can therefore be written as a temperature dependent growth rate modulated by the light and nutrient effects

$$G = k_g T F N \quad (3.15)$$

where

k_g = optimum growth rate coefficient (1/day/°C),

T = temperature, °C,

F = attenuation of growth due to non-optimal light and

N = attenuation of growth due to nutrient limitation.

The effect of non-optimal light intensity is to reduce the growth rate. Steele (1962) proposed that the reduction in growth rate be represented by

$$F = \frac{I}{I_s} e^{(1 - \frac{I}{I_s})} \quad (3.16)$$

where

I = light intensity in the water column (langleys),

I_s = saturating or optimal light intensity (langleys) and

e = 2.1718.

In the water column, light intensity decreases exponentially with depth. For a given value of surface light intensity, the light intensity at any depth can be calculated by

$$I = I_0 e^{-k_e z} \quad (3.17)$$

where

I_0 = surface light intensity,

z = depth and

k_e = light extinction coefficient.

In order to obtain the average light intensity in the water column, equation (3.16) is integrated over the depth. The resultant expression

for depth averaged light is

$$F = \frac{e}{k_e H} \left(1 - e^{-\frac{I_0}{I_s}} \right) \quad (3.18)$$

where

H = water depth.

To obtain the average growth rate per day, Di Toro et al. (1971) integrated equation (3.18) over a day with the following result

$$F = \frac{ef}{k_e H} (e^{-\alpha_1} - e^{-\alpha_2}) \quad (3.19)$$

where

f = photoperiod,

$$\alpha_1 = \frac{I_a}{I_s} e^{-k_e H}$$

$$\alpha_2 = \frac{I_a}{I_s} \quad \text{and}$$

I_a = mean daily light intensity.

However, the daily average in equation (3.19) above does not reflect the diurnal variation of the growth rate. The ability of the original Steele's equation to express surface light inhibition is also lost. Kremer and Nixon (1978) found that Di Toro's expression overestimated the actual growth rate by about 15% and suggested the use of a correction factor of 0.85. Since Steele's formula has found widespread support in the literature and since it is not necessary to average the growth rate over time in a real time model, therefore in this study, the surface light intensity is allowed to vary diurnally following a sine curve peaking at midday, such that

$$I = \begin{cases} \frac{I_m \pi}{2L_d} \sin\left(\frac{\pi(t_d - t_s)}{L_d}\right) & \text{for } t_s < t_d < (t_s + t_d) \\ 0 & \text{otherwise} \end{cases} \quad (3.20)$$

where

$L_d = 12 + 2.7 \sin\left\{\frac{2\pi(t_y - 20)}{365}\right\}$ is the day length (hours),

$t_s = 12 - L_d/2$ is the sunrise time (hours),

I_m = total daily solar radiation (langleys),

t_y = days since January 1st,

t_d = time of the day (hours) and

$\pi = 3.14159$.

As the phytoplankton concentration increases, the absorption of light by the cells themselves reduces the solar energy available at deeper levels. The reduction, known as the self shading effect, is modeled by increasing the light extinction in proportion to the concentration of phytoplankton. The empirical equation of Riley (1956) is used in this model

$$k_e = k'_e + 0.054C_1^{0.66} + 0.0088C_1 \quad (3.21)$$

k'_e = light extinction coefficient at zero chlorophyll *a'* concentration (m^{-1}).

The attenuation of light is chiefly caused by the suspended matter in the water (Colijn, 1982). The value of the extinction coefficient can be estimated from the formula $k'_e = 1.7/D_s$, where D_s is the Secchi disk visibility reading (Sverdrup, 1970). The reported range of the extinction coefficient is 0.4 to 8 m^{-1} .

The optimum light level for photosynthesis has been found to vary over short spans of time and space. These changes may be due to a variety of external factors. Some authors suggest the use of average values for the simulation span. This is reasonable for short time intervals. However, for a long period simulation, time varying optimum light is necessary. It has been established that under certain conditions the photosynthetic capacity reflects to some degree the past light history (Kremer and Nixon, 1978). The basic assumption is that the optimum light for growth tracks the light history to which the algae has been exposed. Based on these conditions, the optimum light in this study is determined as a weighted moving average of the light intensity at the 1 meter depth for the previous three days.

$$I_s = (0.7I_1 + 0.2I_2 + 0.1I_3) e^{-ke} \quad (3.21a)$$

where

I_j = the average surface light j days earlier, $j = 1, 2$ and 3 .

This equation clearly has no limit to acclimation, however. It may be necessary to include light thresholds above and below which acclimation may not occur, such as the low radiation levels in winter.

The hyperbolic effect of nutrient limitation on the growth rate of microorganisms has long been recognized. Generally, the Michaelis-Menton enzyme kinetics is extended to nutrient uptake and to growth rates of phytoplankton. This extension is reasonable since growth processes are the result of a combination of enzymic reactions. The Michaelis-Menton kinetics can be further extended to multi-nutrient limiting conditions. Di Toro (1977) and Kremer and Nixon (1978) used

the products of the Michaelis-Menton reaction when there is simultaneous limitation of several nutrients. This assumption has been supported by empirical observations. The nutrient limitations on chlorophyll growth rate due to the inorganic nitrogen and inorganic phosphorous in this model is expressed by

$$N = \left(\frac{C_3 + C_4}{C_3 + C_4 + k_{mn}} \right) \left(\frac{C_6}{C_6 + k_{mp}} \right) \quad (3.22)$$

where

- k_{mn} = Michaelis-Menton constant for inorganic nitrogen (mg/l),
- k_{mp} = Michaelis-Menton constant for inorganic phosphorous (mg/l),
- C_3 = ammonia nitrogen (mg/l),
- C_4 = nitrite-nitrate nitrogen (mg/l) and
- C_6 = inorganic phosphorous (mg/l).

The endogenous respiration rate, D , and the zooplankton grazing rate, Z , are assumed to be temperature dependent, thus

$$D = k_r' T \quad (3.23)$$

$$Z = k_z' T \quad (3.24)$$

where

k_r' = endogenous respiration coefficient (1/day/°C) and

k_z' = zooplankton grazing coefficient (1/day/°C).

3.3.2 Organic Nitrogen, C_2

In natural waters organic nitrogen undergoes a series of transformations mediated by bacteria. Organic nitrogen is transformed into ammonia nitrogen which itself is subsequently transformed to nitrite and then to nitrate nitrogen. In this model, the internal sources of organic nitrogen are considered to be phytoplankton and zooplankton endogenous respiration. The sink of organic nitrogen is the hydrolysis of organic nitrogen to nitrite and nitrate. The kinetics is of the first order type

$$R_2 = r_n(D_z + f_1 Z)C - k_2 C_2 \quad (3.25)$$

$$k_2 = k_2' T$$

where

- C_2 = organic nitrogen (mg/l),
- r_n = nitrogen-chlorophyll ratio (mg-N/ μ g-chlorophyll),
- k_2 = organic nitrogen to ammonia nitrogen hydrolysis rate (1/day),
- k_2' = organic nitrogen to ammonia nitrogen hydrolysis coefficient (1/day/ $^{\circ}$ C) and
- f_z = assimilation efficiency, value ranges from 0.4 to 0.8.

3.3.3 Ammonia Nitrogen, C_3

The kinetics for ammonia nitrogen is

$$R_3 = k_2 C_2 - k_3 C_3 - r_n(1 - P)GC_1 \quad (3.26)$$

$$P = \frac{C_4}{C_4 + k_{mn}} \quad \text{for nitrate preference} \quad (3.27a)$$

$$P = 1 - \frac{C_3}{C_3 + k_{mn}} \quad \text{for ammonia preference} \quad (3.27b)$$

$$k_3 = k_3' T$$

where

C_3 = ammonia nitrogen (mg/l),

C_4 = nitrite-nitrate nitrogen (mg/l),

k_3 = ammonia to nitrate nitrification rate (1/day),

k_3' = ammonia to nitrate nitrification coefficient (1/day/°C) and

P = nitrate or ammonia nitrogen preference.

The first term on the right hand side of equation (3.26) represents the hydrolysis from organic nitrogen, the second term is the sink of ammonia nitrogen due to nitrification, the third term represents the uptake by phytoplankton, and the factor P represents the nitrate nitrogen or ammonia nitrogen preference.

3.3.4 Nitrite-Nitrate nitrogen, C_4

In this model nitrite and nitrate nitrogen are combined as one variable, this is due to the fact that in natural estuarine waters, the concentration of nitrate nitrogen is normally at an order of magnitude larger than the concentration of nitrite nitrogen. The combined variable simplifies the model yet retains the effects of nitrite nitrogen. The kinetics for nitrite-nitrate nitrogen is

$$R_4 = -Pr_n GC_1 + k_3 C_3 \quad (3.28)$$

The first term on the right hand side is the uptake by phytoplank-

ton, the second is the source of nitrite-nitrate nitrogen from nitrification of ammonia nitrogen.

3.3.5 Organic Phosphorus, C_5

The biochemical kinetics of organic phosphorous consists of hydrolysis of organic phosphorous to inorganic phosphorous, and the release of organic phosphorous from death of phytoplankton and zooplankton. The kinetic expression for organic phosphorous is

$$R_5 = r_p(D + f_z Z)C_1 - k_5 C_5 \quad (3.29)$$

$$k_5 = k_5' T$$

where

C_5 = organic phosphorous (mg/l),

k_5 = organic phosphorous to inorganic phosphorous conversion rate (1/day),

k_5' = organic phosphorous to inorganic phosphorous conversion coefficient (1/day/°C) and

r_p = phosphorus-chlorophyll ratio (mg-P/ μ g-chlorophyll).

3.3.6 Inorganic Phosphorus, C_6

Only the inorganic phosphorous fraction of the total phosphorous is considered to be taken up by phytoplankton. The internal source of inorganic phosphorous is the hydrolysis of organic phosphorous, such that

$$R_6 = -r_p C_6 C_1 + k_5 C_5 \quad (3.30)$$

3.3.7 CBOD, C_7

CBOD is handled as a first order decaying substance in a classical manner. The sink of CBOD is the oxidation by bacteria and the internal sources are the die off of phytoplankton and zooplankton.

$$R_7 = 2.67r_c(f_z Z)C_1 - k_7 C_7 \quad (3.31)$$

$$k_7 = k_7'(1.047)^{T-20}$$

where

$$C_7 = \text{CBOD (mg/l),}$$

$$k_7 = \text{CBOD oxidation rate (1/day),}$$

$$k_7' = \text{CBOD oxidation rate at 20°C and}$$

$$r_c = \text{carbon-chlorophyll ratio (mg-C/μg-chlorophyll)}$$

The factor 2.67 arises from the fact that the complete oxidation of one gram of carbon to carbondioxide requires 2.67 grams of oxygen.

3.3.8 DO Deficit, C_8

DO is coupled to CBOD, nitrogen and phytoplankton. The external source of DO is atmospheric reaeration; the sinks are oxidation of CBOD, oxidation of ammonia nitrogen and nitrite nitrogen, and the respiration of zooplankton and phytoplankton. The equation is written in terms of DO deficit

$$R_8 = k_7 C_7 + 4.57k_3 C_3 - a_p C C_1 + a_r D C_1 + b_8 - k_8 C_8 \quad (3.32)$$

$$a_p = 2.67r_c k_{op}$$

$$a_r = 2.67r_c / k_{or}$$

$$k_g = k'_g(1.024)^{\frac{T-20}{H}} \quad \begin{matrix} -1.5 \\ H \end{matrix} \quad \begin{matrix} 0.5 \\ U \end{matrix}$$

$$b_g = b'_g(1.065)^{T-20}$$

where

C_g = dissolved oxygen deficit (mg/l),

a_p = rate of oxygen production from photosynthesis (1/day),

a_r = rate of oxygen depletion by respiration (1/day),

k_{op} = photosynthetic quotient,

k_{or} = respiration ratio,

k_g = reaeration rate (1/day),

k'_g = reaeration coefficient at 20°C,

b_g = benthic oxygen demand (gm-O₂/m²/day) and

b'_g = benthic oxygen demand at 20 °C.

DO is calculated by subtracting the DO deficit from the saturation values of DO. The saturation DO depends on temperature and salinity of the water, C_g , and is determined by the empirical formula

$$\begin{aligned} DO = 9.0806 - (0.18725 - 0.0044972(T-20) - 0.00205C_g)(T-20) \\ - (0.0556 - 0.0002739C_g)C_g \end{aligned} \quad (3.33)$$

3.3.9 Salinity, C_g

Salinity is treated as a conservative substance without source/sink term, since there are no biochemical reactions.

$$R_g = 0 \quad (3.34)$$

where

$$C_g = \text{salinity (ppt)}.$$

3.3.10 Coliform Bacteria, C_o

Coliform bacteria die off rate is handled as a first order decay process

$$R_o = - k_o C_o \quad (3.35)$$

$$k_o = k'_o (1.040)^{T-20}$$

where

C_o = coliform bacteria (number/100 ml),

k_o = coliform bacteria die off rate (1/day) and

k'_o = coliform bacteria die off rate at 20°C.

So finally we have arrived at ten partial differential equations that constitute the biochemical water quality model. These equations will be solved successively using the finite element method as described in the next chapter.

4 FINITE ELEMENT FORMULATION

4.1 Introduction

Equations (3.1), (3.2) (3.13) and their associated initial and boundary conditions are the governing equations for the biochemical water quality model. This is an initial-boundary value problem with twelve equations for twelve unknowns η , Q and C_i ($i = 1, 2, 3, \dots, 9, 0$). In this study the finite element method (FEM) is used for the numerical solution. For practical and economic reasons equation (3.2) will be linearized by using the value of Q from the previous integration time step and equation (3.13) will be solved successively for each water quality constituent.

The FEM is a numerical technique for obtaining approximate solutions to mathematical problems defined by differential equations. This method was originally developed for studying complex structural mechanics, but because of its flexibility as an analysis tool, the FEM has been rapidly applied to many other engineering and science problems. The theory of FEM is quite well known, and is described in a number of excellent text books written on this subject, e.g. Zienkiewicz (1977) or Huebner (1975).

The FEM discretizes the solution domain into a number of subregions called elements, each element is represented by a number of points called the nodes where the dependent variables are determined. The

unknown variable is approximated within each element by an interpolation function expressed in terms of the values at the nodes. The system equations for the entire solution domain are obtained by assembling the contributions from the individual elements.

4.2 Variational Statements and the Finite Element Approximation

Using the Galerkin weighted residual method, the variational statements for equations (3.1), (3.2) and (3.13) are obtained by multiplying the equations with arbitrary weighting functions $\delta\eta$, δQ and δC respectively, integrating over the length of the estuary L and requiring the resulting expression to vanish

$$\int_L \left(R \frac{\partial \eta}{\partial t} + \frac{\partial Q}{\partial x} - q \right) \delta \eta dx = 0 \quad (4.1)$$

$$\int_L \left(\frac{\partial Q}{\partial t} + \frac{\partial QU}{\partial x} + gA \frac{\partial \eta}{\partial x} + g \frac{Q|Q|}{AC^2 R_h} + gA \frac{d_c \partial \rho}{\rho \partial x} \right) \delta Q dx = 0 \quad (4.2)$$

$$\int_L \left(\frac{\partial AC}{\partial t} + \frac{\partial QC}{\partial x} - \frac{\partial}{\partial x} \left(AE \frac{\partial C}{\partial x} \right) - AR + Ak_s C - W \right) \delta C dx + \int_L F_x^* \delta C dx = 0 \quad (4.3)$$

where

$$F_{x_B}^* = AE \frac{\partial C}{\partial x} \Big|_{x = x_B}$$

is the prescribed dispersive flux boundary condition at $x = x_B$.

For clarity the surface wind term in equation (3.2) and the subscript i in equation (3.13) have been omitted. An additional step is performed to reduce the order of the derivative in equation (4.3) by integrating the dispersive term by parts, the equation becomes

$$\int_L \left\{ \left(\frac{\partial AC}{\partial t} + \frac{\partial QC}{\partial x} - AR + Ak_s C - W \right) \delta C + AE \frac{\partial C \partial \delta C}{\partial x \partial x} \right\} dx + F_o^* \delta C - F_l^* \delta C = 0 \quad (4.4)$$

where

$$F_o^* = AE \frac{\partial C}{\partial x} \Big|_{x=0}$$

and

$$F_l^* = AE \frac{\partial C}{\partial x} \Big|_{x=l}$$

are the given dispersive boundary conditions at the downstream end, $x = 0$, and at the upstream end, $x = l$, respectively.

For convenience the first two terms in equation (4.4) can be written as

$$\begin{aligned} \frac{\partial AC}{\partial t} + \frac{\partial QC}{\partial x} &= A \frac{\partial C}{\partial t} + Q \frac{\partial C}{\partial x} + C \left(\frac{\partial A}{\partial t} + \frac{\partial Q}{\partial x} \right) \\ &= A \frac{\partial C}{\partial t} + Q \frac{\partial C}{\partial x} + Cq \end{aligned}$$

In the finite element method the solution domain is divided into a number of elements and the field variables η , Q and C in each element are approximated by trial functions

$$\eta \approx \hat{\eta} = \{N\}^T \{\eta\} \quad (4.5a)$$

$$Q \approx \hat{Q} = \{N\}^T \{Q\} \quad (4.5b)$$

$$C \approx \hat{C} = \{N\}^T \{C\} \quad (4.5c)$$

where

- $\hat{\eta}$, \hat{Q} , \hat{C} = approximate solutions in an element,
 $\{N\}^T$ = a row vector of the interpolation function and
 $\{\eta\}$, $\{Q\}$, $\{C\}$ = the vectors of the unknown nodal variables to be determined.

The interpolations are usually defined locally for elements or subdomains. In a one dimensional problem, the elements will be line segments along the x-axis. The simplest line element is a line segment with two nodes. This is the type of element used in the present study. Higher polynomials can be used, but a linear variation is preferred because it is simple to use and simple to interpret physically. Using a local coordinate system as shown in Figure 4.1, the linear variation of the field variable such as the concentration C in equation (4.5c) can be written as

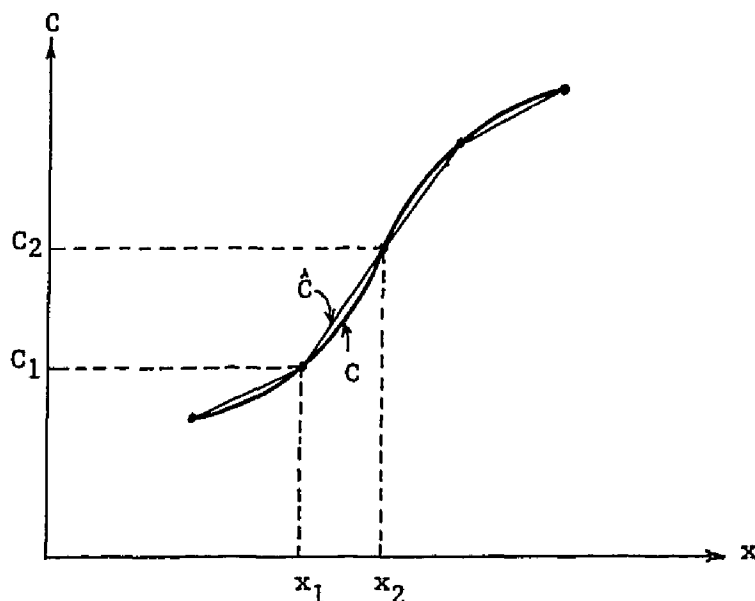


Figure 4.1 Finite element approximation to the exact solution.

$$C = \hat{C} = N_1 C_1 + N_2 C_2 \quad (4.6a)$$

where

$$N_1 = (x_2 - x) / (x_2 - x_1),$$

$$N_2 = (x - x_2) / (x_2 - x_1),$$

x_1, x_2 = coordinates of the two ends of the element and

C_1, C_2 = the nodal values at x_1 and x_2 respectively.

Equation (4.6a) can also be written in matrix form as

$$\hat{C} = \{N\}^T \{C\} \quad (4.6b)$$

where

$$\{C\} = \begin{Bmatrix} C_1 \\ C_2 \end{Bmatrix}$$

$$\{N\}^T = \{N_1 \ N_2\}$$

The weighting functions $\delta\eta$, δQ , and δC also have the same form as the trial functions as in equations (4.5a to c). All the other variables such as A and B are expressed in a similar fashion.

Substituting the trial functions (4.5a, b and c) and the similar weighting functions into equations (4.1), (4.2) and (4.4). The resulting element integrals can be evaluated explicitly for every element. The global equations are obtained by assembling the individual element equations. After cancelling the terms $\{\delta\eta\}^T$, $\{\delta Q\}^T$ and $\{\delta C\}^T$, the results can be written as

$$[M_\eta] \frac{d\{\eta\}}{dt} + [K_\eta]\{\eta\} = \{F_\eta\} \quad (4.7)$$

$$[M_Q] \frac{d\{Q\}}{dt} + [K_Q]\{Q\} = \{F_Q\} \quad (4.8)$$

$$[M_C] \frac{d\{C\}}{dt} + [K_C]\{C\} = \{F_C\} \quad (4.9)$$

Where the matrices are obtained from the assemblage of all the elements. The details of the integration and the matrices are given in Appendix A.

4.3 Time Integration

The FEM has reduced the original set of partial differential equations in space and time into a set of ordinary differential equations in time. Several integration methods can be used to advance the solution in time from a given initial condition. The choice of time integration schemes has been discussed by Wang (1975) and by Roache (1972). In this study, the hydrodynamic and water quality equations are solved separately in two sub-models; and the trapezoidal rule with split time scheme (Wang, 1975) is used to advance the solution in time.

4.3.1 Hydrodynamic Model

Equations (4.7) and (4.8) are used to solve for η and Q respectively. In the split time scheme, these two equations are staggered in time such that η is evaluated at times $t_{n+\frac{1}{2}}$ and Q at times t_n ($n = 1, 2, 3, \dots$). Equations (4.7) and (4.8) can be written as

$$[M_\eta] (\{\eta\}_{n+\frac{1}{2}} - \{\eta\}_{n-\frac{1}{2}}) = (\{F_\eta\} - [K_\eta]\{Q\}_n) \Delta t \quad (4.10)$$

$$[M_Q] \{Q\}_{n+1} - \{Q\}_n + [K_Q] \{Q\}_{n+1} + \{Q\}_n \Delta t/2 = \Delta t \{F_Q\} \quad (4.11)$$

where

Δt = the size of the integration time step.

Using given initial values $\{\eta\}_{n-1/2}$ and $\{Q\}_n$, the solution proceeds by first solving equation (4.10) for $\{\eta\}_{n+1/2}$; and then solving equation (4.11) for $\{Q\}_{n+1}$ using initial values $\{Q\}_n$ and $\{\eta\}_{n+1/2}$ from the previous half time step. The process is then repeated for the subsequent time steps.

4.3.2 Water Quality Model

The ten water quality constituents C_i are obtained by solving equation (4.9) successively for each water quality constituent. Employing the trapezoidal rule of integration, the finite difference form of equation (4.9) can be written as

$$[M_C] \{C\}_{n+1/2} - \{C\}_{n-1/2} + [K_C] \{C\}_{n+1/2} + \{C\}_{n-1/2} \Delta t/2 = \Delta t \{F_C\} \quad (4.12)$$

Equation (4.12) is used to solve for C_i at times $t_{n+1/2}$ from the given initial values $\{C\}_{n-1/2}$ and the values of $\{\eta\}_{n+1/2}$ and $\{Q\}_{n+1/2}$ from the hydrodynamic model. The process is then repeated for the subsequent time steps.

As mentioned in chapter three, there are two types of boundary conditions, corresponding to the essential and the natural boundary conditions. The essential boundary conditions are imposed by modifying the final system equations; the natural boundary conditions are imposed by evaluating the dispersive flux (Harleman, 1972). For the water

quality model, the ocean boundary condition is handled by checking the discharge at each time step. If discharge is into the boundary, concentration of the incoming water is specified. If discharge is out of the boundary, dispersive flux is specified.

4.4 Stability Conditions

The stability criteria for a given set of equations is commonly determined by the method of von Neumann (Roache, 1972). The objective is to determine whether the spurious errors introduced in the numerical method will amplify. The procedure is to follow a Fourier expansion as time progresses. This method, however, is only applicable to the greatly simplified set of equations; and the nonlinear terms are invariably omitted in the analysis. The stability criteria in the present study is difficult to obtain analytically. But guidelines for stability criteria for the hydrodynamic model can be obtained using the Courant condition

$$\Delta t_{cr} < \frac{\Delta x}{\sqrt{2gh}} \quad (4.13)$$

where

- Δt_{cr} = critical time step for the onset of instability,
- Δx = typical grid size,
- H = typical water depth and
- g = gravitational acceleration.

For the convective-diffusion equation, Roache (1972) has shown that using the explicit integration scheme when the grid Reynolds number

$$\frac{u\Delta x}{E} < 2 \quad (4.14)$$

the diffusion restrictions

$$\frac{E\Delta t}{\Delta x^2} < 0.5 \quad (4.15)$$

and

$$\Delta t < \frac{2E}{U^2} \quad (4.16)$$

are necessary and sufficient for the stability of the linear and constant U case. The effects of spatially varying U can not be ascertained, however. Similarly the implicit integration scheme using the trapezoidal rule has been found to be unconditionally stable.

In practice the stability criteria varies from problem to problem, since the stability of the numerical solution is governed by a number of factors such as the particular way of formulating the equations and the truncation errors of the computer. Guidelines can be established by using equation (4.13) for the hydrodynamic model and equations (4.15) and (4.16) for the water quality model. It is interesting to note that the stability criteria for hydrodynamic models are much more stringent than the water quality counterparts. Therefore it is more efficient to separate the hydrodynamic and water quality systems into two sub-models as is done in the present study. The stability conditions found in this study are generally more relax than those given by equations (4.13), (4.15) and (4.16); these will be further discussed in the individual case studies.

Another problem that may occur with the numerical solution of the conservation of mass equation is the presence of spatial oscillations. Spatial oscillatory solutions generally occur in a node to node manner, hence called 2 x oscillations. The occurrence of spatial oscillation is not a true stability problem because it is not unbounded, but the result oscillates about the correct solution. Lee and Harleman (1971) found that the solution tended to oscillate in the vicinity of steep concentration gradients. If the oscillations can be tolerated, a smoothing technique can be used to suppress the oscillations; since this is done on output only, it has no internal effect on the solution.

The oscillations can also be suppressed by introducing damping mechanisms such as by adding artificial dispersion terms to the equation or by using numerical schemes such as the upwind differencing method which introduces artificial dispersion into the equation (Chow, 1979). The best approach, however, is to make judicious mesh refinements and to reexamine the specification of boundary conditions (Gresho and Lee, 1981).

5 VERIFICATION

It is important to first check to see if the numerical models are formulated correctly. This can be done by comparing numerical results to analytical solutions. In this chapter, the hydrodynamic and water quality models will be used to solve three simple problems and compare the results with exact analytical solutions. This will offer a level of confidence that the models have been formulated correctly and that the computer programs have been written correctly.

5.1 Standing Wave in a Rectangular Channel

The first example is to use the hydrodynamic model to solve the problem of a standing wave in a rectangular channel. For a linearized one dimensional problem, the governing equations are

$$\frac{\partial U}{\partial t} + g \frac{\partial \eta}{\partial x} = 0 \quad (5.1)$$

$$\frac{\partial \eta}{\partial t} + h \frac{\partial U}{\partial x} = 0 \quad (5.2)$$

The channel length is L and closed at one end at $x = L$. At the open end, $x = 0$, the water level is forced by a simple sine wave

$$\eta = a \sin(\omega t) \quad (5.3)$$

where

a = amplitude,

$\omega = 2\pi/T$ = angular frequency and

T = period.

The boundary condition at the closed end is

$$U = 0 \quad \text{at } x = L \quad (5.4)$$

The analytical solution of the problem is a standing wave with the velocities and water surface elevations given by equations

$$U = \frac{-ac}{h \cos B} \sin\left\{B\left(\frac{x}{L} - 1\right)\right\} \cos(\omega t) \quad (5.5)$$

$$\eta = \frac{a}{\cos B} \cos\left\{B\left(\frac{x}{L} - 1\right)\right\} \sin(\omega t) \quad (5.6)$$

where

$c = \sqrt{gh}$ is the wave speed and

$B = \omega L/c$

The hydrodynamic model was run using four elements of equal length.

The following values were used in the model

No. of elements = 4;

No. of nodes = 5;

$L = 200$ m;

$h = 4$ m;

$T = 600$ sec;

$a = 0.1$ m;

$g = 9.81$ m/sec²;

$\Delta x = 50$ m;

$\Delta t = 5$ sec.

A relatively small amplitude, $a/h = 0.025$, is chosen to minimize the non-linear effects. The problem was solved without coupling to the salinity submodel. The solution is started using initial conditions calculated from equations (5.6) and (5.7). The time history of the computed surface elevation at $x = L$ is plotted together with the analytical solution as shown in Figure 5.1. The time history of the computed velocity at $x = 0$ is shown in Figure 5.2. In general, the computed solutions agree very well with the exact analytical solutions.

The size of the integration time step used was 5 seconds. The critical time step, Δt_{cr} , determined from the Courant condition is

$$\Delta t_{cr} < \frac{\Delta x}{\sqrt{2gh}} = \frac{50}{2 \times 9.81 \times 4} = 5.6 \text{ seconds}$$

The model was also run using time step of 9 seconds without any stability problems. Time steps larger than this were not tested, however.

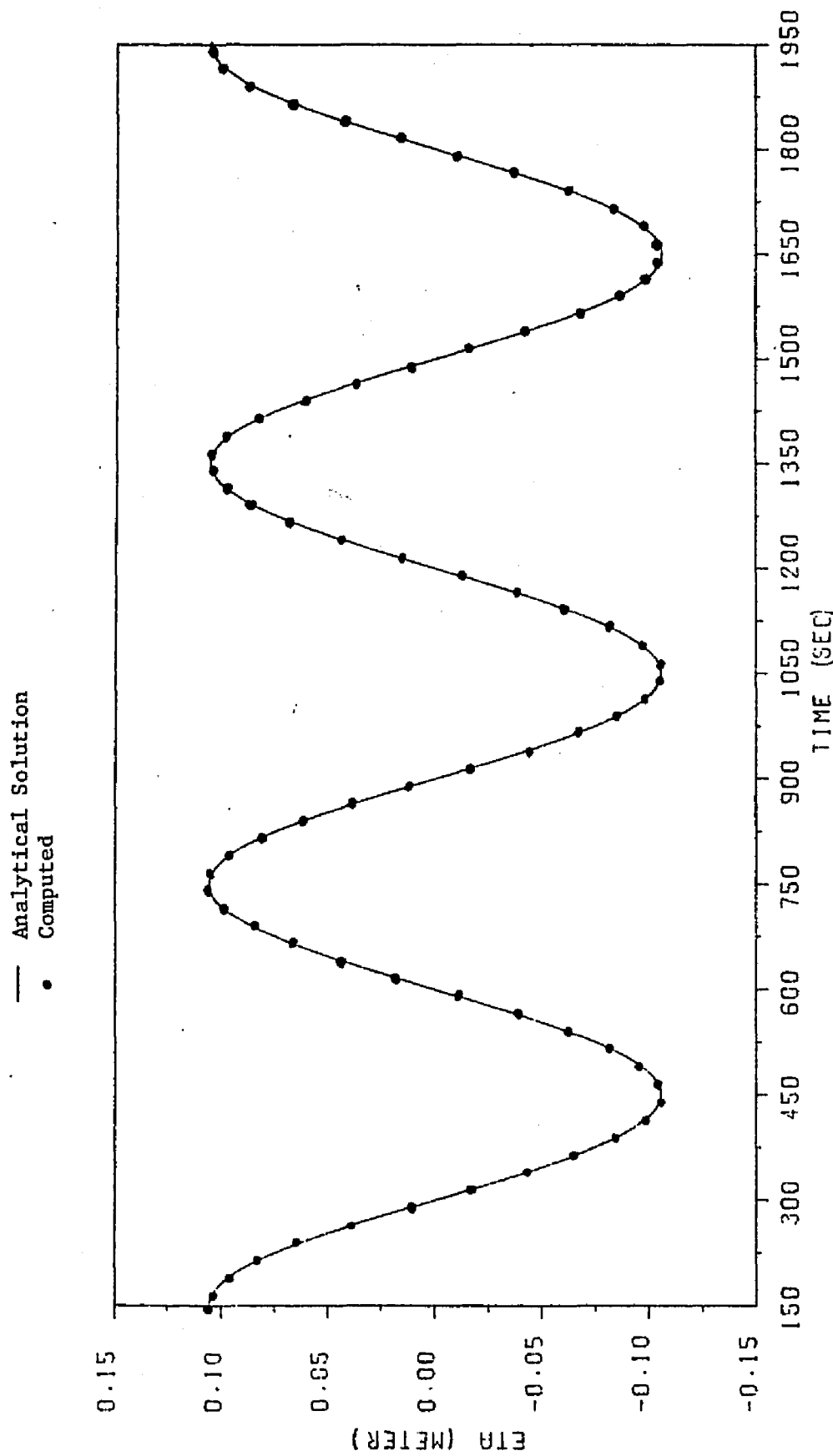


FIG 5.1 COMPARISON OF SURFACE ELEVATION AT X = L.

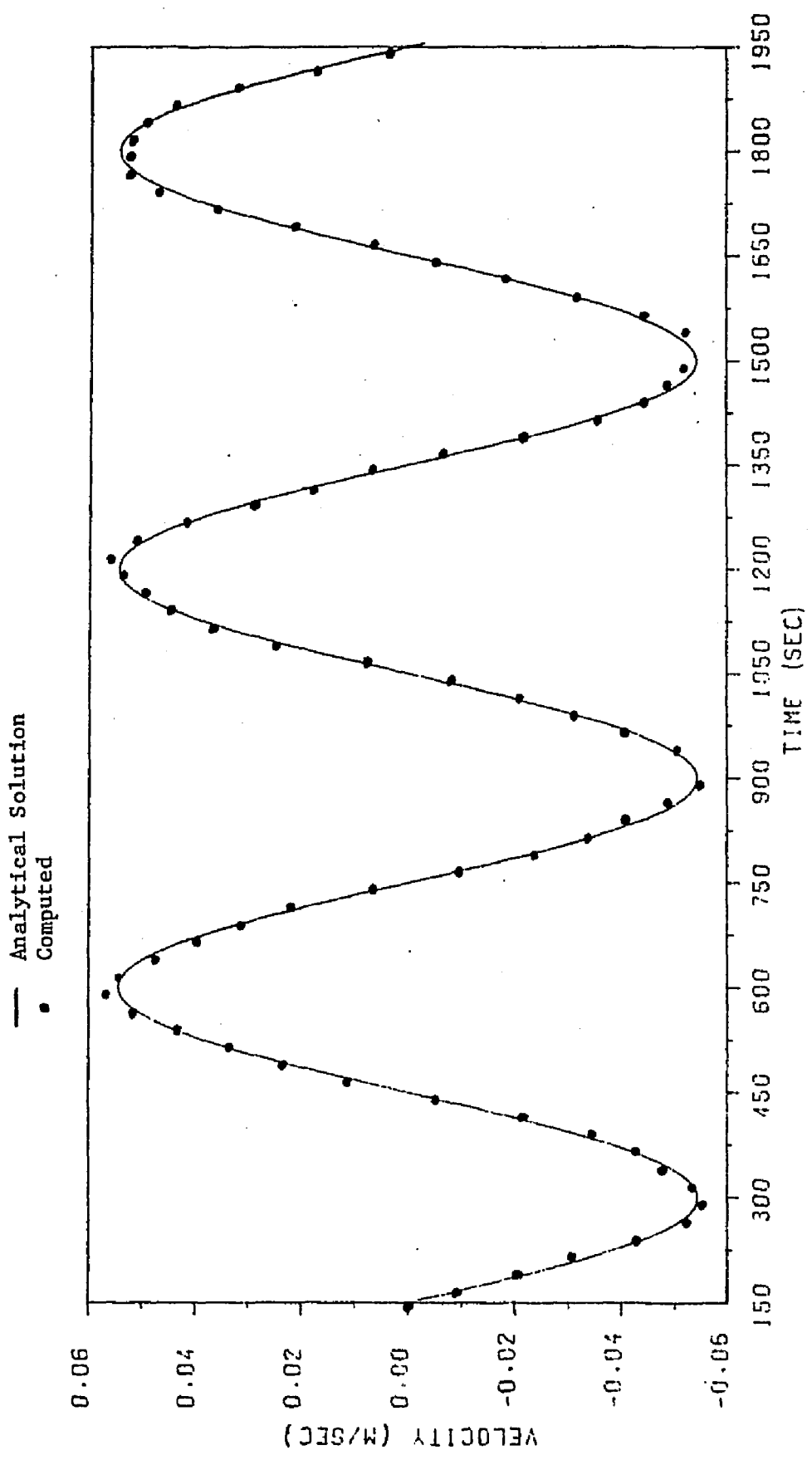


FIG 5.2 COMPARISON OF VELOCITY AT X = 0.

5.2 Dispersion in a Rectangular Channel

In the second example, the water quality model is used to calculate the dispersion of a conservative substance in a rectangular channel with a steady and uniform flow. The upstream boundary concentration is held constant. The concentration at the downstream boundary is specified as zero. The mathematical formulation of this problem is

$$A \frac{\partial C}{\partial t} + Q \frac{\partial C}{\partial x} = \frac{\partial}{\partial x} A E \frac{\partial C}{\partial x} - kC \quad (5.7)$$

$$\text{for } 0 < x < \infty$$

and the boundary conditions are

$$C = C_0 \quad \text{at } x = 0 \quad (5.8a)$$

$$C = 0 \quad \text{at } x = \infty \quad (5.8b)$$

The analytical solution of this problem is

$$C = 0.5C_0 e^{\chi U} \left(e^{\chi \Omega} \operatorname{erfc} \left(\frac{x + \Omega t}{\sqrt{4Et}} \right) + e^{-\chi \Omega} \operatorname{erfc} \left(\frac{x - \Omega t}{\sqrt{4Et}} \right) \right) \quad (5.9)$$

where

k = decay rate,

erfc = the complementary error function,

$$\Omega = \sqrt{U^2 + 4kE} \quad \text{and}$$

$$\chi = x/2E.$$

The model was run using 40 elements of equal length. The following values were used in the computer simulation

No. of elements = 40;

No. of nodes = 41;
L = 400 m;
A = 1 m²;
C = 1 mg/l at x = 0 m;
C = 0 at x = 400 m;
E = 3,600 m²/hr;
k = 0 hr⁻¹.
U = 360 m/hr;
 Δx = 10 m;
 Δt = 9 and 72 seconds.

The initial conditions are set to zero everywhere in the channel and the model is run from time = 0 to time = 1.5 hour. The computed concentrations at various times plotted together with the analytical solutions are shown in Figure 5.3. Generally the computed solutions agree very well with the analytical solutions. Note that after time = 1 hour, the computed solutions at the downstream end begin to diverge from the analytical solutions. This is due to the difference in the downstream boundary conditions between the analytical solution and the model, namely; the analytical solution is for an infinitely long channel, but the computed solution is for a channel with finite length. When the concentration plume reaches the downstream end, the numerical solution is affected by the downstream boundary conditions which is specified equal to zero in this case.

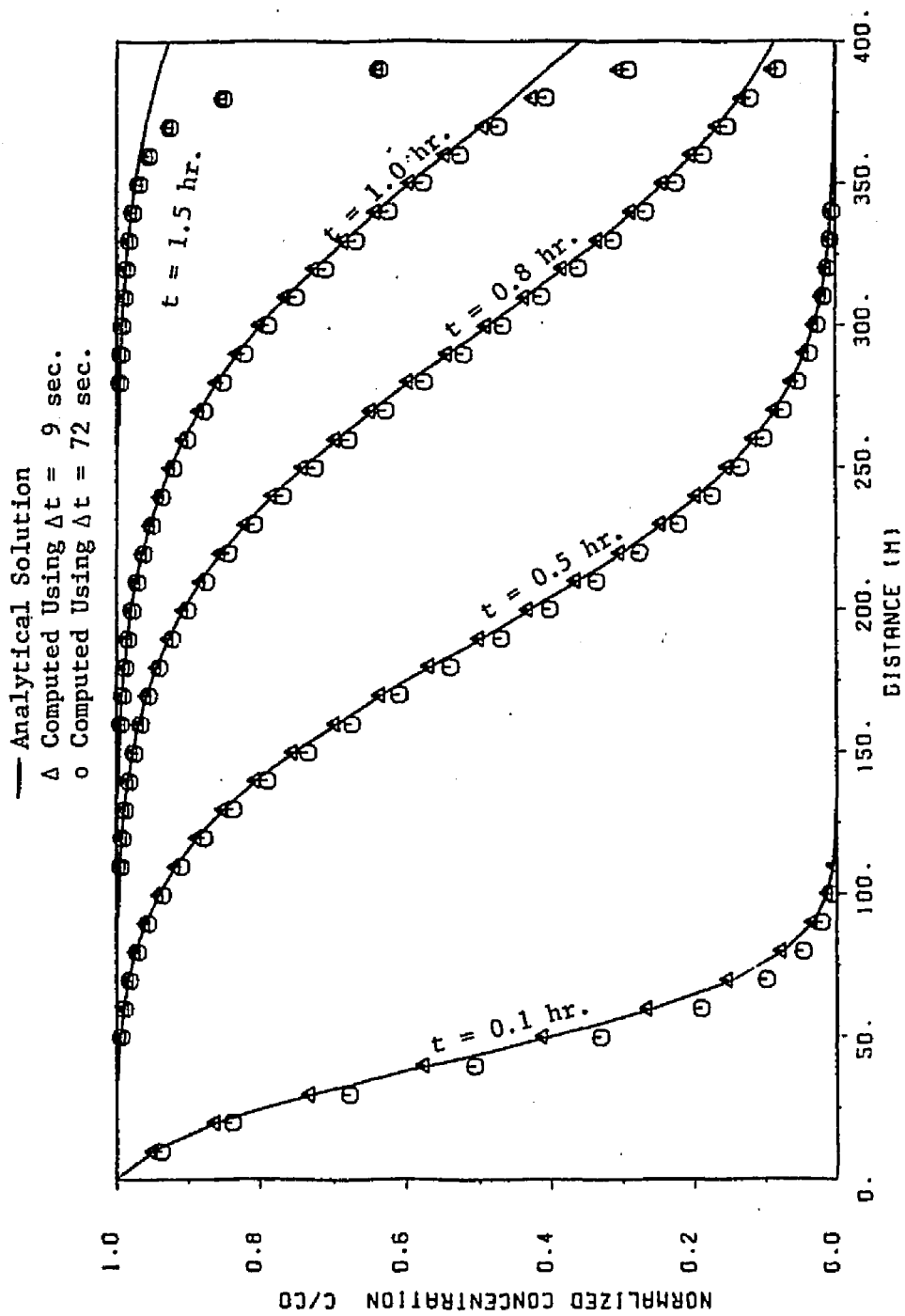


FIGURE 5.3 COMPARISON OF FINITE ELEMENT SOLUTIONS TO ANALYTICAL SOLUTIONS. WITH NO DECAY RATE.

5.3 Dispersion in a Rectangular Channel With Decay

This example is the same as the one in section 5.2 except that a non-conservative substance with a first order decay rate is used. The analytical solution of this problem is the same as in equation (5.9).

Using decay rate $k=0.5$ per hour, the computed results along the channel at various times together with the analytical solutions are plotted in Figure 5.4. In general the agreement between the analytical solution and the model is very good.

In the last two examples above, the size of the critical time step according to equation (4.15) is

$$\Delta t < \frac{100}{2 \times 3600} \times 3600 = 50 \text{ seconds}$$

In the test runs, stability is maintained for time steps up to 72 seconds, which shows the excellent stability of the trapezoidal integration scheme. Still larger time steps are thought possible but they were not tested.

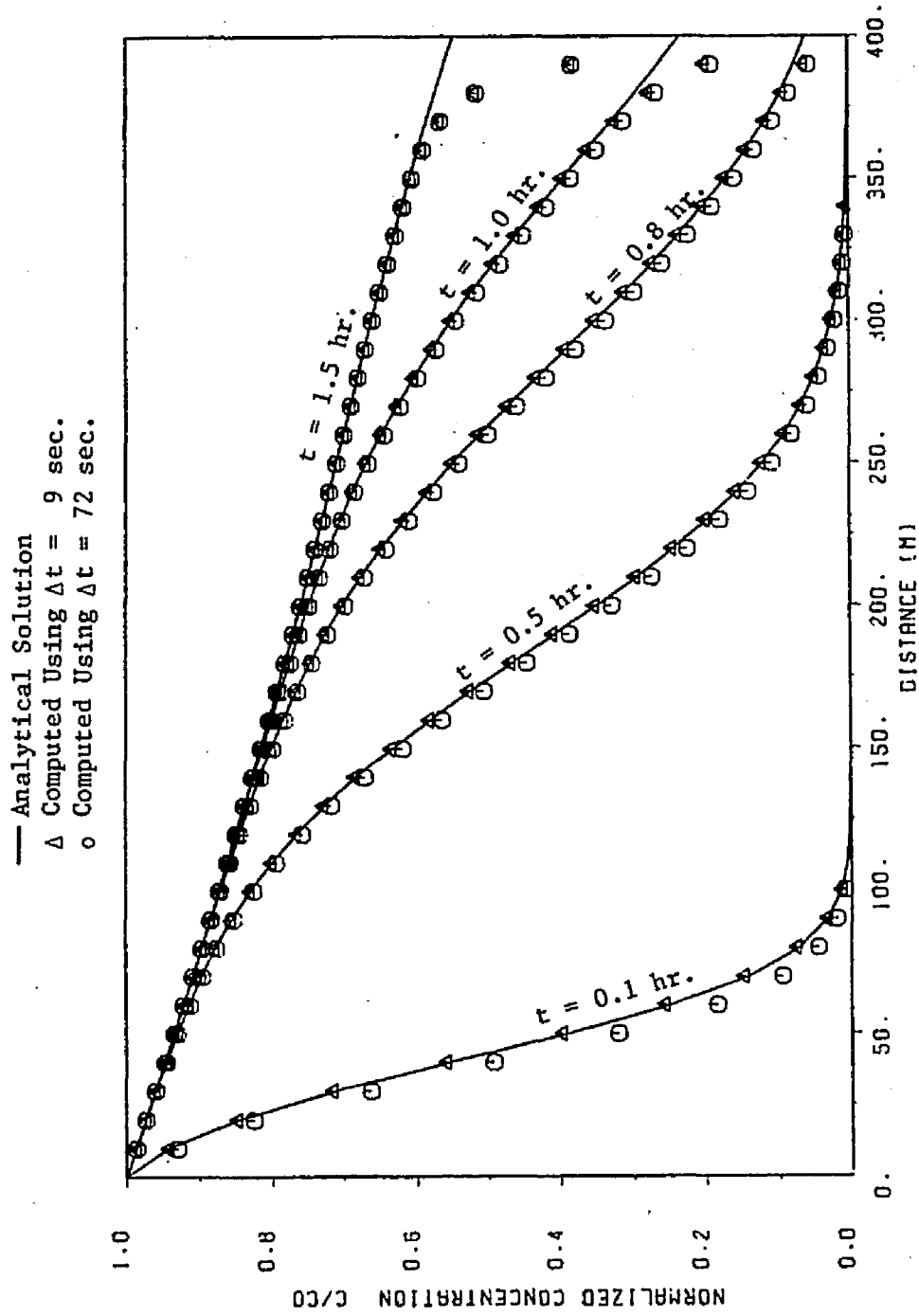


FIGURE 5.4 COMPARISON OF FINITE ELEMENT SOLUTIONS TO ANALYTICAL SOLUTIONS.
DECAY RATE = 0.5 PER HOUR.

6 APPLICATION TO THE JAMES RIVER

To demonstrate the capability of the model, further verification using real world cases is necessary. This step is important in establishing the applicability of the model. However, the natural systems are very complex, therefore the agreement between the model and the field data cannot be expected to be perfect. When judging a model of this nature, the quality of the input data and the field data to which the model is compared should always be considered. The ultimate purpose of a model is not to obtain a perfect fit of the field data, but rather to get the model to reproduce the key features of the system, such as the extent of the salinity intrusion or the general trends of water quality concentrations. When the agreement between the calculated results and field data is satisfactory, the model is said to be calibrated. It can then be used to calculate the response of the estuary to alternative waste discharge levels.

In this chapter, the application of the hydrodynamic and water quality models to the James River in Virginia is described. The reach of the estuary to be modeled extends from the river mouth to Richmond. This reach of river is tidal and is approximately 160 kilometers long. The river has a maintained channel up to Richmond, with a minimum mid-channel depth of approximately 8 meters. Cross-sectional average depth of the river varies from 3 to 9 meters. The top width varies from approximately 3000 meters at the mouth to 300 meters at Richmond. The

average tidal range varies from 0.76 meter near the mouth at Sewell's Point to 0.58 meter near the Chickahominy (km 80) to 0.98 meter at Richmond.

Average freshwater inflow at Richmond is 200 cubic meters per second. In 1971 the fresh water inflow varied from 2500 cubic meters per second during the spring flood to 50 cubic meters per second during summer. The major tributaries to the James River are the Appomatox River, the Chickahominy River and the Nansemond River. Figure 6.1 shows the freshwater inflows used in the model from the period March to October 1971. In the model, flows below the fall line are distributed into each element proportional to the drainage area the element subtends. The James River estuary is classified as partially-mixed. Near the mouth, a relationship between stratification-destratification and the spring-neap cycle has been observed by Haas (1977). Therefore strictly speaking, the assumption of one-dimensionality is not valid at the times when stratification occurs. The average salinity at the mouth is 22 ppt for year 1971. Normally salt intrudes up to the vicinity of Jamestown Island (km 68), but during periods of low flow the intrusion may go up as far as Hopewell (km 120); during periods of high fresh water inflow the intrusion can be pushed down to Newport News (km 25).

The models were used to make an 8 month simulation starting from March 1st. to Oct 31st. of 1971. An attempt was made to calibrate the models using 1971 field data collected for the Chesapeake Bay Nutrient Input Study, EPA (1972). The time steps used were 6 and 60 minutes for the hydrodynamic and the water quality models respectively. The procedure was to run the hydrodynamic model coupled with salinity first until calibration was achieved. The resulting tidal elevations and

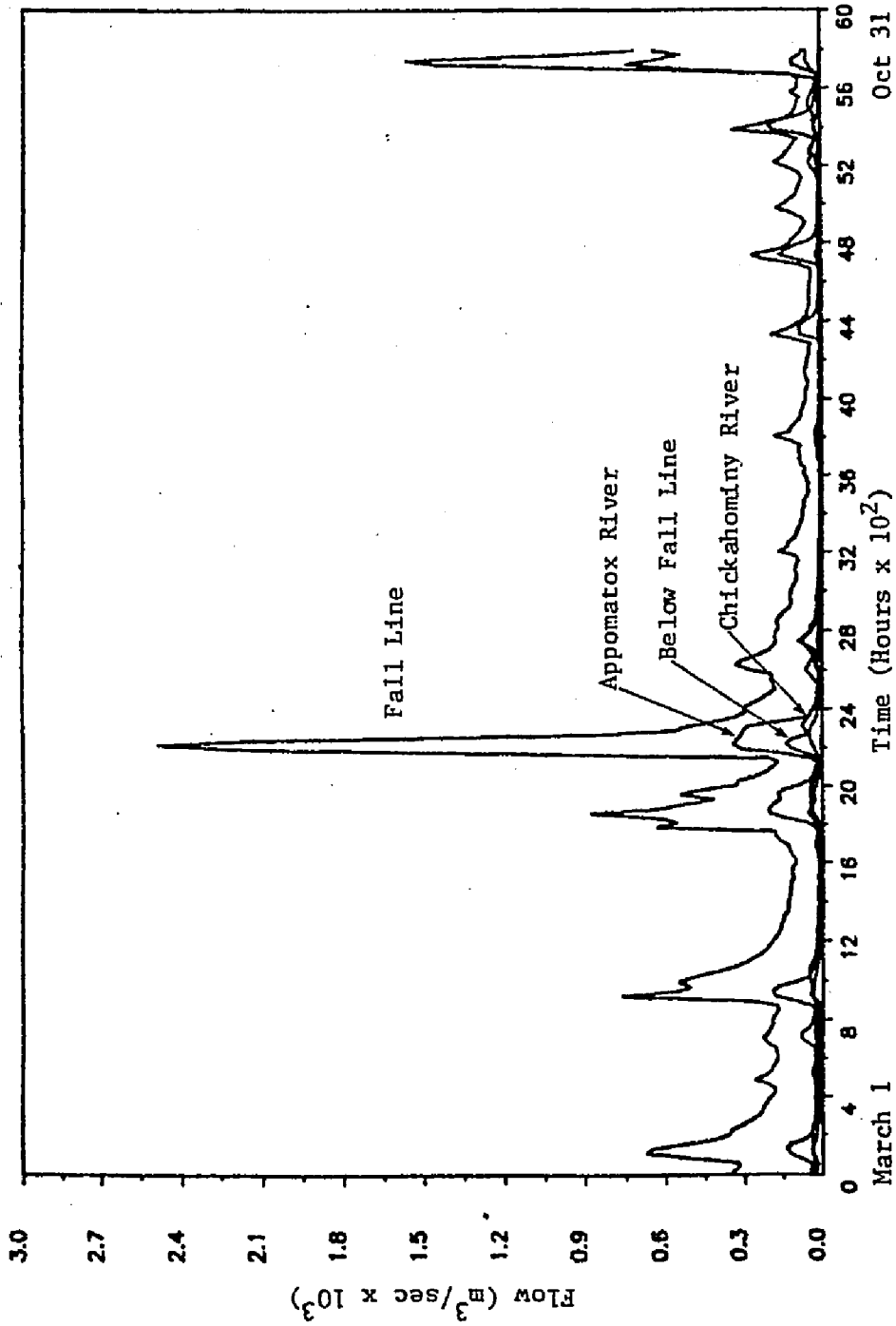


Figure 6.1 Fresh water inflows to the James River model.

current velocities were then stored on magnetic disks to be used as inputs to the water quality model.

6.1 Schematization

The estuary is divided into 40 elements and 41 nodes as shown in Figure 6.2. The lengths of the elements range from 2.4 to 6 kilometers. This spacing is chosen to give an integration time step of 6 minutes for the hydrodynamic model (124 steps per tidal cycle). The geometric properties required at each node include the top width, the cross-sectional area, mean water depth and side slopes. Figure 6.3 shows a typical schematic cross-section of the river. The cross-sectional area is divided into two sections, namely the conveyance area and the storage area, A_c and A_s respectively. It is assumed that flow is confined to the conveyance area only and the shallow areas on the sides contribute little to the longitudinal flow but they provide water storage. This concept has been previously used by several authors such as Daily and Harleman (1972). The purpose is to try to approximate the non-uniform velocity distribution in the cross-section. However, the determination of shallow areas in a cross-section is somewhat arbitrary and requires some trial and error. In the James River model, areas with water depth less than 0.8 meter are assumed to be shallow.

At each transect, the cross-sectional area comprised of the mean cross-sectional area and the fluctuation area due to tide. The mean cross-sectional areas are measured from cross-sectional bathymetric profiles (unpublished VIMS data) using a planimeter. The conveyance and storage widths are also measured from the cross-sectional profiles.

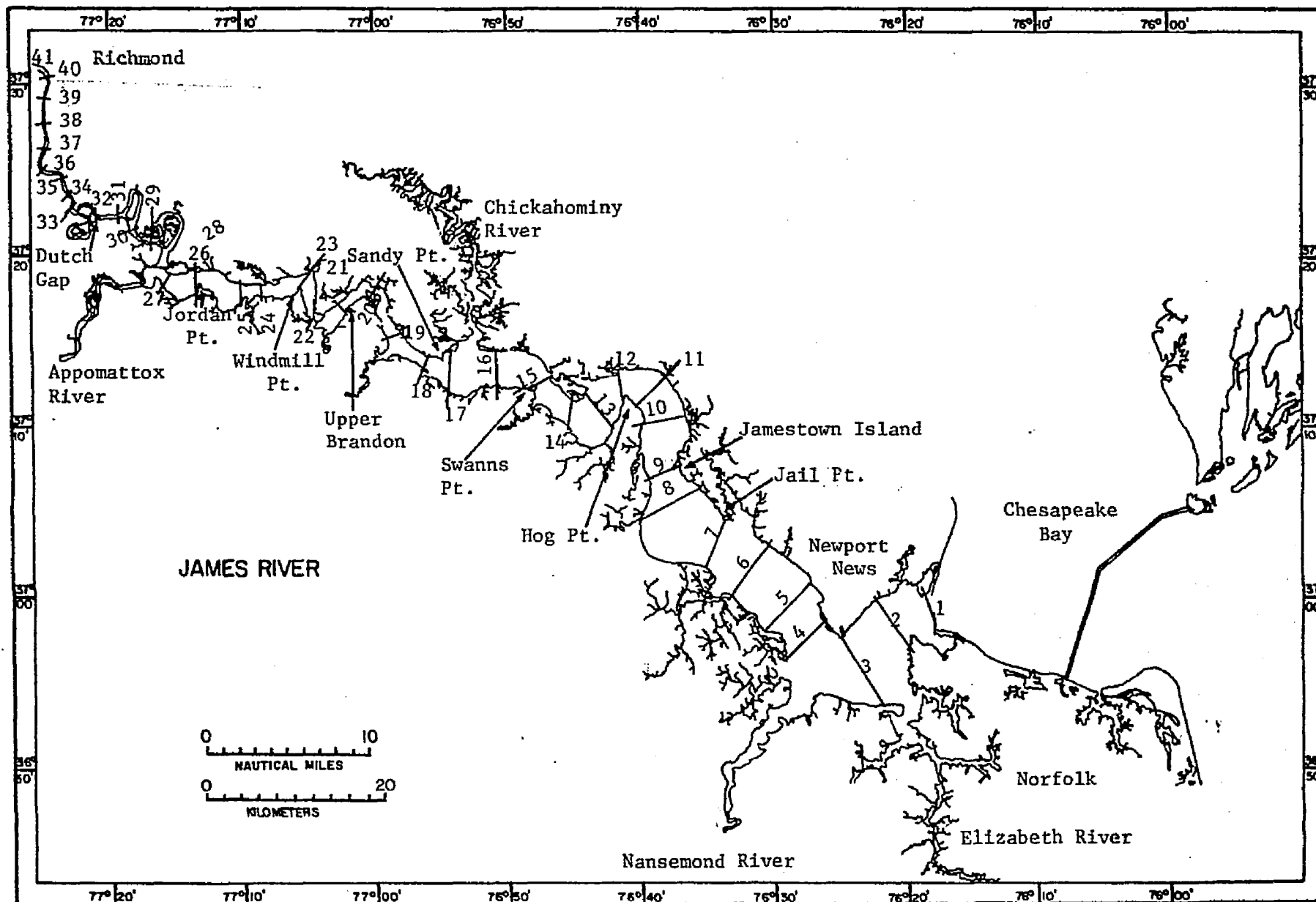


Figure 6.2 Model segments for the James River estuary.

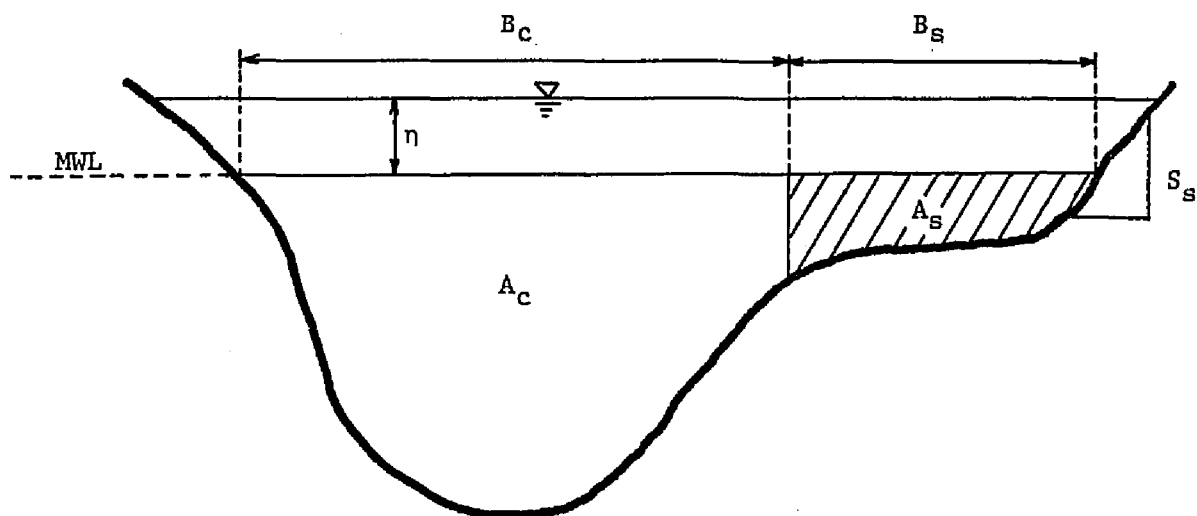


Figure 6.3 Schematic cross-section of the river.

At each integration time step the total top width, B , is calculated by

$$B = (B_c + B_s) + 2\eta S_s \quad (6.1)$$

Similarly, the total cross-sectional area at each time step is given by

$$A = (A_c + A_s) + \eta(B_c + B_s + B)/2 \quad (6.2)$$

where

η = the instantaneous water surface above mean water level and

S_s = the average side slope of the channel.

The specification of side slopes of the channel is necessary only when the tidal height is expected to exceed normal flood levels, otherwise the sides may be assumed vertical ($S_s = 0$).

6.2 Initial and Boundary Conditions

The tidal elevation imposed at the mouth is calculated by the equation

$$\eta = \sum_{i=1}^3 a_i \cos(\omega_i t + \theta_i) \quad (6.3)$$

where

a_i = the amplitude of the i th constituent,

ω_i = frequency,

θ_i = phase and

t = time.

The values of amplitude, frequency and phase of the three constituents used are as follows

i	Amplitude (m)	Frequency (Radians per hour)	Phase (Radians)
1	0.3430	0.5059	6.2480
2	0.0786	0.4964	0.2600
3	0.0671	0.5236	5.0310

These three constituents correspond to the principal lunar semi diurnal (M_2), larger lunar elliptic (N_2), and principal solar semidiurnal (S_2) respectively. These values are obtained from National

Ocean Survey for year 1971 (unpublished data).

At the downstream boundary, salinity is held constant during flood tide, during ebb tide the dispersive flux $AE\partial C/\partial x$ is specified. This term is calculated in the model based on the salinity values from the previous integration time step.

Initial conditions are determined by linearly interpolating the available field data along the entire length of the river.

The dispersion coefficient is approximated by

$$E(x) = e(x)UR^{5/6} \quad (6.4)$$

U = the instantaneous velocity,

R = the hydraulic radius and

e = is a factor to be adjusted during calibration.

The values of e used for James River vary spatially from 260 at the mouth to 130 at Richmond. This corresponds to the maximum dispersion coefficient of 30 to 15 sq.m/sec respectively.

The Manning coefficient varies spatially and increases gradually from 0.026 at the mouth to 0.034 at Richmond, where the channel is narrow.

During the simulation, node to node oscillations of tidal elevations and velocities are observed at a few upstream nodes. The effects of this are minor, because the oscillations are about the solution and do not become unbounded. They are believed to be caused by the coarse grid spacings at the upstream end. Although it would be possible to reduce the oscillations by using smaller grid sizes,

decreasing the grid size would mean that a smaller integration time step would be required. Because the oscillations are confined to a few upstream nodes, a compromise is made by smoothing the results at each time step using a smoothing operator as described by Wang (1977)

$$U_i^S = bU_i + (1 - b) \frac{\sum U_j \ell_j}{\sum \ell_j} \quad (6.5)$$

where

U_i = velocity at node i ,

U_i^S = the smoothed value at node i ,

U_j = velocity at the neighbouring node j ($j = 1, 2$),

ℓ_j = distance to the neighbouring node j and

$b = 0.5$ is an arbitrary weighting factor.

The computed results are presented as time history plots of tidal elevation, current velocity and salinity at various nodal points. In the figures to follow, the x-axis represents time, with output plotted at every two hours and time zero being March 1, 1971. The y-axis represents the tidal elevations, current velocities or salinity. Due to the volume of the model output and in order to present the entire eight month of simulation on one plot, the time scales in the plots are not fine enough to resolve the diurnal fluctuations. The plots are seen as a dark band instead. The width of the band is actually the diurnal variations.

The computed and observed time history of tidal elevations at Sandy Point, Jordan Point, Dutch Gap and Richmond are shown in Figures 6.4 to 6.7 respectively. The comparison between the computed and the observed

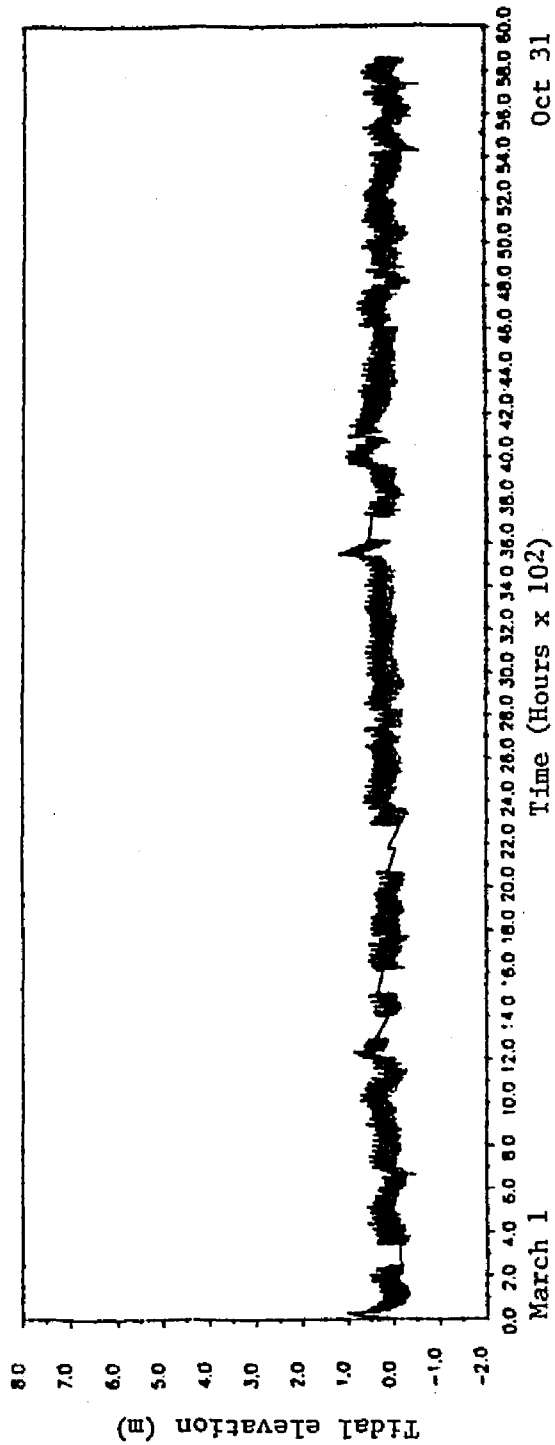


Figure 6.4a Observed tidal elevation at Sandy Point.

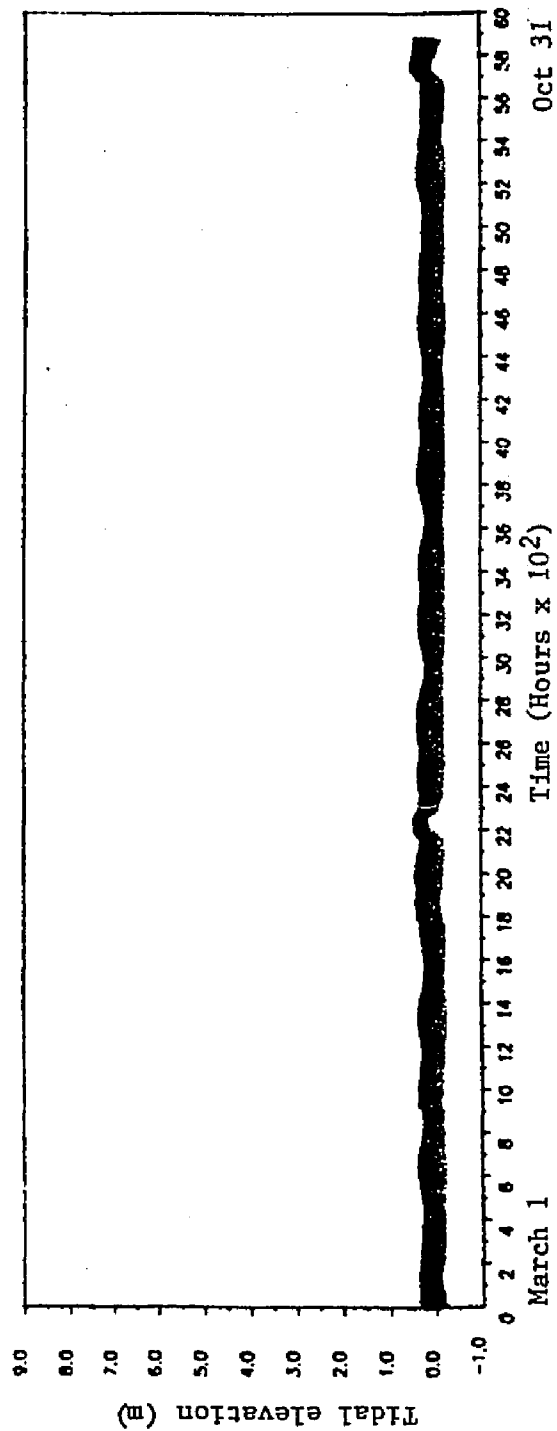


Figure 6.4b Computed tidal elevation at node 18 (Sandy Point).

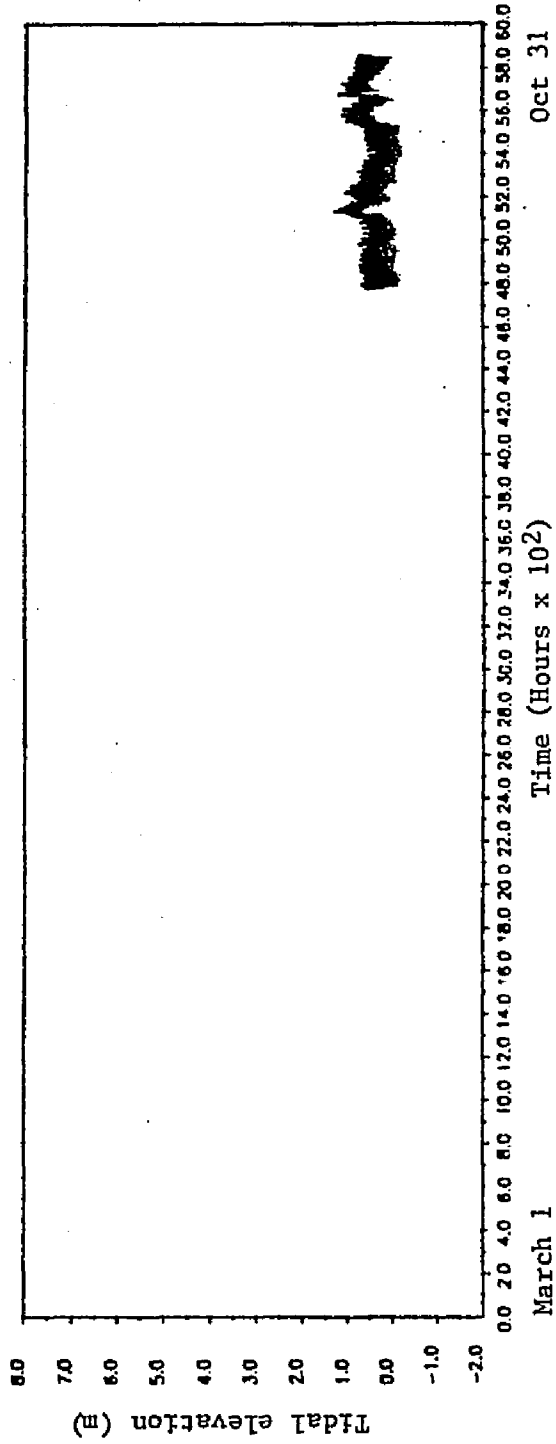


Figure 6.5a Observed tidal elevation at Jordan Point.

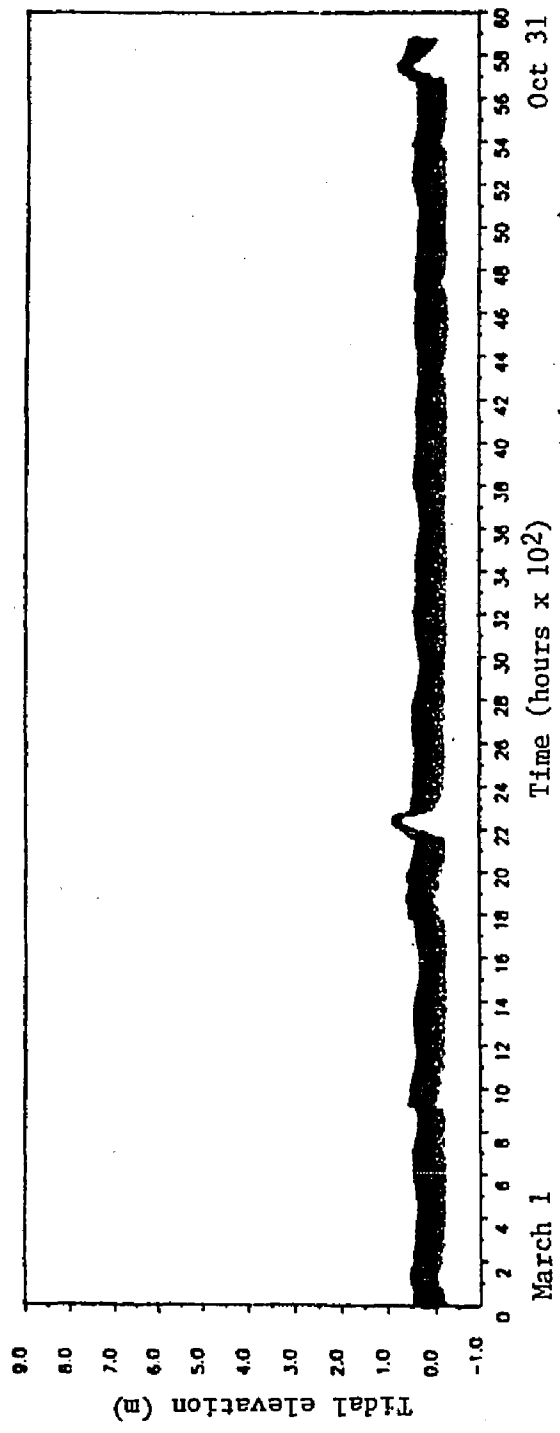


Figure 6.5b Computed tidal elevation at node 26 (Jordan Point).

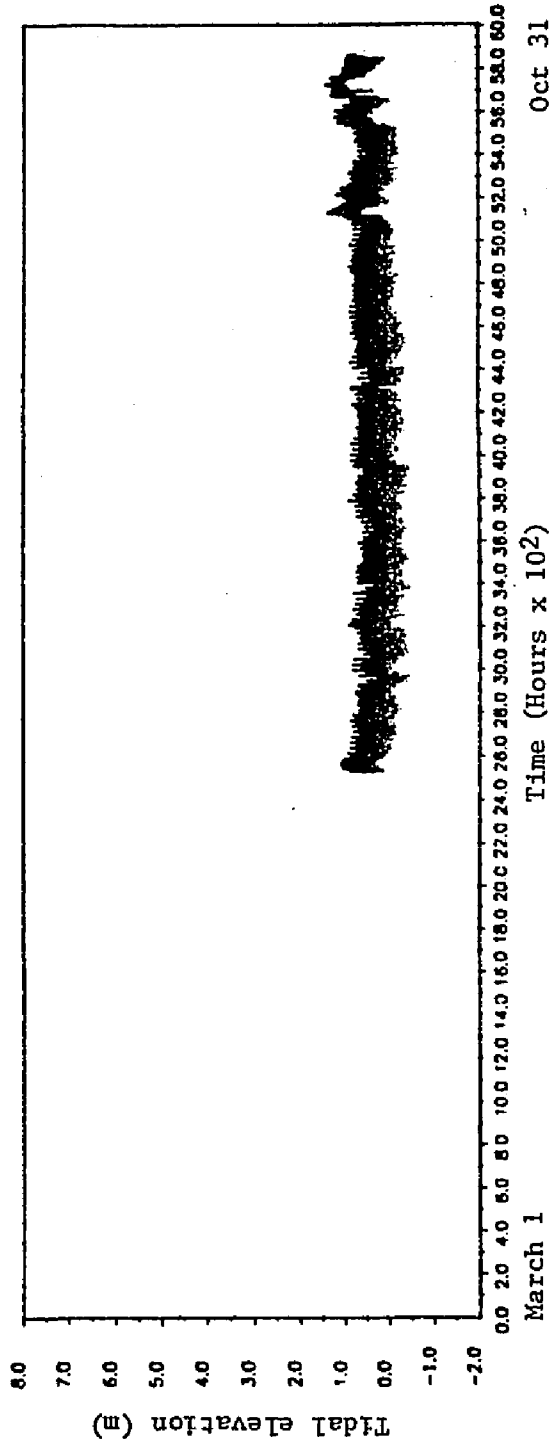


Figure 6.6a Observed tidal elevation at Dutch Gap.

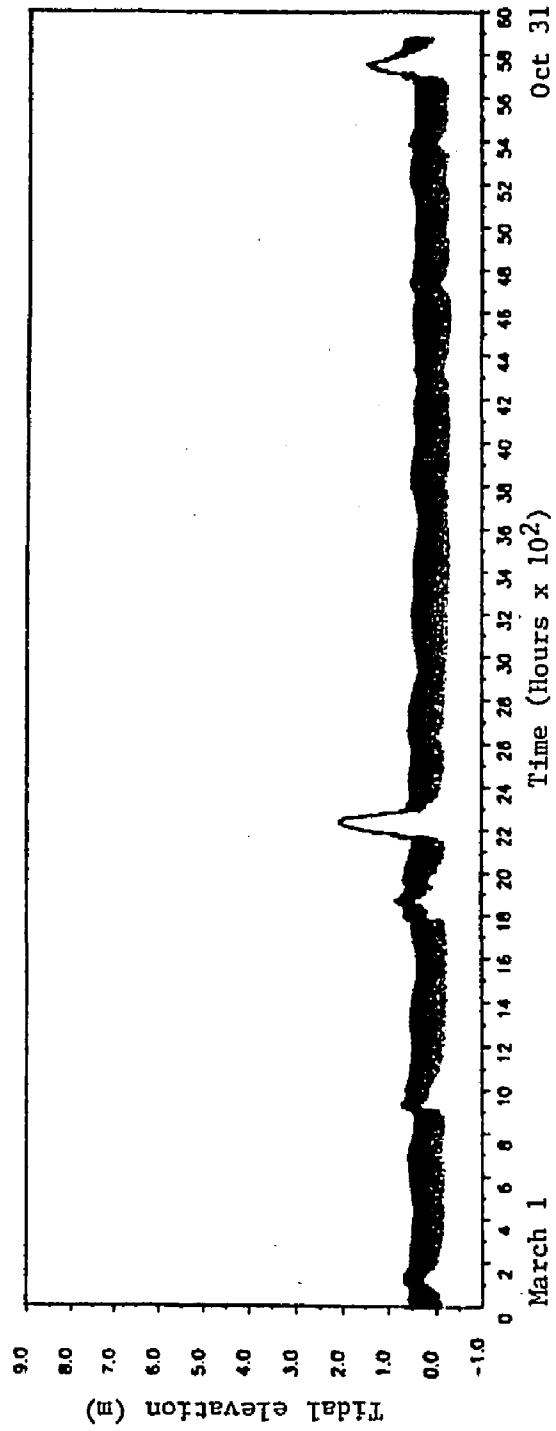


Figure 6.6b Computed tidal elevation at node 31 (Dutch Gap).

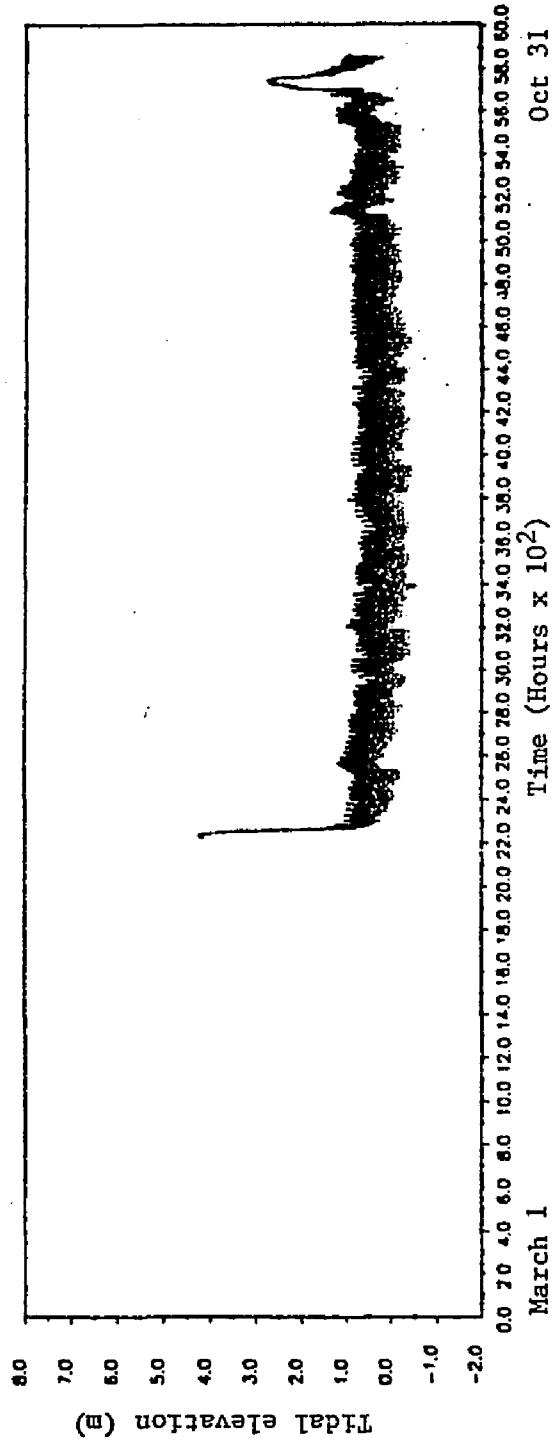


Figure 6.7a Observed tidal elevation at Richmond.

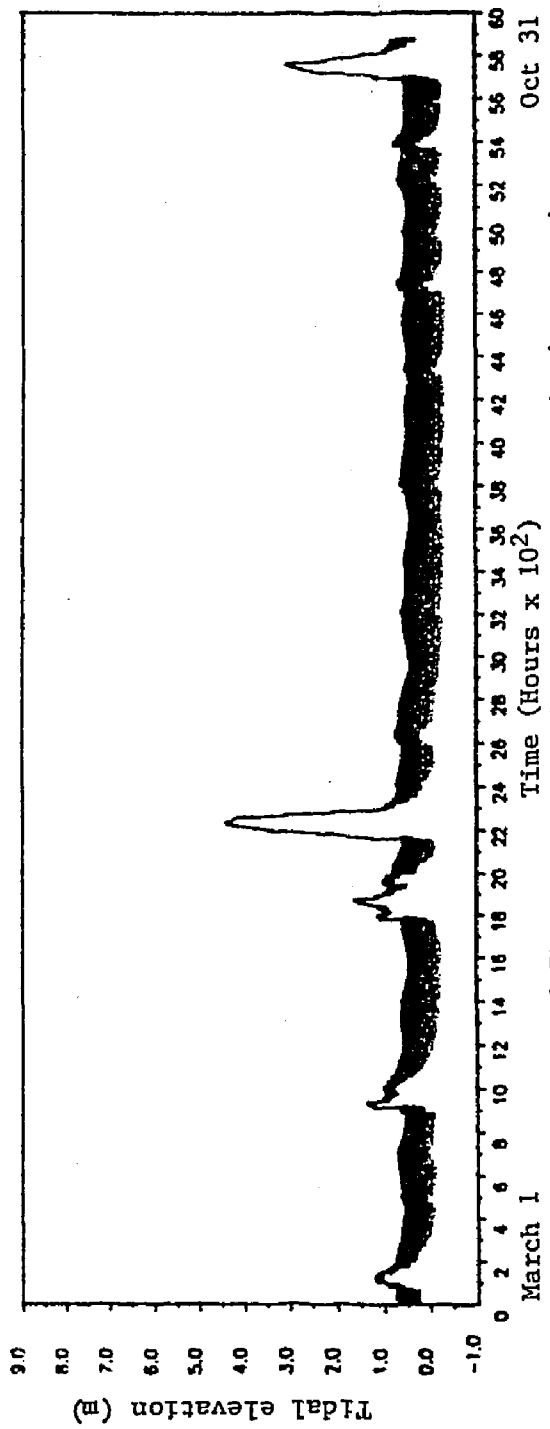


Figure 6.7b Computed tidal elevation at node 40 (Richmond).

tidal elevations are quite good in general. The observed data tend to have more fluctuations and sometimes have a larger diurnal tidal range. Continuous current records are not available, but comparison between computed currents and some field data points shows that the computed currents have the correct order of magnitude in general. The computed current at the same stations as the tidal elevation plots are shown in Figures 6.8 to 6.11 respectively.

Figures 6.12 to 6.17 show the computed and observed time history of salinity at the river mouth, Newport News, Jail Point, Hog Point, Swann's Point and Sandy Point respectively. The observed values are plotted as the vertical maximum, average and minimum respectively. The comparison between the computed results and observed salinity is very good. Note that Figure 6.12 is the plot of salinity at node 1, which is the downstream boundary node of the model. The upper limit of 22 ppt is the fixed boundary concentration specified during flood tide. During ebb tide, the dispersive flux is specified. This allows a more realistic specification of the downstream boundary conditions.

Figure 6.13 is the computed salinity at node 4 (near Newport News). During the spring runoffs, the computed salinity goes all the way down to zero. This is in general agreement with field observations. Figure 6.17 shows the computed salinity at node 18 (near Sandy Point). Salt barely intrudes up to this point even during the summer low flow months, so this is near the upper limit of salt intrusion in 1971.

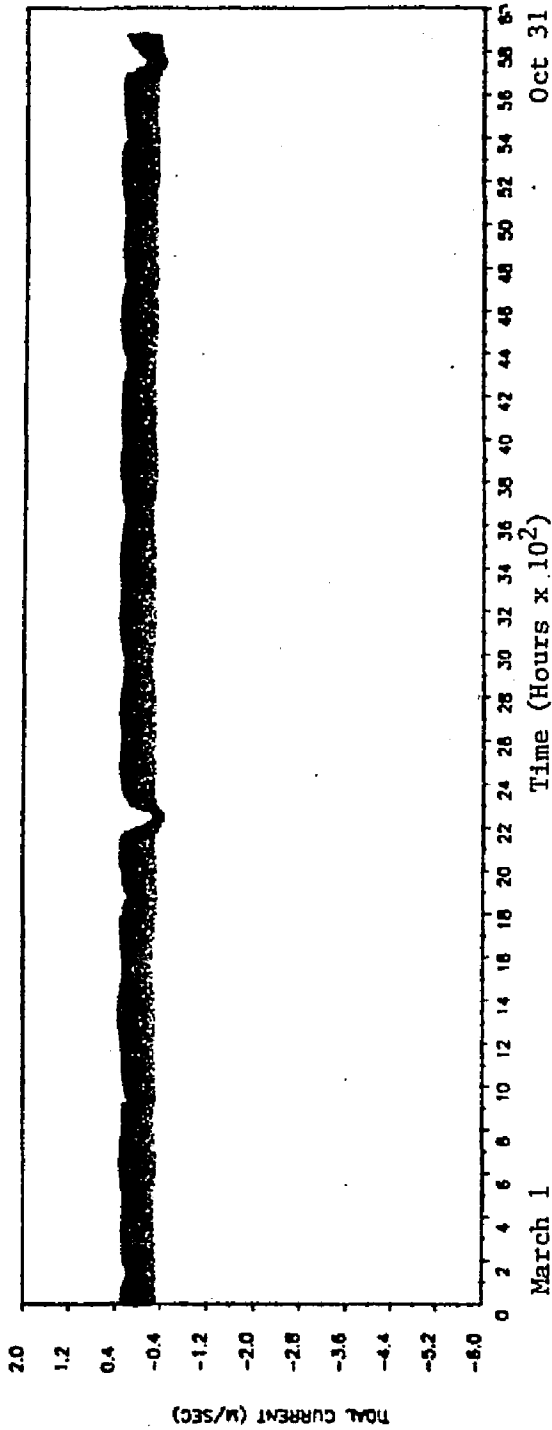


Figure 6.8 Computed current at node 18 (Sandy Point).

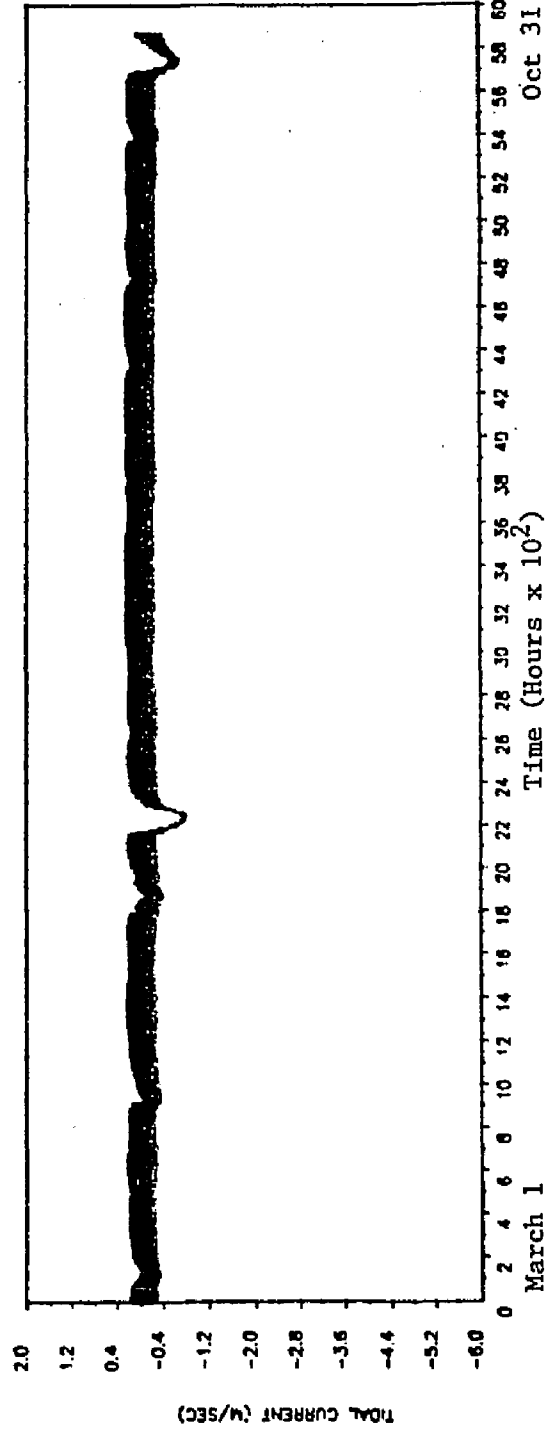


Figure 6.9 Computed current at node 26 (Jordan Point).

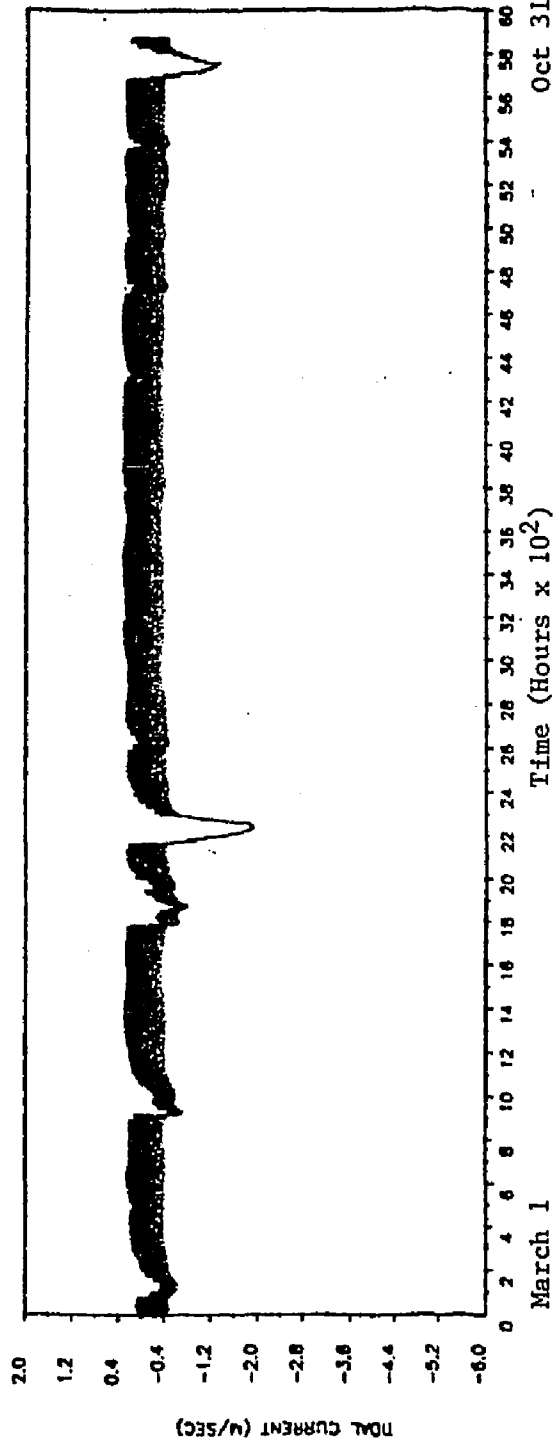


Figure 6.10 Computed current at node 31 (Dutch Gap).

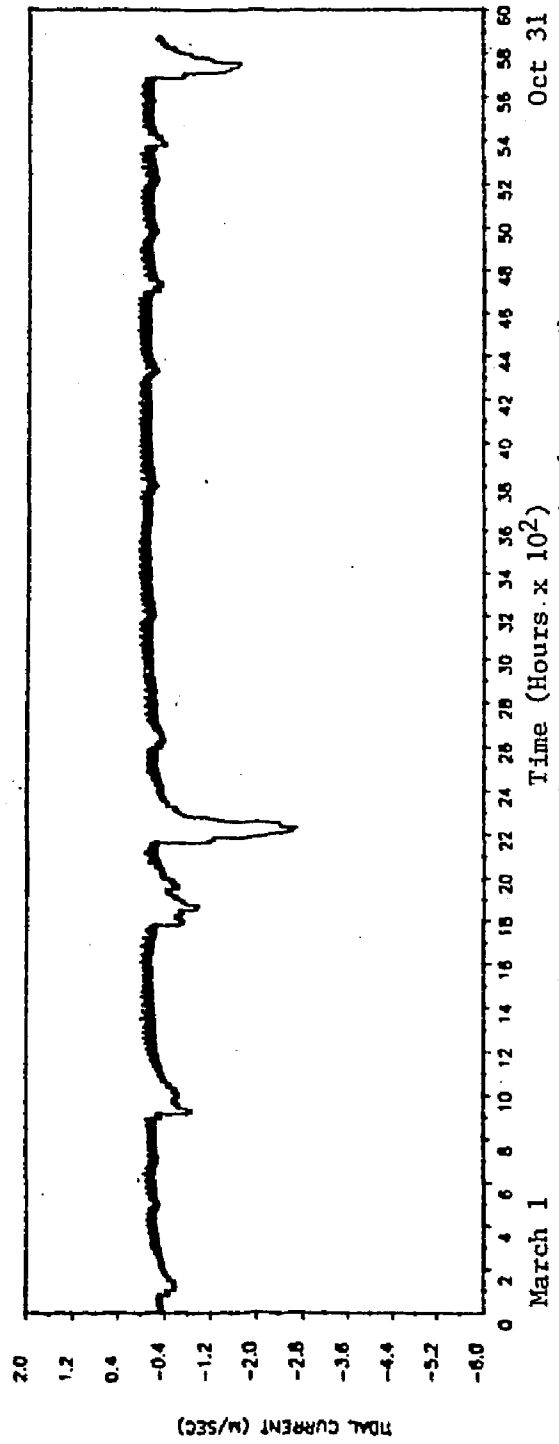


Figure 6.11 Computed current at node 40 (Richmond).

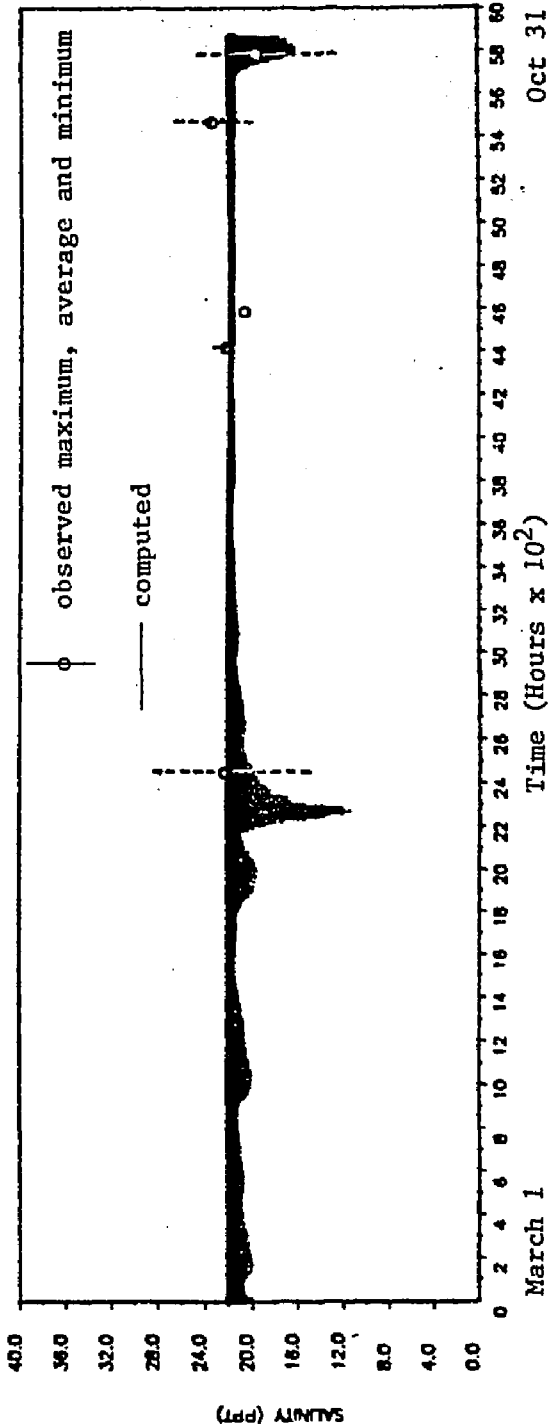


Figure 6.12 Computed and observed salinity at node 1 (River mouth).

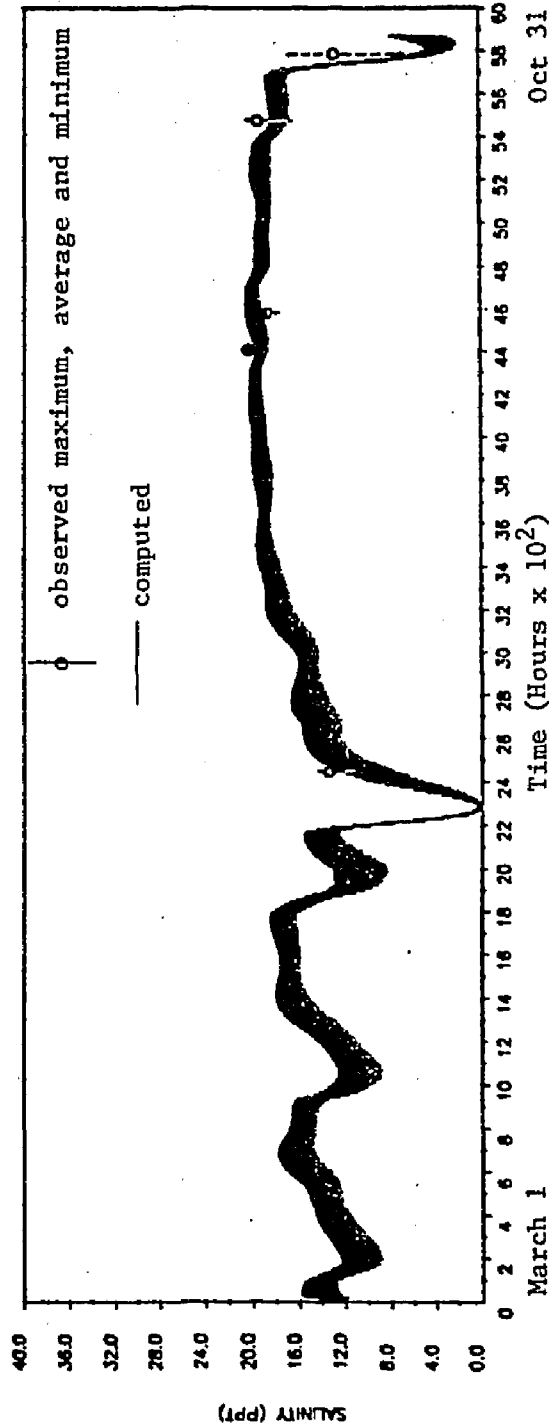


Figure 6.13 Computed and observed salinity at node 4 (Newport News).

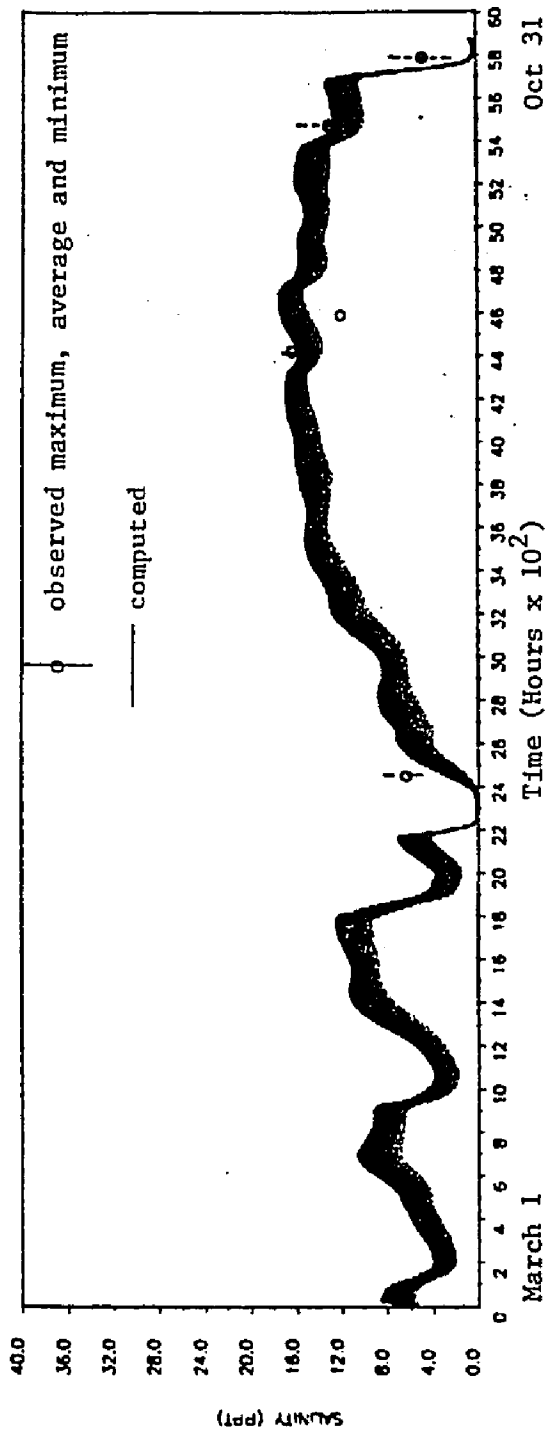


Figure 6.14 Computed and observed salinity at node 7 (Jail Point).

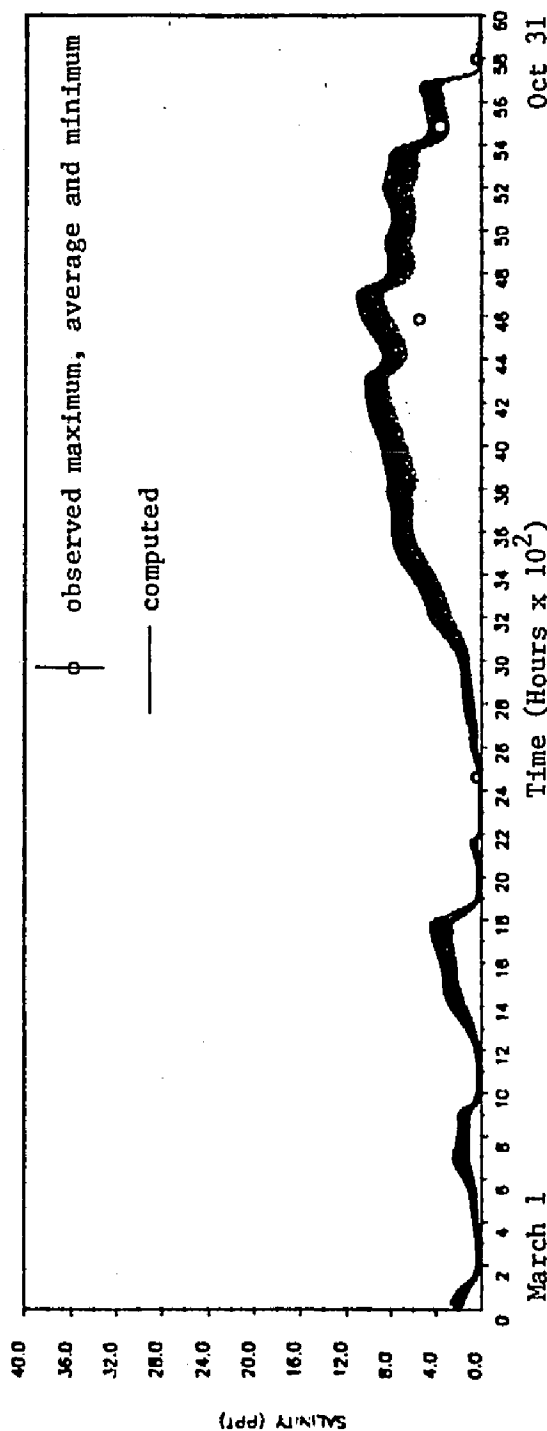


Figure 6.15 Computed and observed salinity at node 11 (Hog Point).

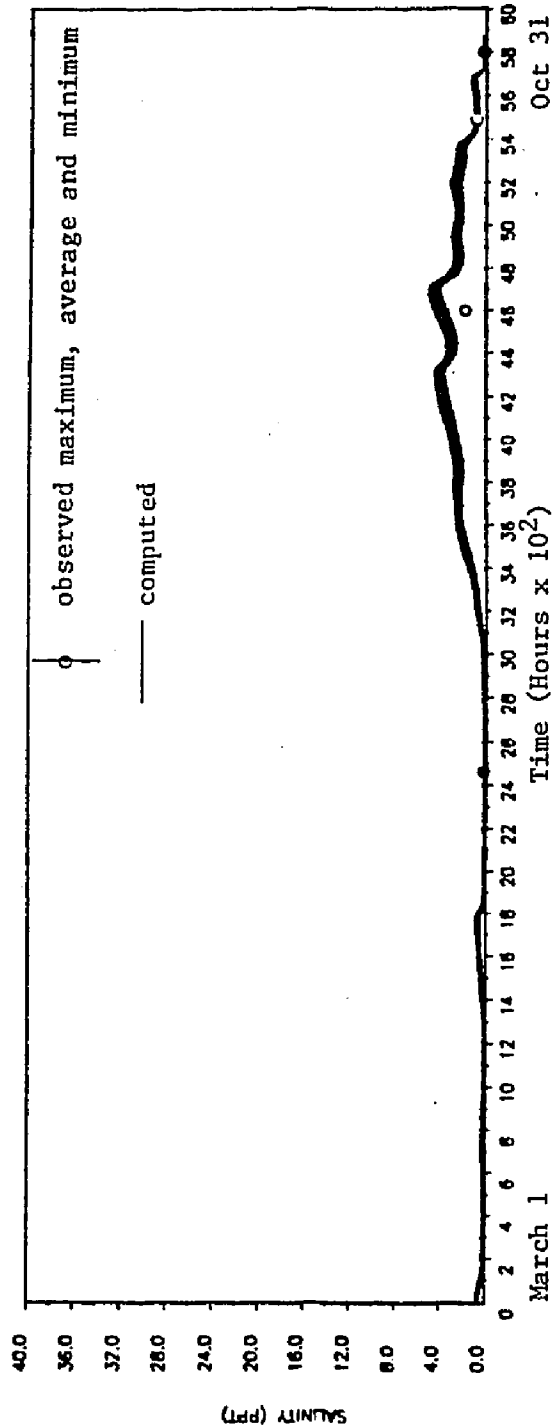


Figure 6.16 Computed and observed salinity at node 15 (Swanns Point).

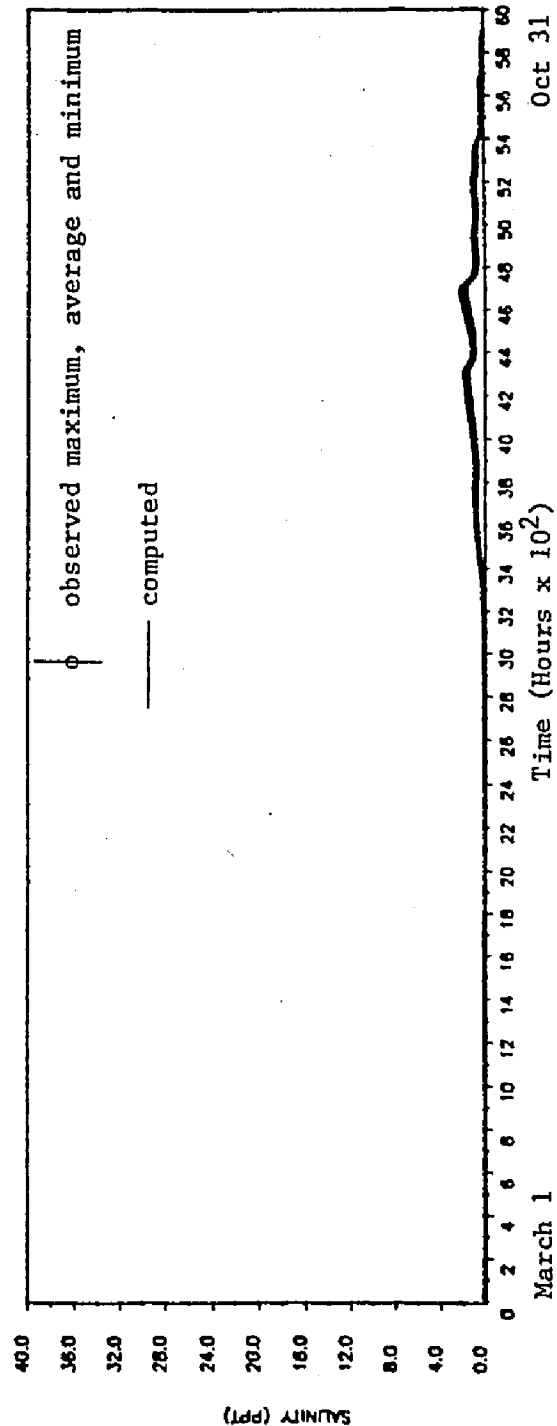


Figure 6.17 Computed and observed salinity at node 18 (Sandy Point).

The non-point and point sources input to the water quality model are obtained from the Chesapeake Bay Nutrient Input Study, EPA (1972). These values are estimated from regression equations. Figures 6.18 to 6.25 show the non-point waste loads used as inputs into the water quality model.

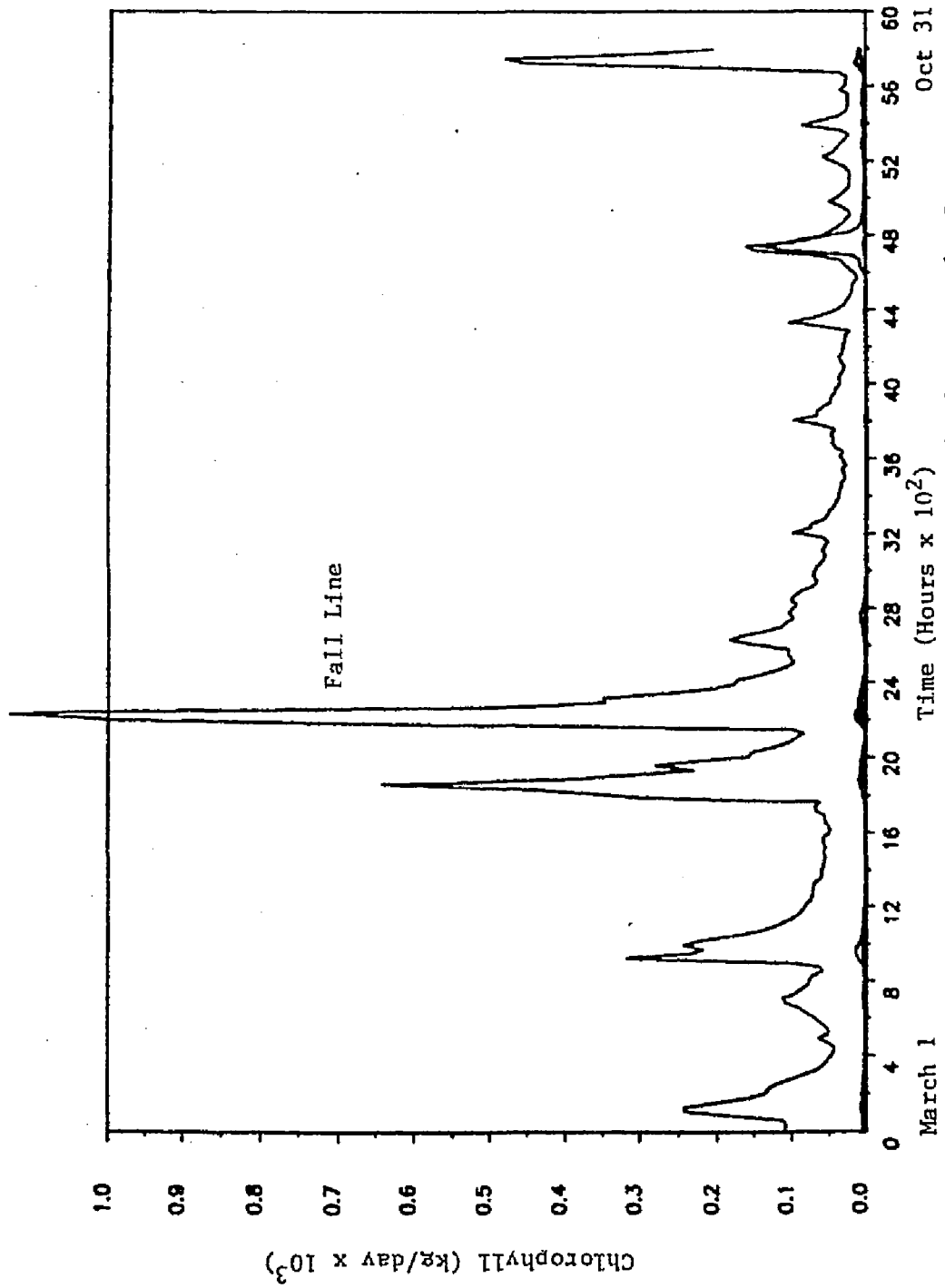
The point-sources used in the model are held constant during the entire simulation period. Values of the point-sources are given in Table 6.1. Estimated benthic releases are divided into four periods corresponding to spring (March-May), early summer (June 1-21), late summer (July 22-August) and fall (September-October) conditions. The values of the benthic releases are given in Tables 6.2 to 6.5.

Actual observed daily solar radiations are used in the model. Figure 6.26 shows the solar radiation measured at the upper and lower James River respectively. These values are linearly interpolated along the length of the river for use in each element of the model. Measured daily temperatures are fitted to an equation of the form

$$T (^{\circ}\text{C}) = a - b \cos (2\pi(\text{day}-c)/365) \quad (6.6)$$

where a , b , and c are the fitted constants. This equation is then used in the model to calculate daily temperatures. Figure 6.27 shows the temperature at the upper and lower James River as calculated using the above equation.

The water quality model is calibrated by adjusting the biochemical parameters in a trial and error manner. To save computer costs, the calibration of the water quality model was carried out in two steps.



March 1
Time (Hours x 10²)
Oct 31
Figure 6.18 Chlorophyll nonpoint source loadings to the James River model.

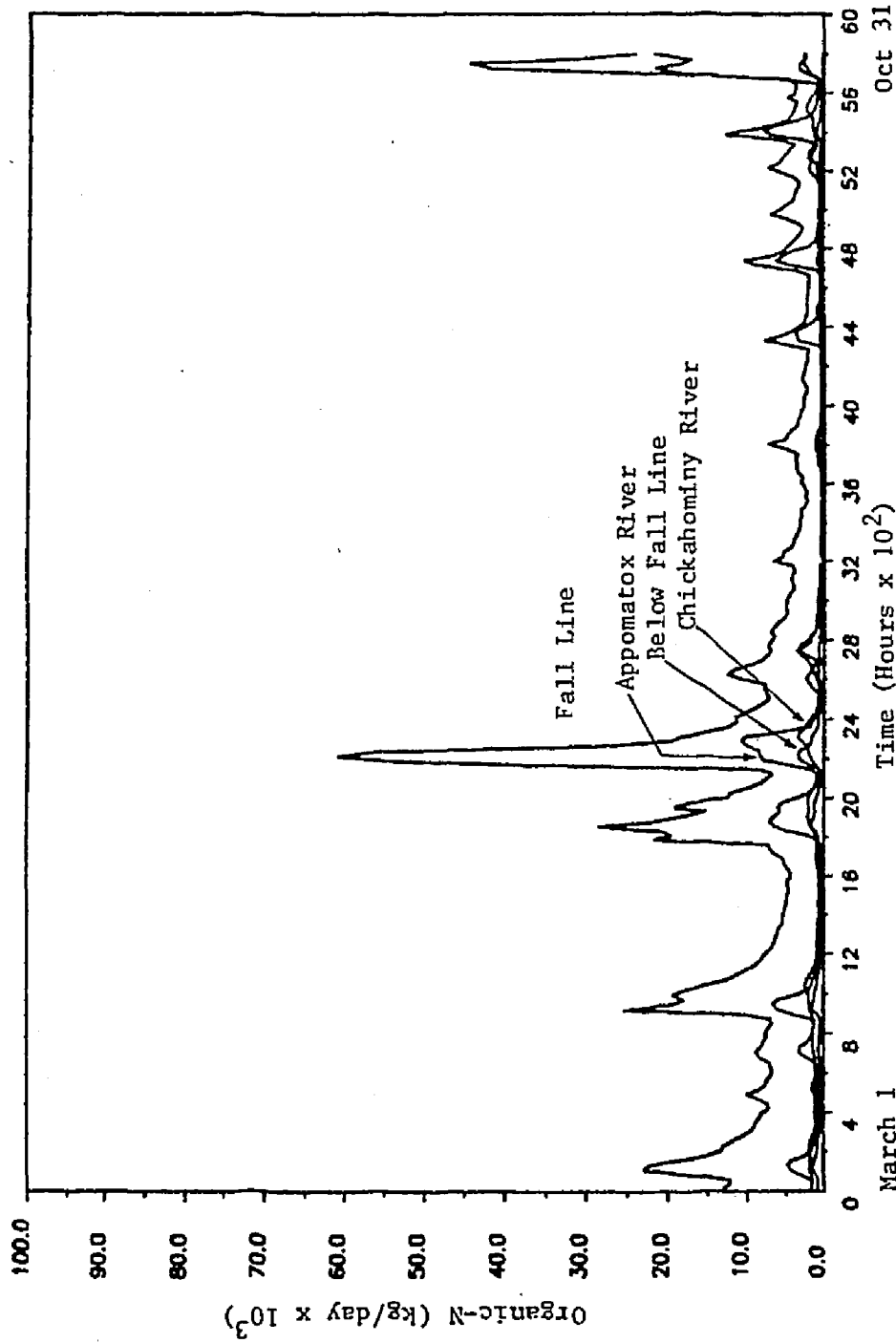
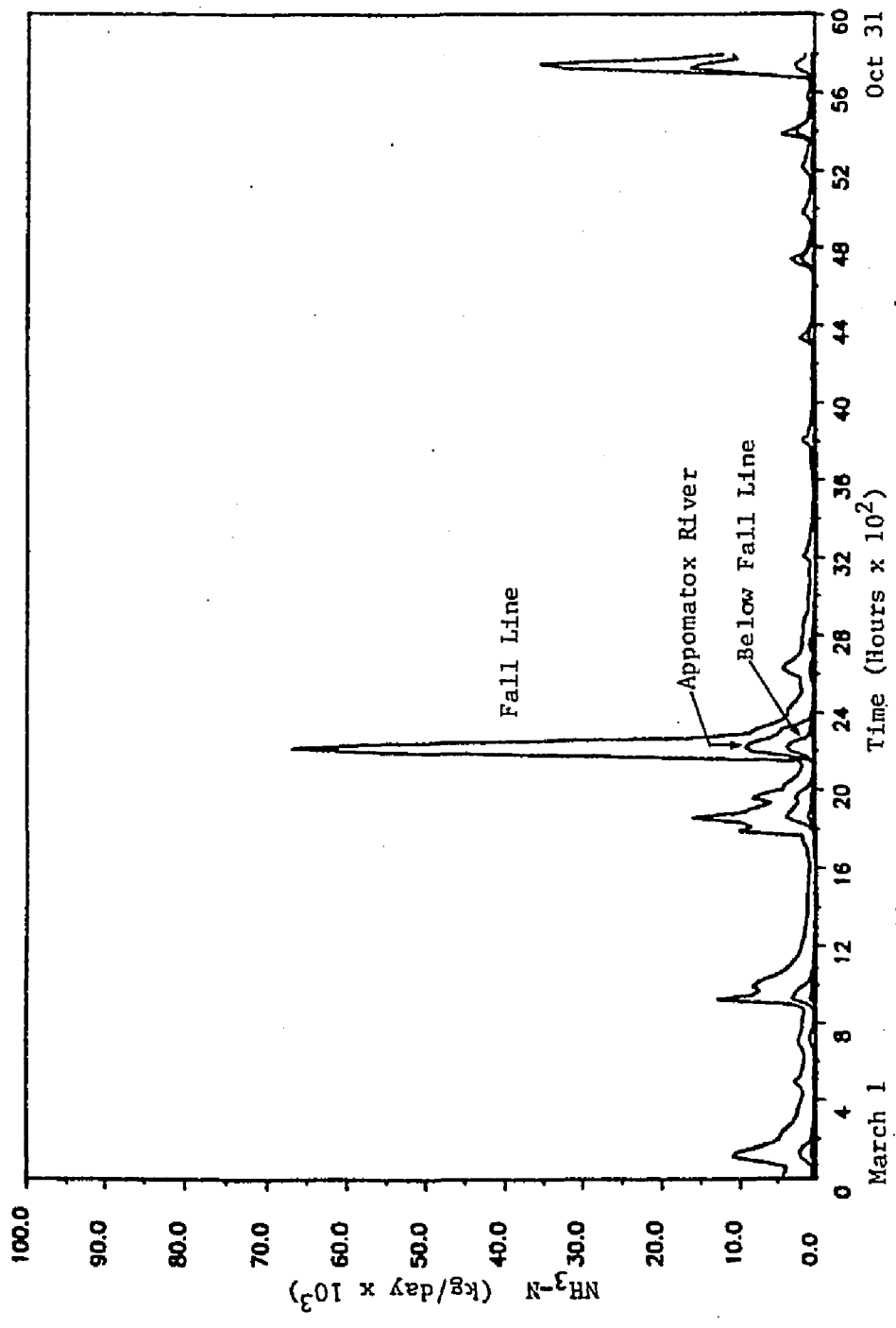


Figure 6.19 Organic-N nonpoint source loadings to the James River model.



March 1
Time (Hours x 10²)
Oct 31
Figure 6.20 Ammonia-N nonpoint source loadings to the James River model.

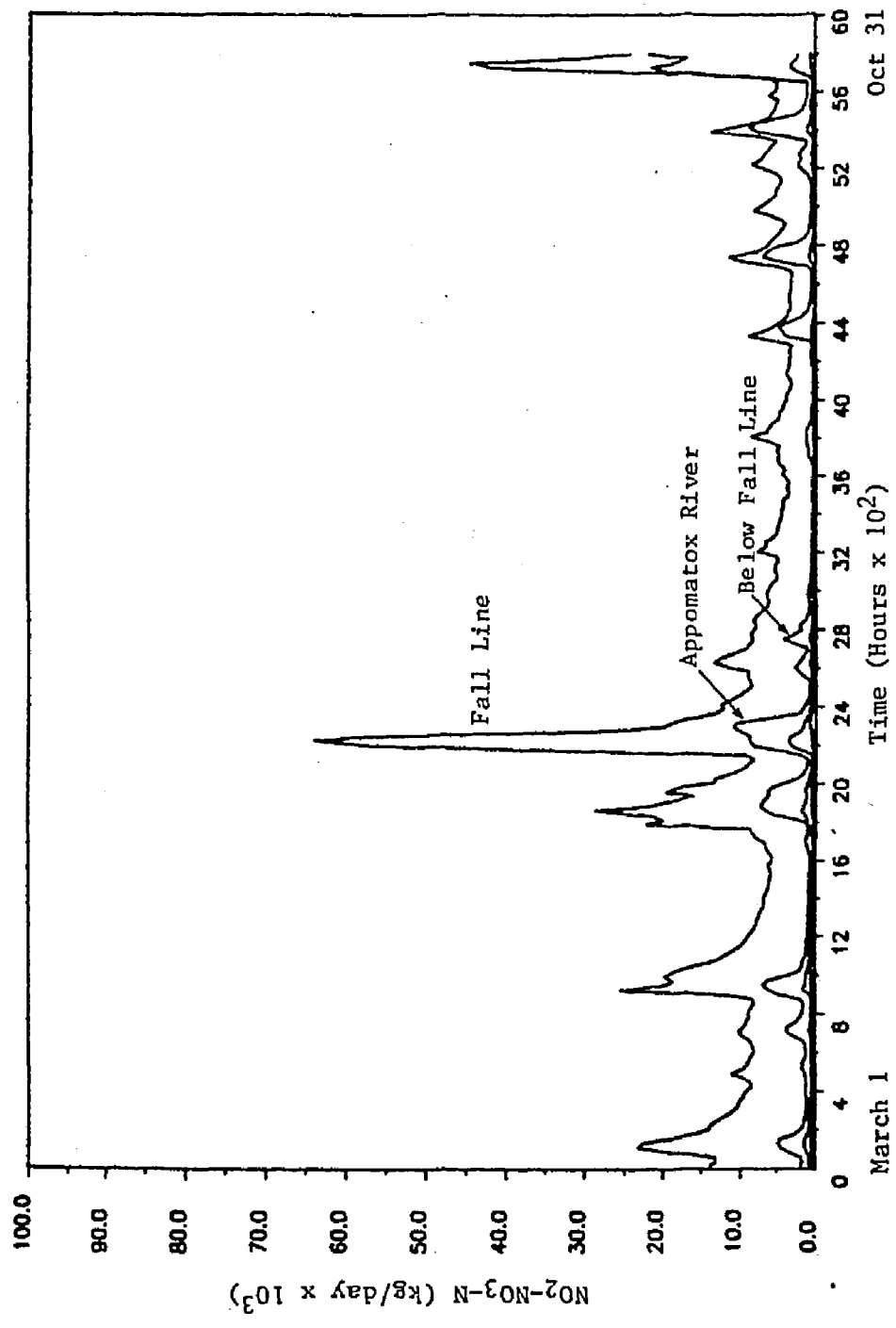
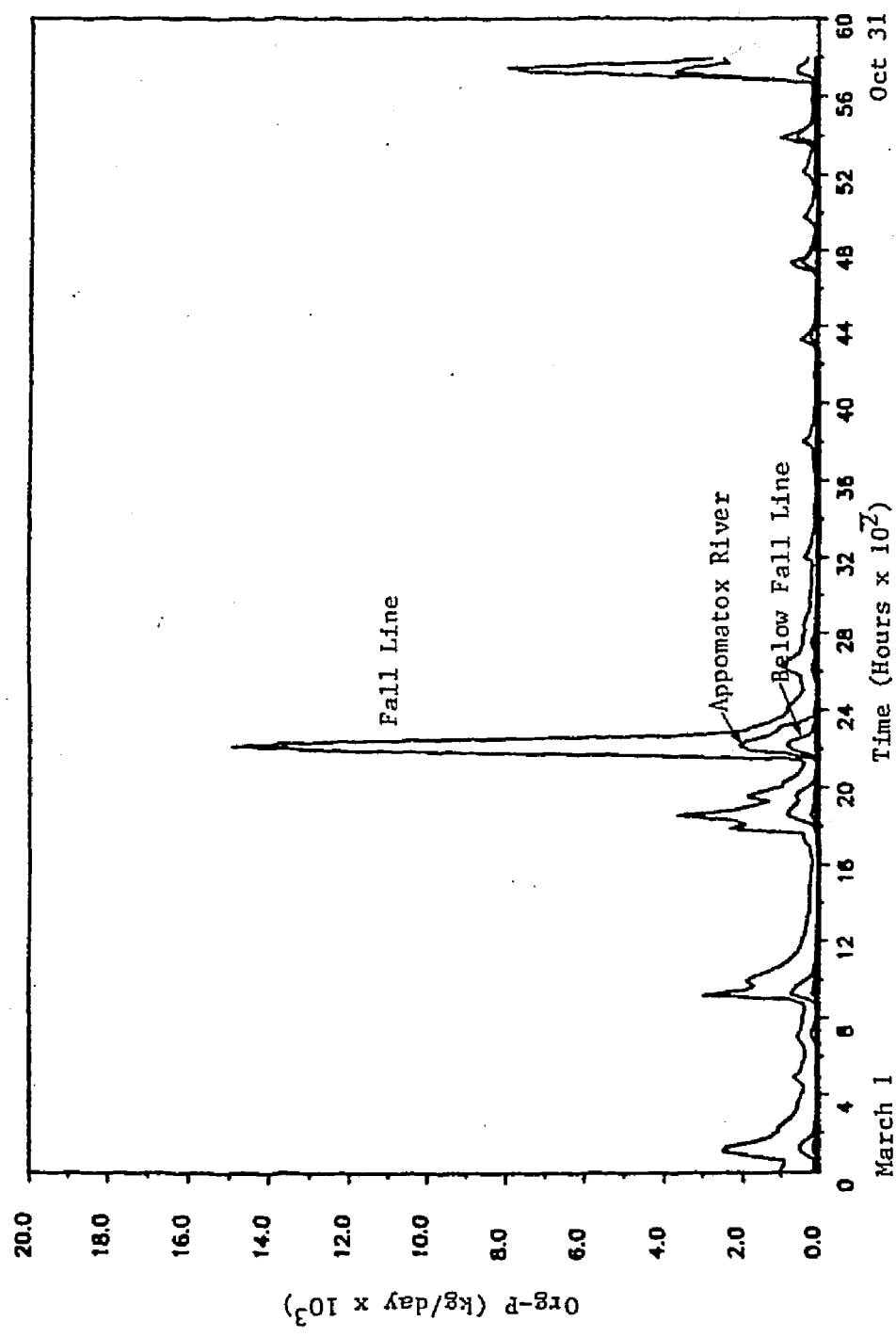
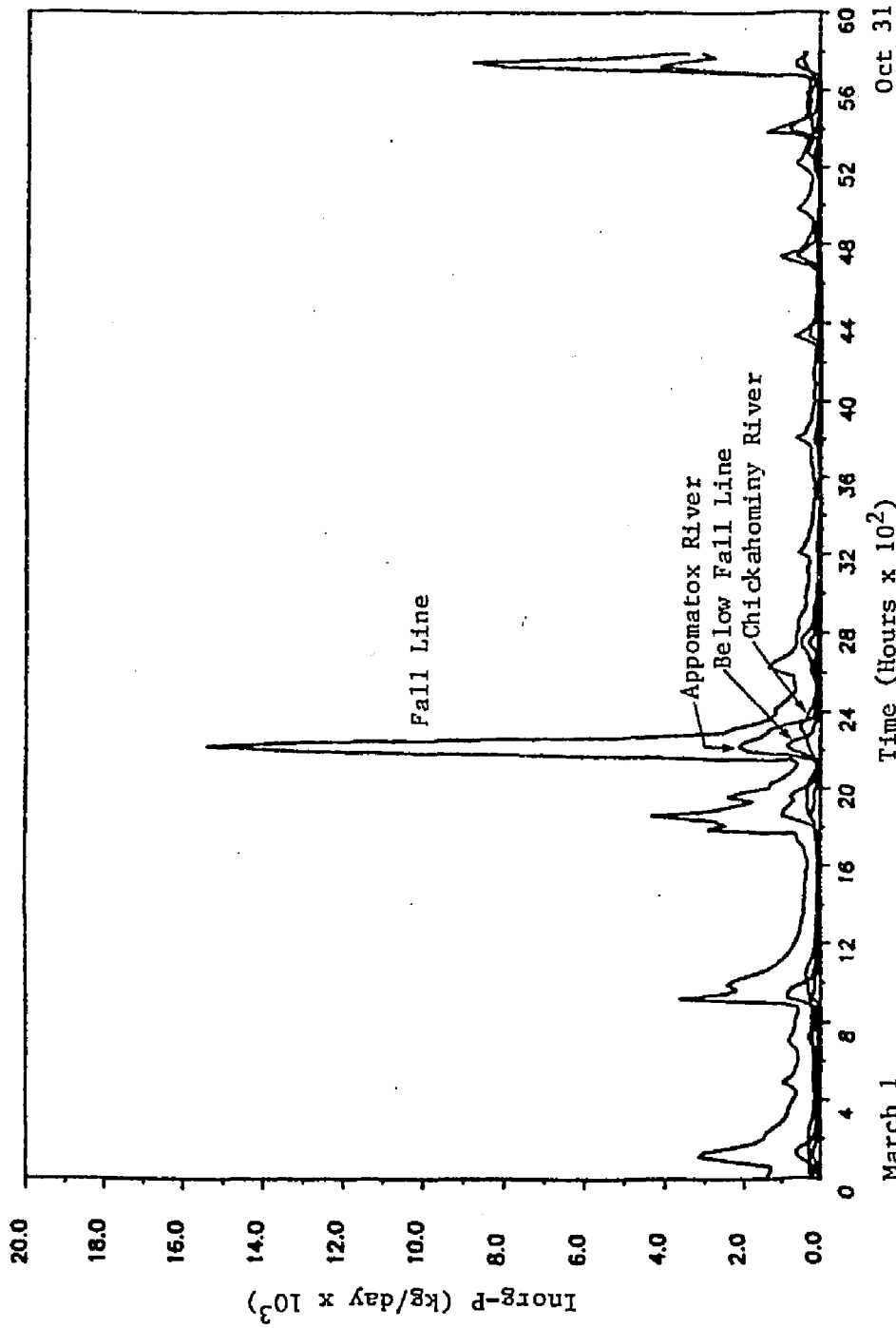


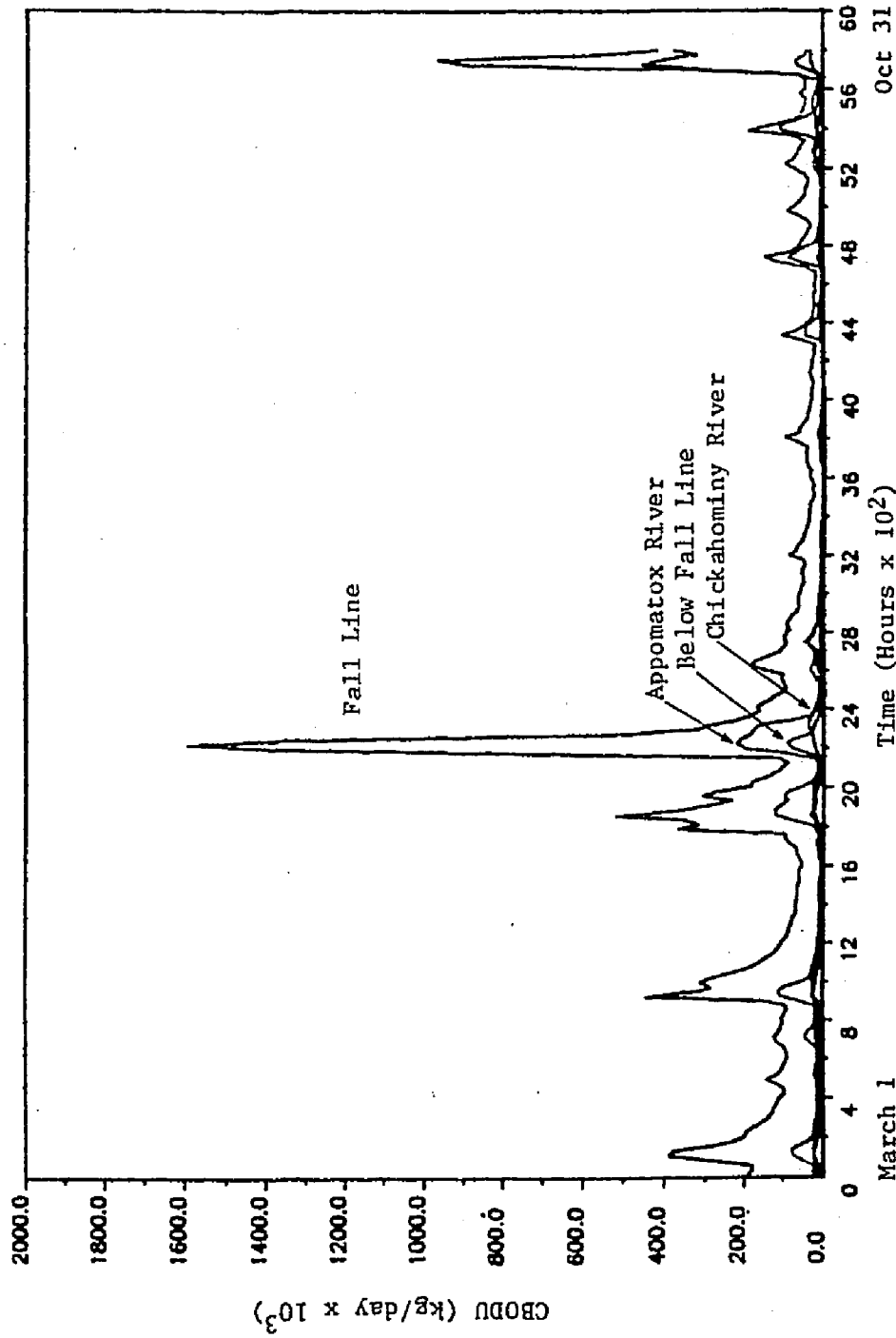
Figure 6.21 Nitrite-Nitrate-N nonpoint source loadings to the James River model.



March 1
Time (Hours x 10²)
Oct 31
Figure 6.22 Organic-P nonpoint source loadings to the James River model.



March 1
Time (Hours x 10²)
Oct 31
Figure 6.23 Inorganic-P nonpoint source loadings to the James River model.



March 1
 Time (Hours x 10²)
 Oct 31
 Figure 6.24 CBODU nonpoint source loadings to the James River model.

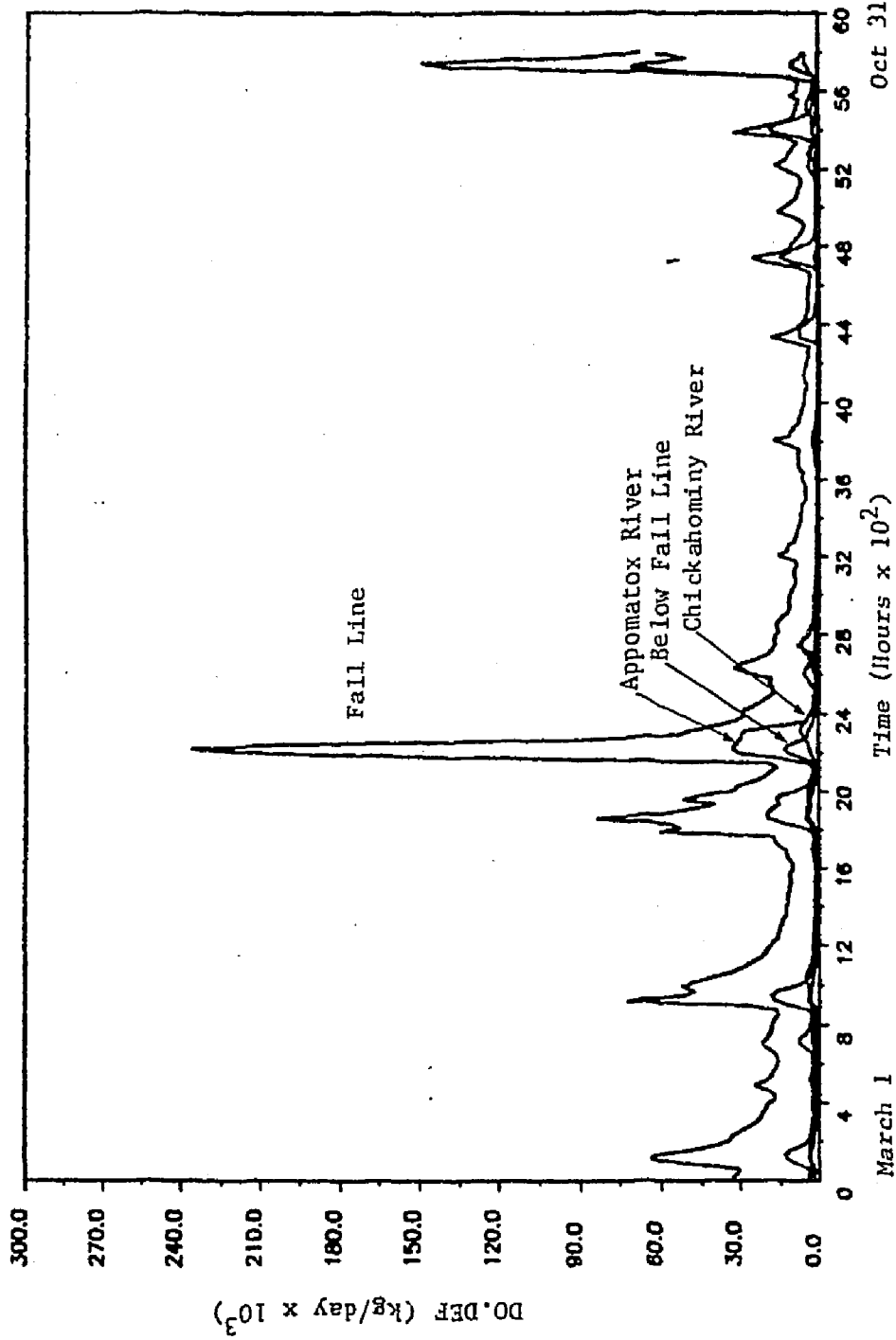


Figure 6.25 DO deficit nonpoint source loadings to the James River model.

Table 6.1 Point Source Loadings to the James River (kg/day)

Element	Org-N	NH ₃ -N	NO ₂ -NO ₃ -N	Org-P	Inorg-P	CBODU	DO.Def
1	0	0	0	0	0	0	1
2	1063	2679	0	797	1089	23682	635
3	42	146	0	32	45	1211	112
4	162	13	0	0	22	1752	4
5	0	0	0	0	0	0	1
6	432	1250	15	308	1002	9618	269
7	0	0	0	0	0	0	1
8	0	0	0	0	0	0	1
9	0	0	0	0	0	0	1
10	0	51	0	0	172	172	4
11	0	0	0	0	0	0	1
12	0	0	0	0	0	0	1
13	0	0	0	0	0	0	1
14	0	0	0	0	0	0	1
15	0	0	0	0	0	0	1
16	0	53	0	0	46	302	394
17	0	0	0	0	0	0	1
18	0	0	0	0	0	0	1
19	0	0	0	0	0	0	1
20	0	0	0	0	0	0	1
21	0	0	0	0	0	0	1
22	0	0	0	0	0	0	1
23	0	0	0	0	0	0	1
24	0	0	0	0	0	0	1
25	0	0	0	0	0	0	1
26	0	8204	5960	0	0	65788	1
27	254	500	0	191	154	4906	109
28	0	0	0	0	0	0	1
29	0	0	0	0	0	340	1
30	0	0	0	0	0	0	1
31	0	0	0	0	0	0	1
32	0	0	0	0	0	0	1
33	0	0	0	0	0	0	1
34	0	0	0	0	0	0	1
35	0	0	0	0	0	0	1
36	0	0	0	0	0	0	1
37	0	76	0	0	0	1012	123
38	0	0	0	0	0	0	1
39	0	0	0	0	0	0	1
40	984	1971	0	738	598	19059	428

Table 6.2 Benthic Releases for Spring (kg/day)

Element	NH ₃ -N	Inorg-P
1	104	0
2	289	0
3	493	0
4	137	0
5	285	0
6	208	0
7	235	0
8	76	0
9	87	0
10	147	0
11	162	0
12	108	0
13	102	0
14	76	0
15	182	0
16	183	0
17	122	0
18	105	0
19	79	0
20	55	0
21	80	0
22	79	0
23	80	0

Table 6.3 Benthic Releases for Early Summer (kg/day)

Element	NH ₃ -N	Inorg-P
1	119	153
2	331	139
3	563	101
4	157	75
5	325	71
6	238	19
7	269	0
8	87	38
9	99	61
10	167	2
11	185	1
12	124	3
13	117	0
14	86	44
15	208	15
16	209	0
17	139	5
18	120	18
19	90	42
20	63	36
21	92	12
22	91	22
23	91	0

Table 6.4 Benthic Releases for Late Summer (kg/day)

Element	NH ₃ -N	Inorg-P
1	119	17
2	331	15
3	563	11
4	157	8
5	325	8
6	238	2
7	269	0
8	87	4
9	99	7
10	167	0
11	185	0
12	124	0
13	117	0
14	86	5
15	208	2
16	209	0
17	139	1
18	120	2
19	90	5
20	63	4
21	92	1
22	91	2
23	91	0

Table 6.5 Benthic Releases for Fall (kg/day)

Element	NH ₃ -N	Inorg-P
1	85	0
2	238	0
3	405	0
4	113	0
5	234	0
6	171	0
7	193	0
8	63	0
9	71	0
10	120	0
11	133	0
12	89	0
13	84	0
14	62	0
15	149	0
16	150	0
17	100	0
18	86	0
19	65	0
20	46	0
21	66	0
22	65	0
23	66	0

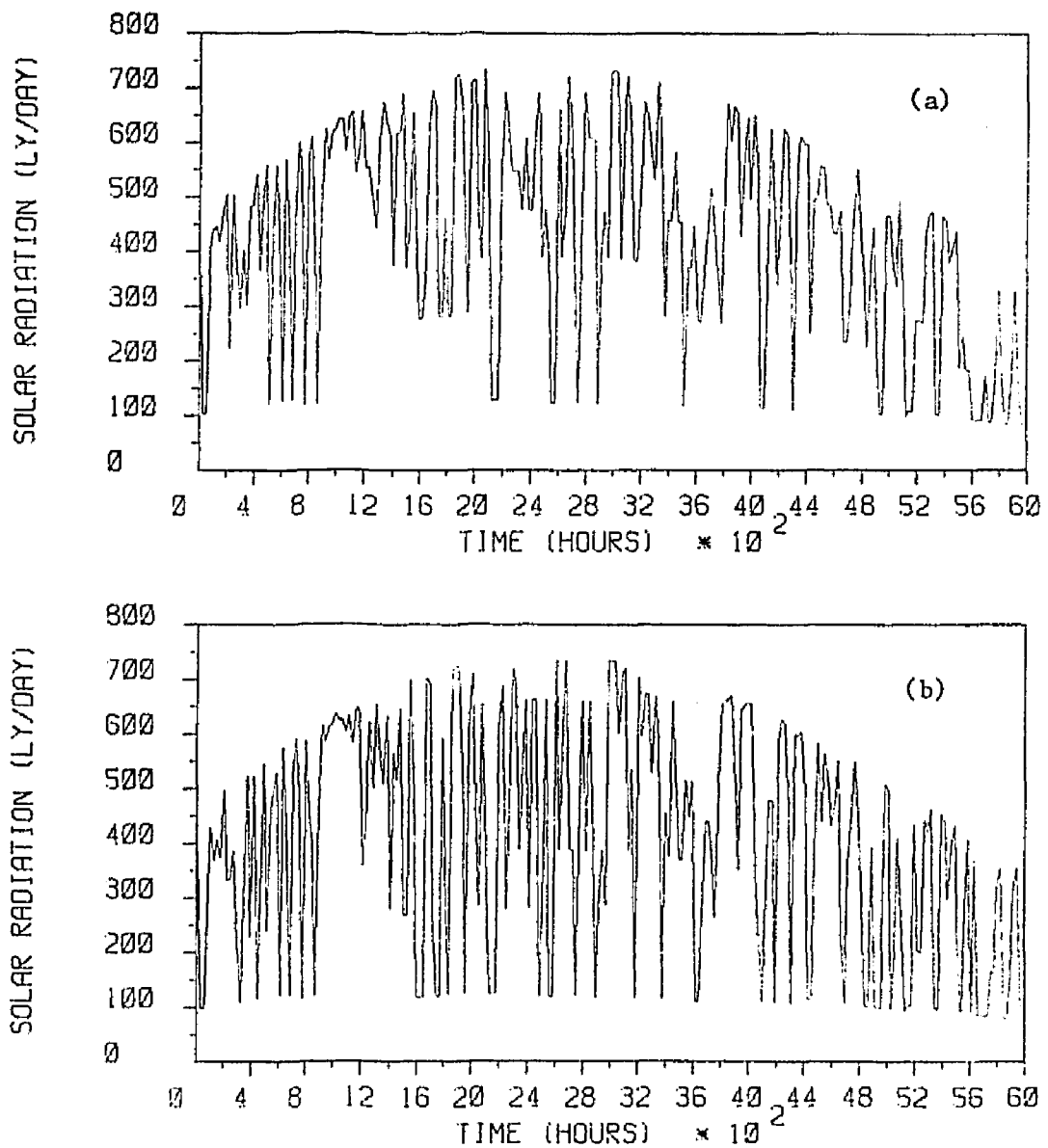
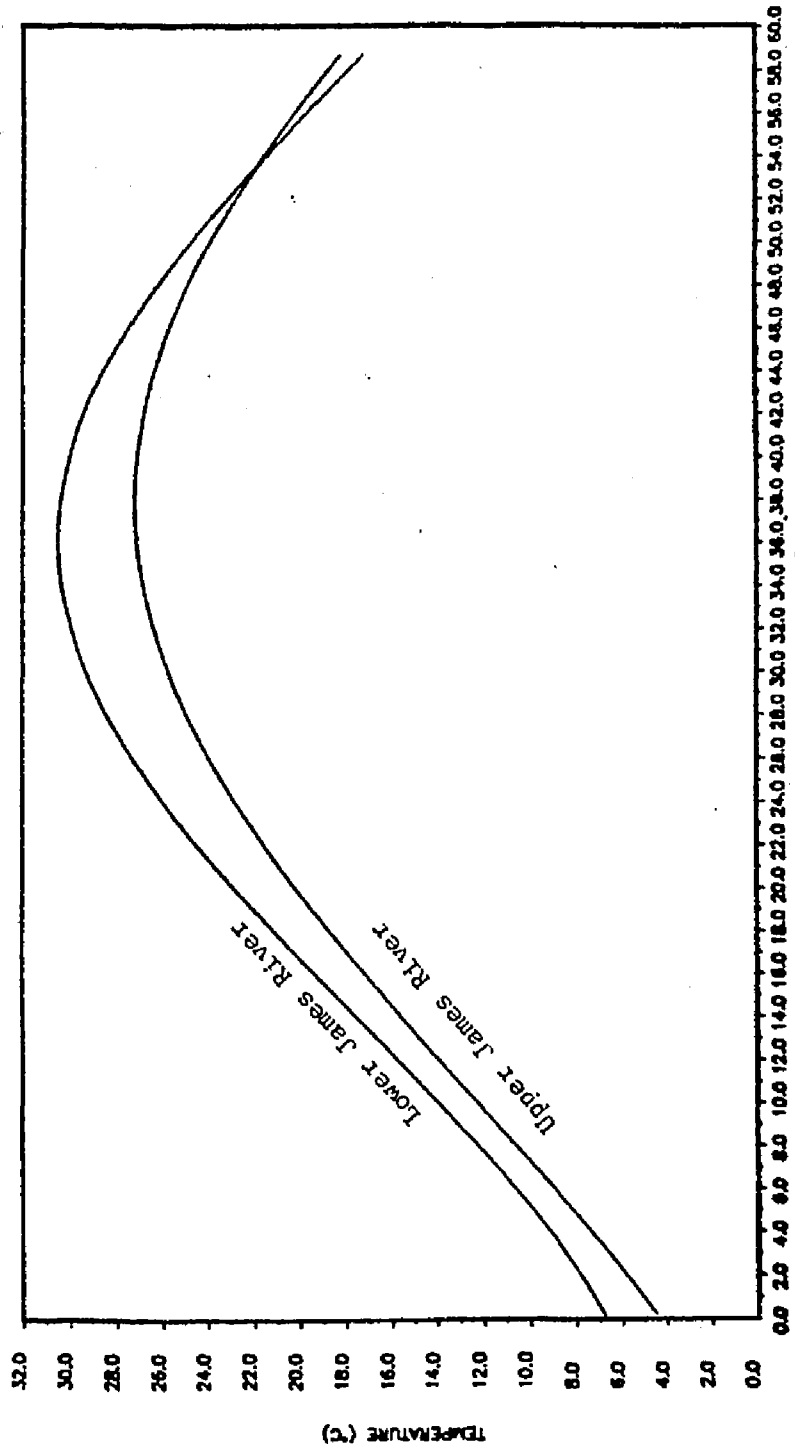
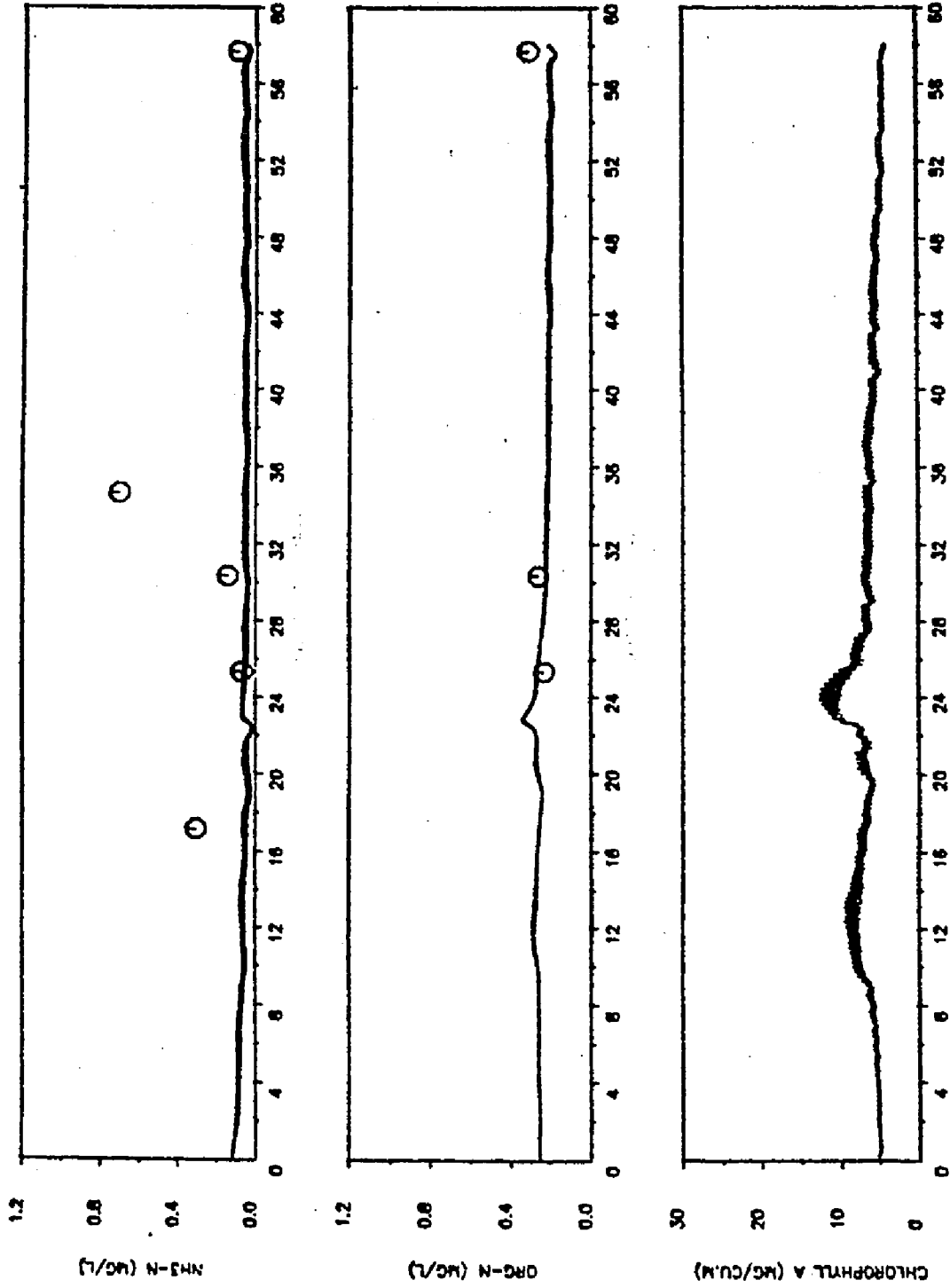


Figure 6.26 James River solar radiation from March 1, 1971 to October 31, 1971, (a) Upper James River, (b) Lower James River.

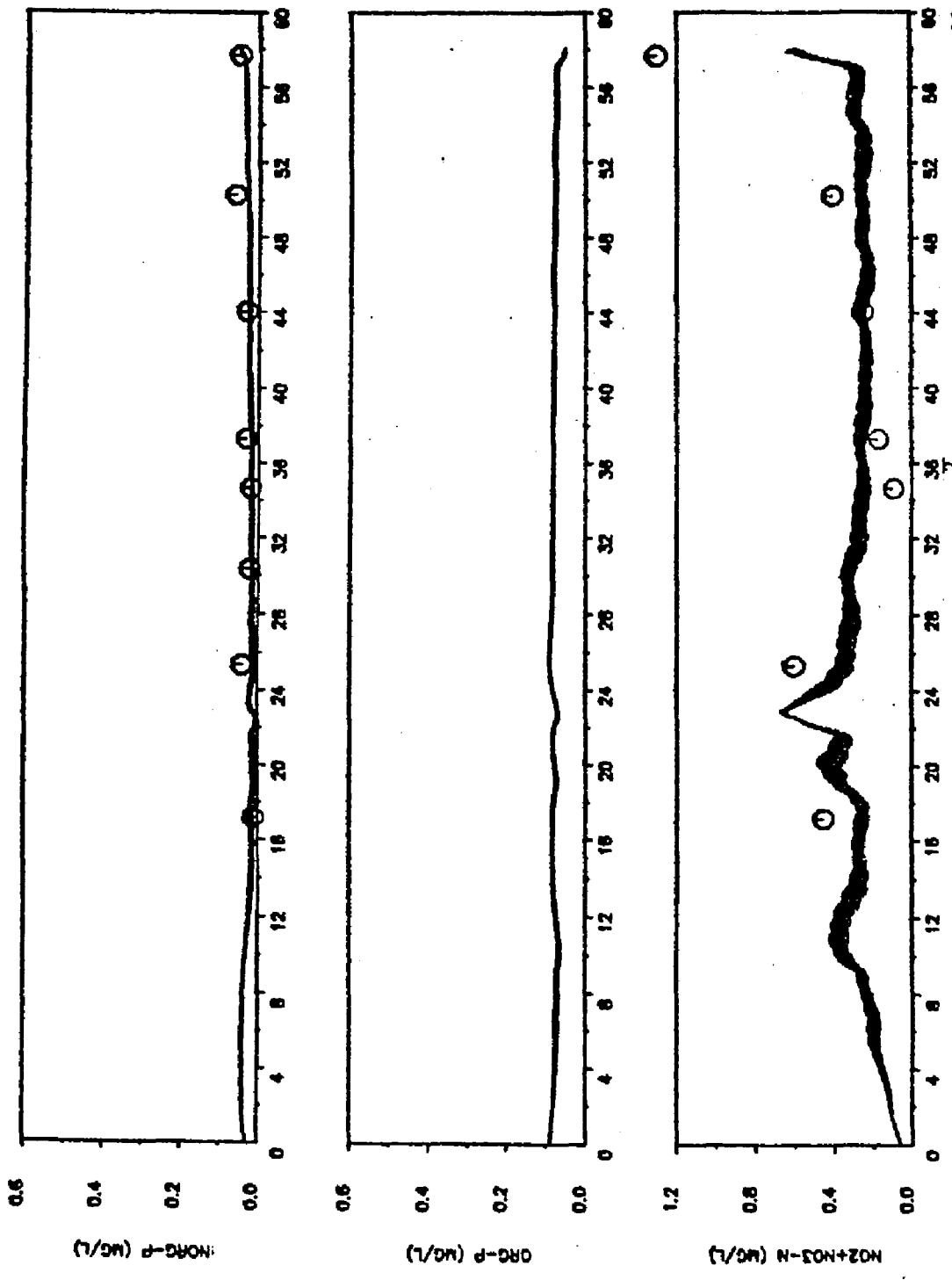


March 1. Time (Hours x 10²) Oct 31
 Figure 6.27 Water temperature variations from March to October 1971.

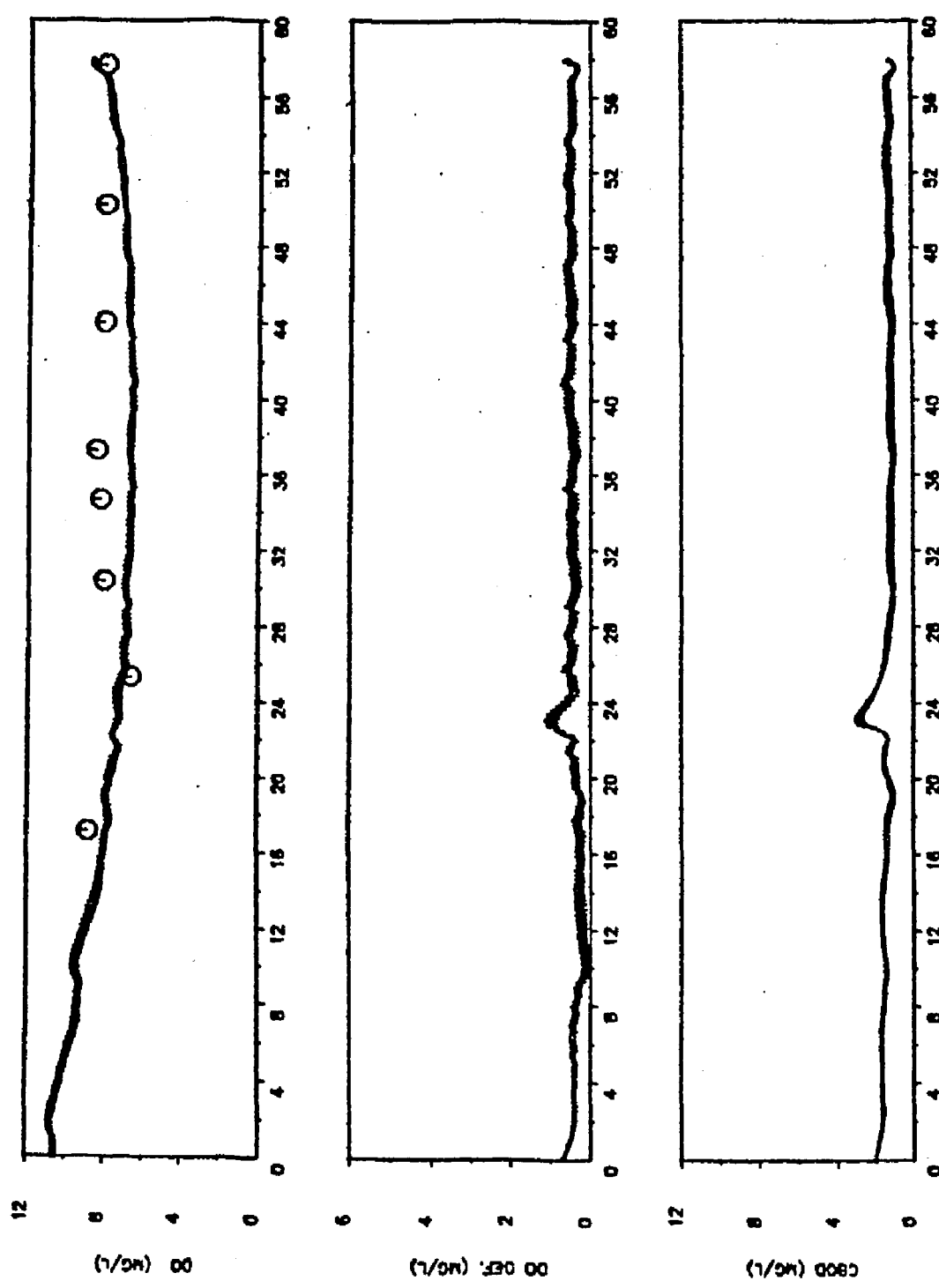
First the model was run to simulate a short period of time (about two months), when the agreement was good, the model was then run for the full eight month period. Experience from this study has shown that even after the model has been adjusted for the two month simulation, it still required considerable adjustment to calibrate for the eight month simulation. Thus the long simulation is considered a rigorous test of the parameters used in the model, since they have to cover the variations that occur from season to season. The set of biochemical parameters used for the final calibration is shown in Table 6.6. Figures 6.28 to 6.35 show the computed water quality concentrations and the observed field values. In general, the agreement between the observed data and the model is good.



March 1 Oct 31
 Time (Hours x 10²)
 Figure 6.28 Computed and observed water quality constituents at node 4
 in the James River.
 ——— computed; ○ observed.



March 1
Time (Hours x 10²) Oct 31
Figure 6.28 (Cont'd) Computed and observed water quality constituents at node 4
in the James River.



March 1
Figure 6.28 (Cont'd) Computed and observed water quality constituents at node 4
in the James River.
— computed; ○ observed.
Oct 31

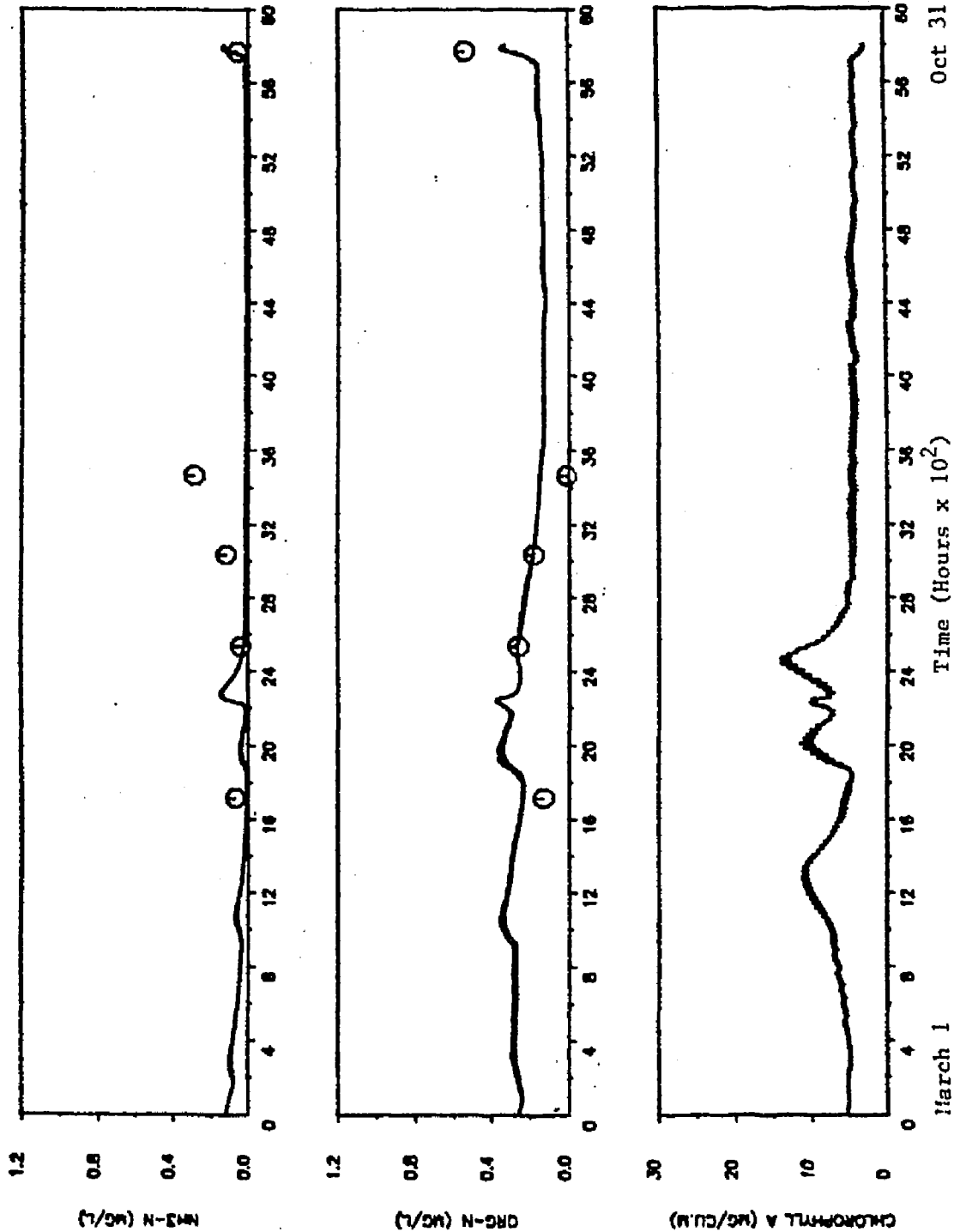
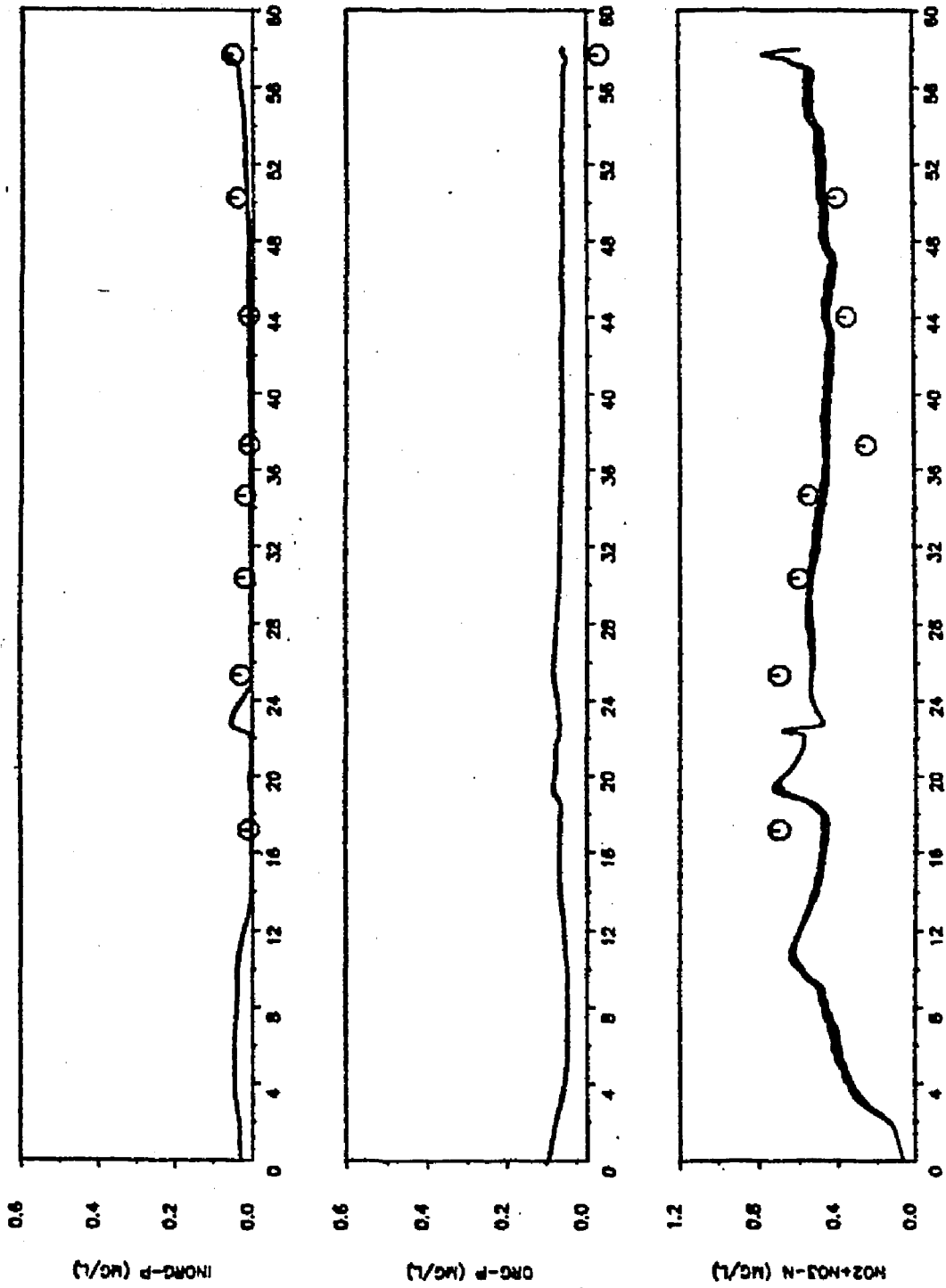


Figure 6.29 Computed and observed water quality constituents at node 9 in the James River.



March 1
Time (Hours x 10^2)
Oct 31
Figure 6.29 (Cont'd) Computed and observed water quality constituents at node 9 in the James River.
— computed; \odot observed.

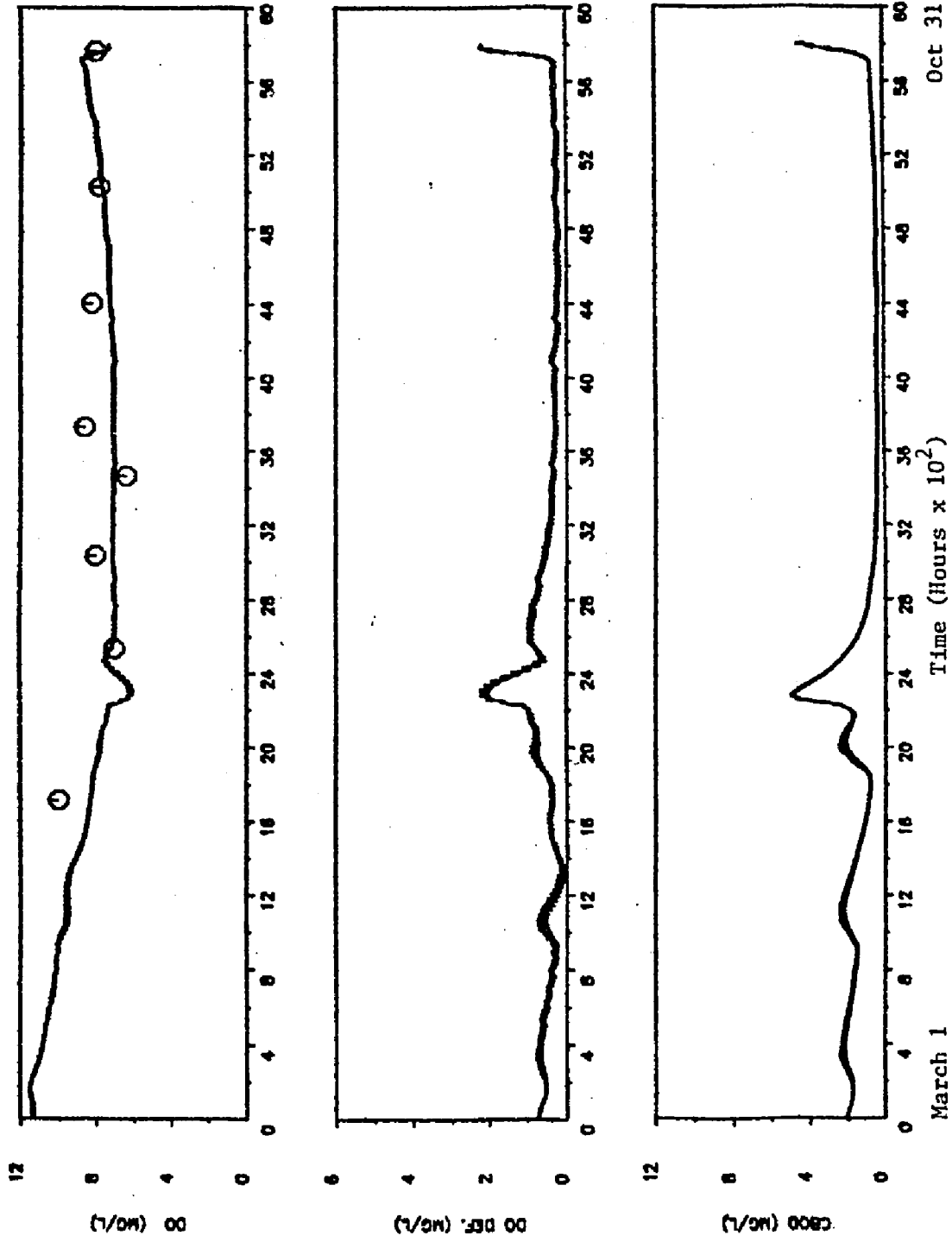
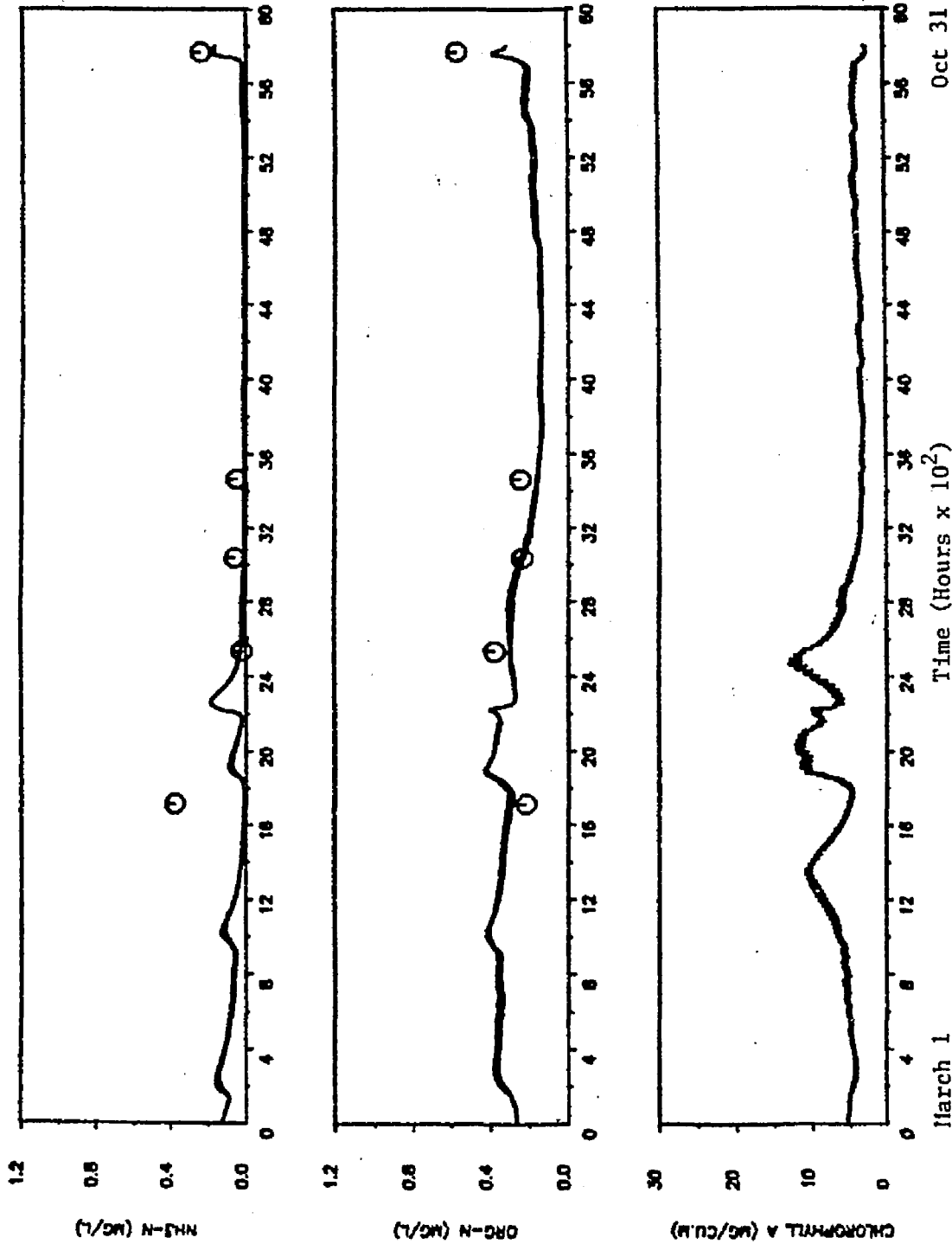


Figure 6.29 (Cont'd) Computed and observed water quality constituents at node 9 in the James River.



March 1
Oct 31
Time (Hours x 10²)
Figure 6.30 Computed and observed water quality constituents at node 12 in the James River.
— computed; ○ observed.

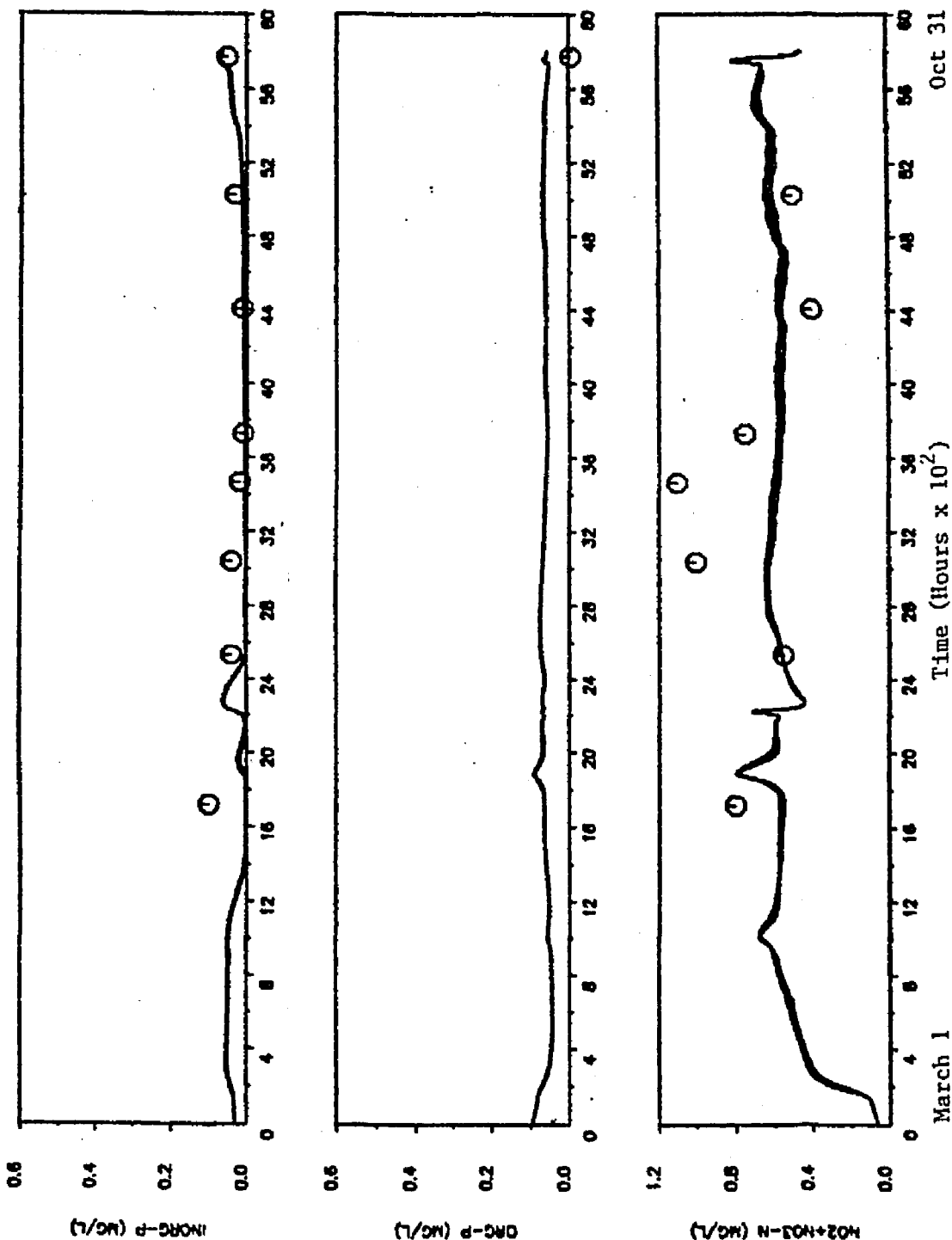
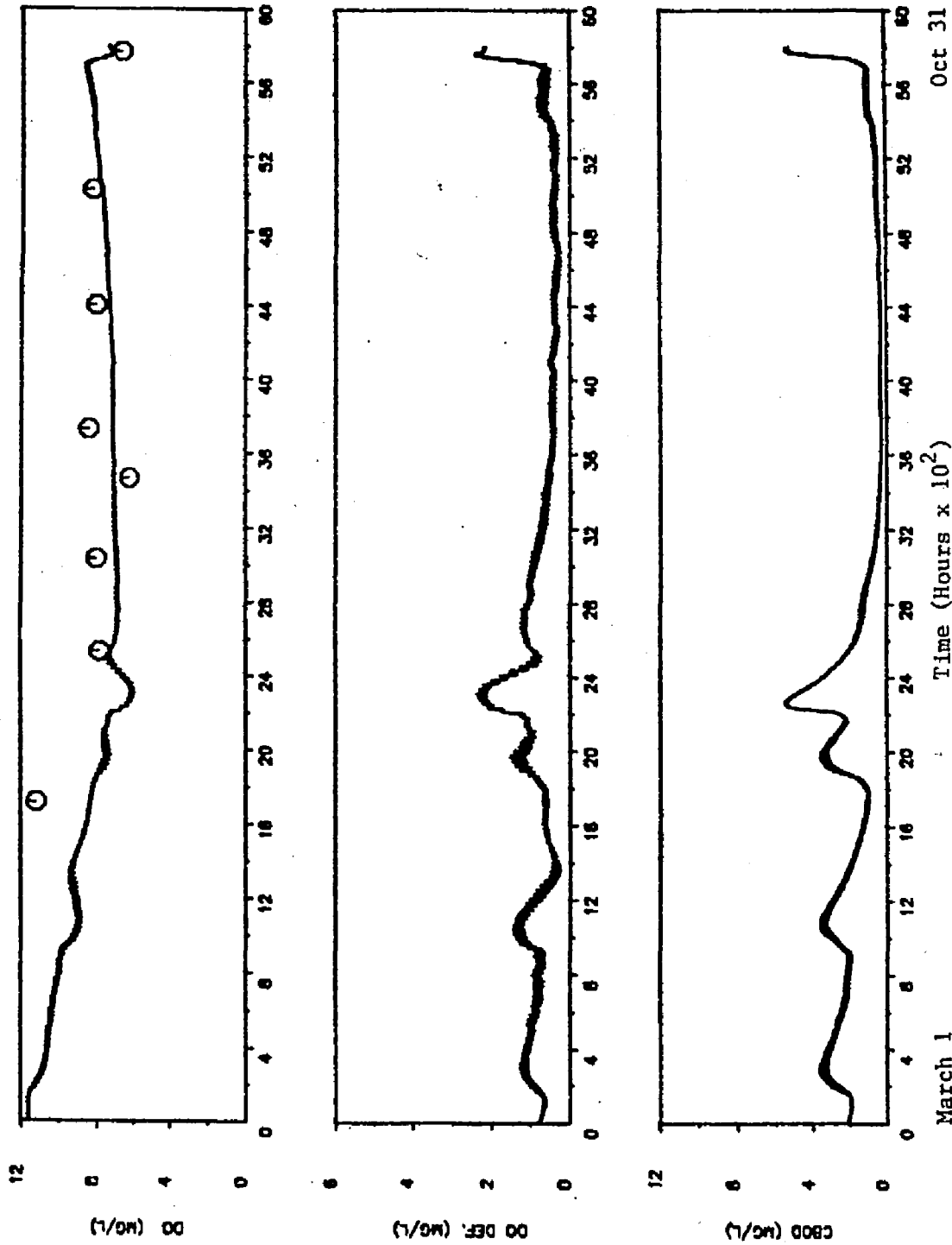
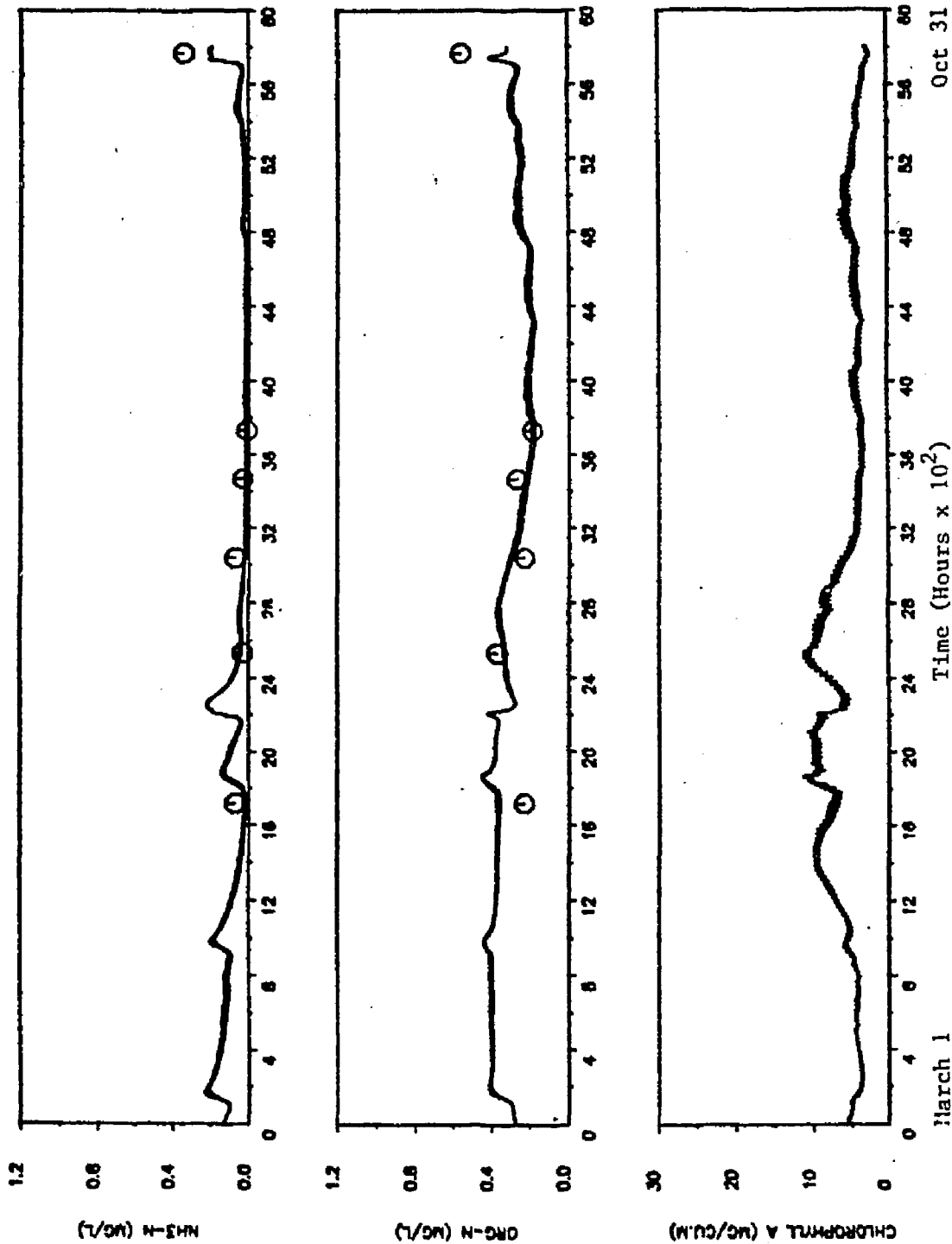
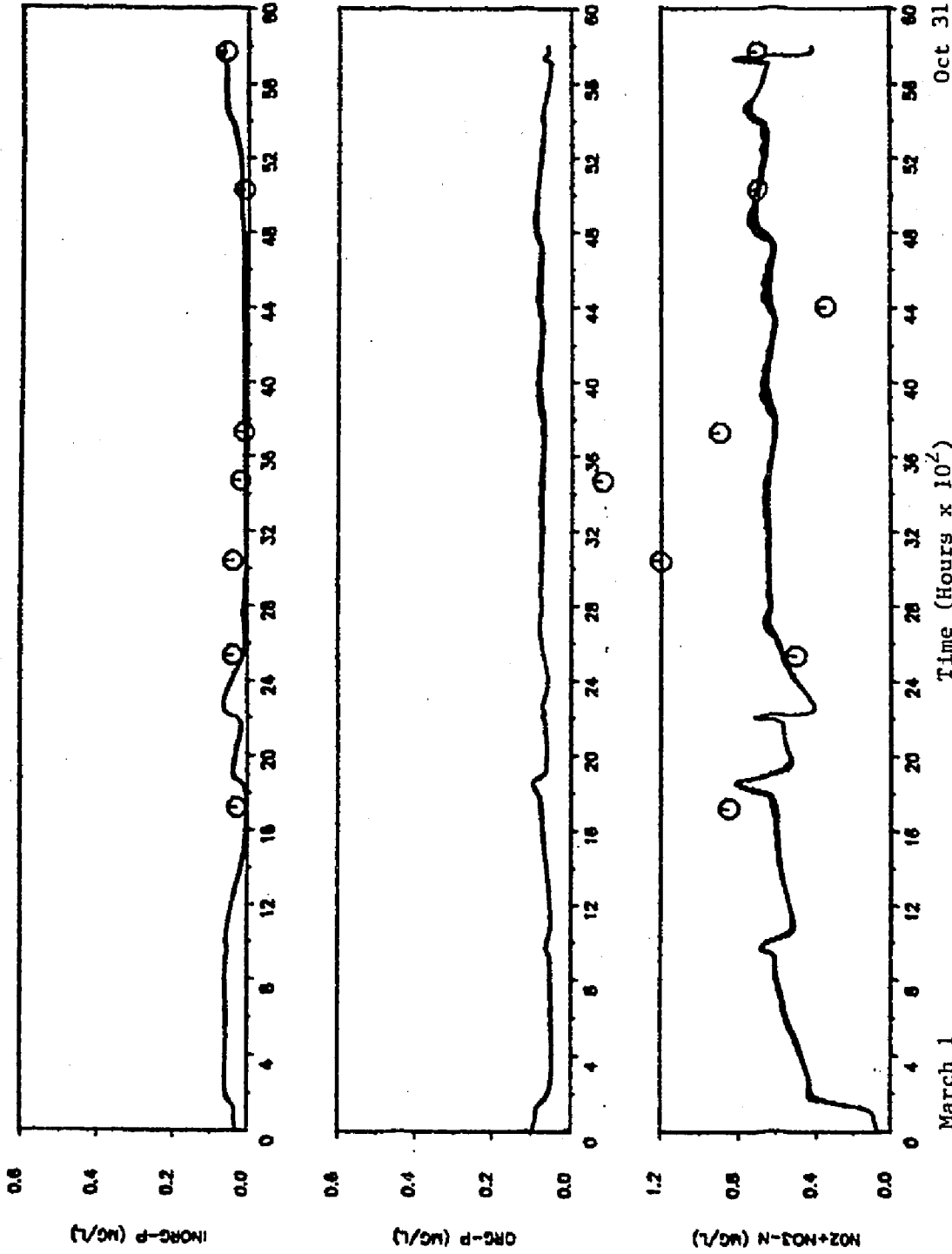


Figure 6.30 (Cont'd) Computed and observed water quality constituents at node 12 in the James River.

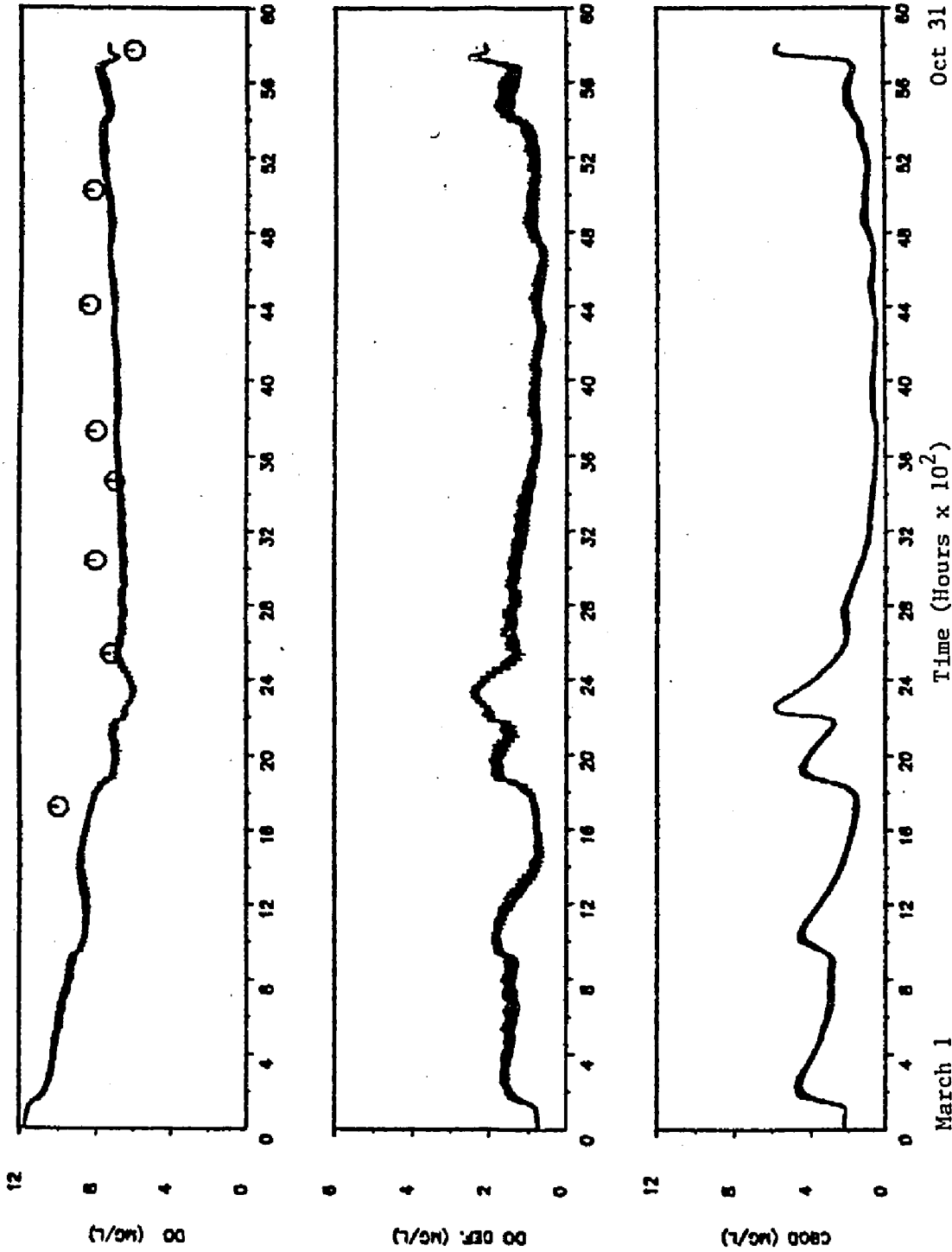


March 1 : Time (Hours x 10²) Oct 31
 Figure 6.30 (Cont'd) Computed and observed water quality constituents at node 12 in the James River.





March 1
Time (Hours x 10²)
Oct 31
Figure 6.31 (Cont'd) Computed and observed water quality constituents at node 16 in the James River.
— computed; ○ observed.



March 1
Time (Hours x 10²)
Oct 31
Figure 6.31 (Cont'd) Computed and observed water quality constituents at node 16 in the James River.
— computed; ○ observed.

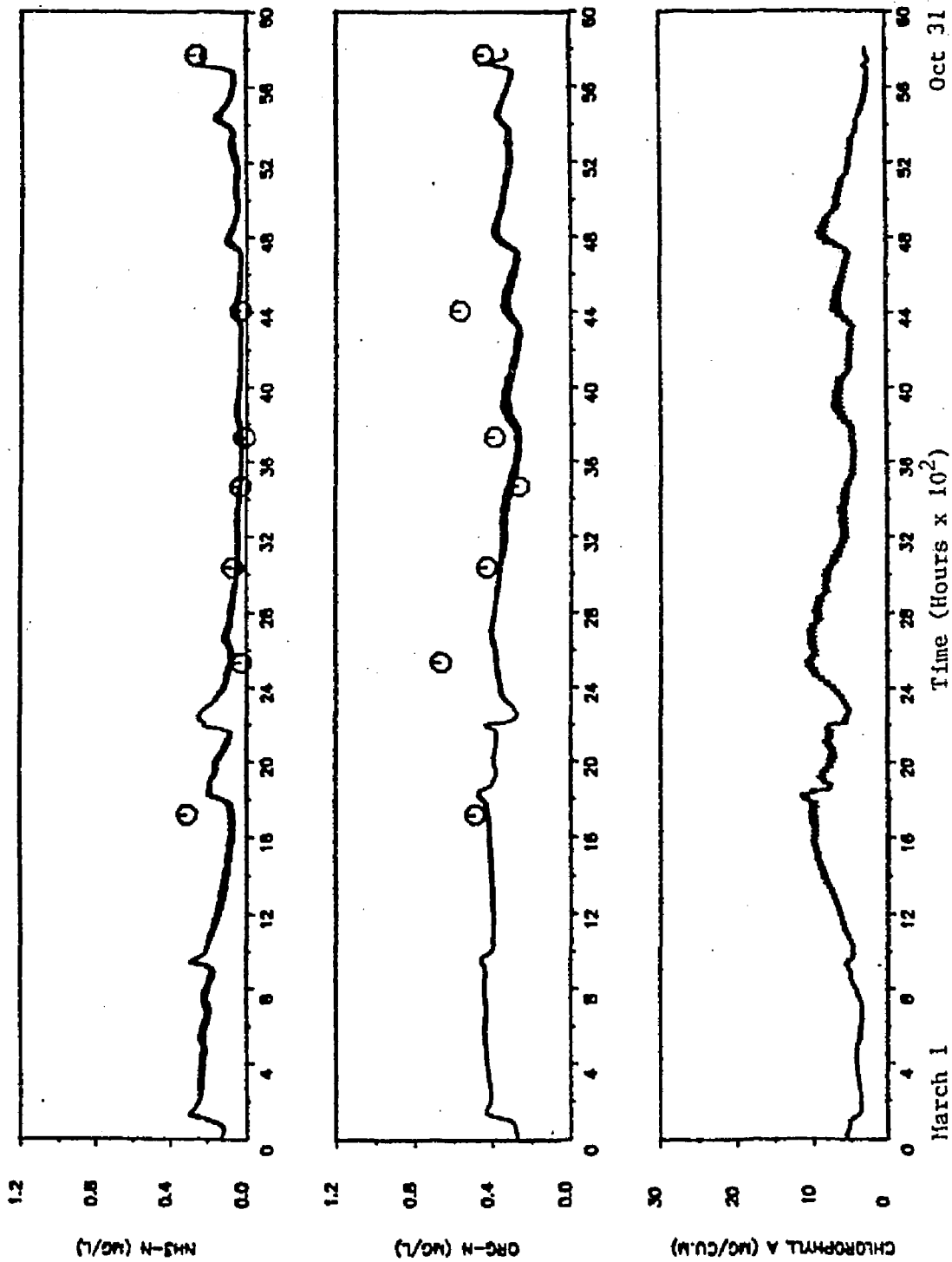
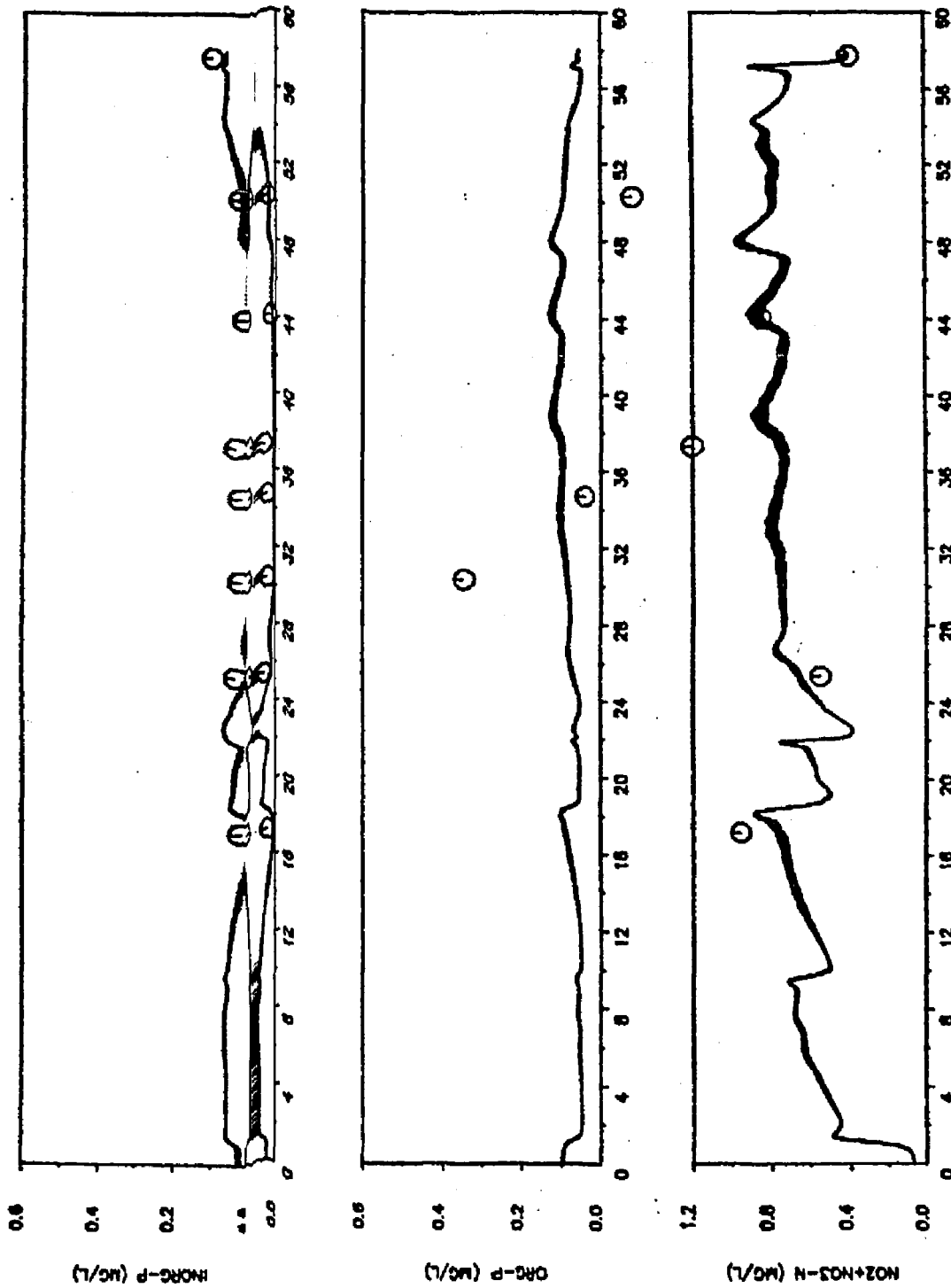


Figure 6.32 Computed and observed water quality constituents at node 19 in the James River.



March 1 Oct 31
 Figure 6.32 (Cont'd) Computed and observed water quality constituents at node 19
 in the James River.

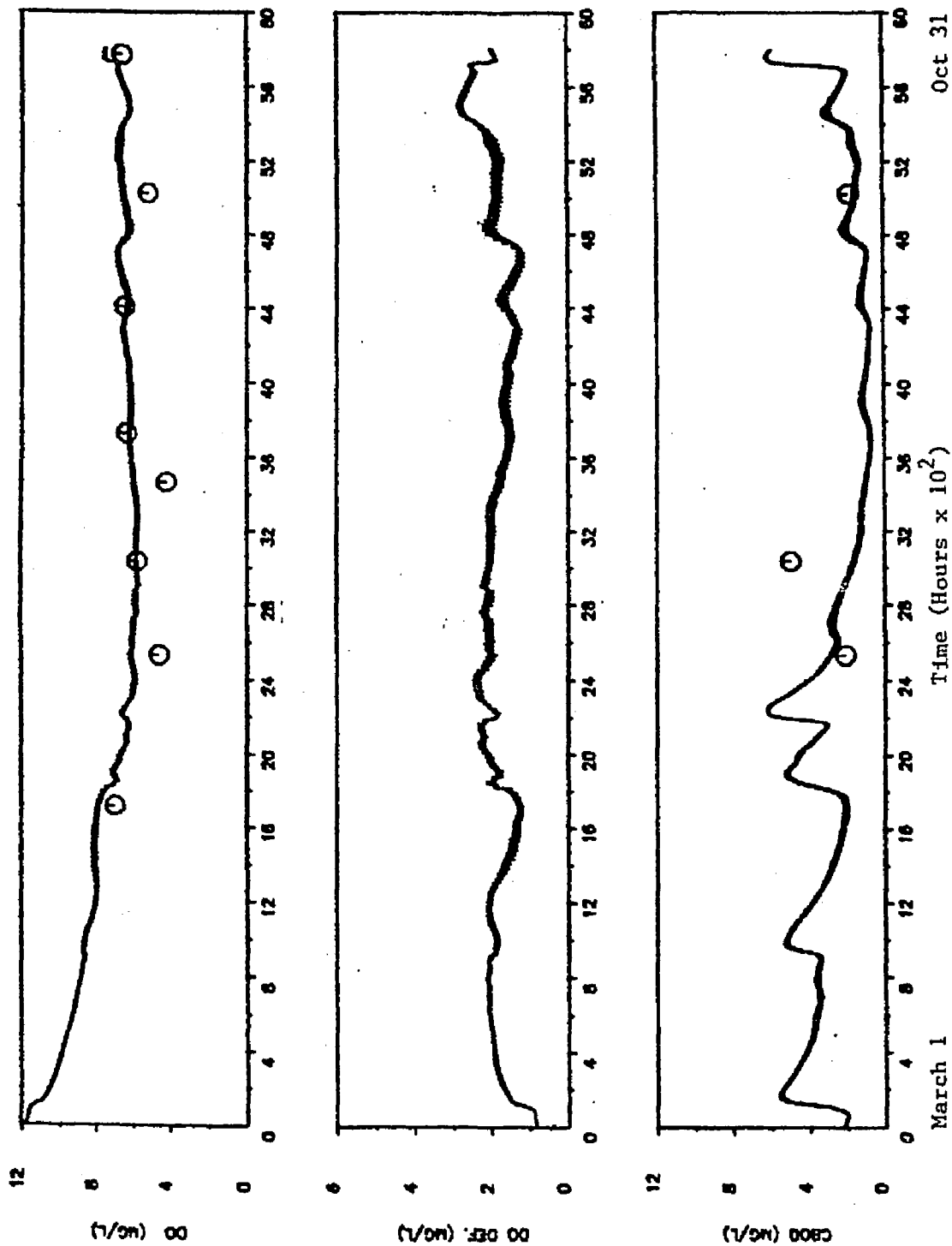
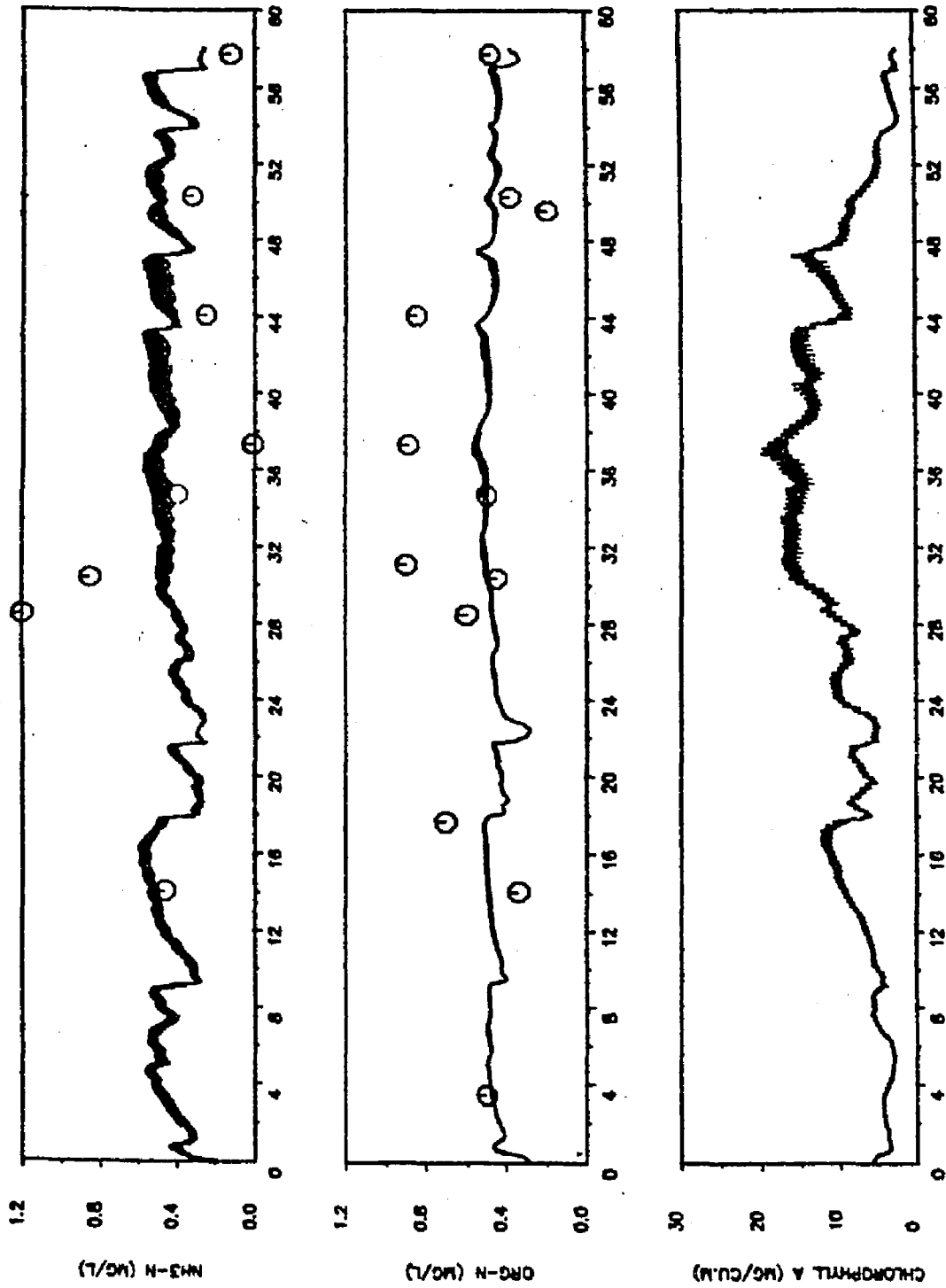


Figure 6.32 (Cont'd) Computed and observed water quality constituents at node 19 in the James River.

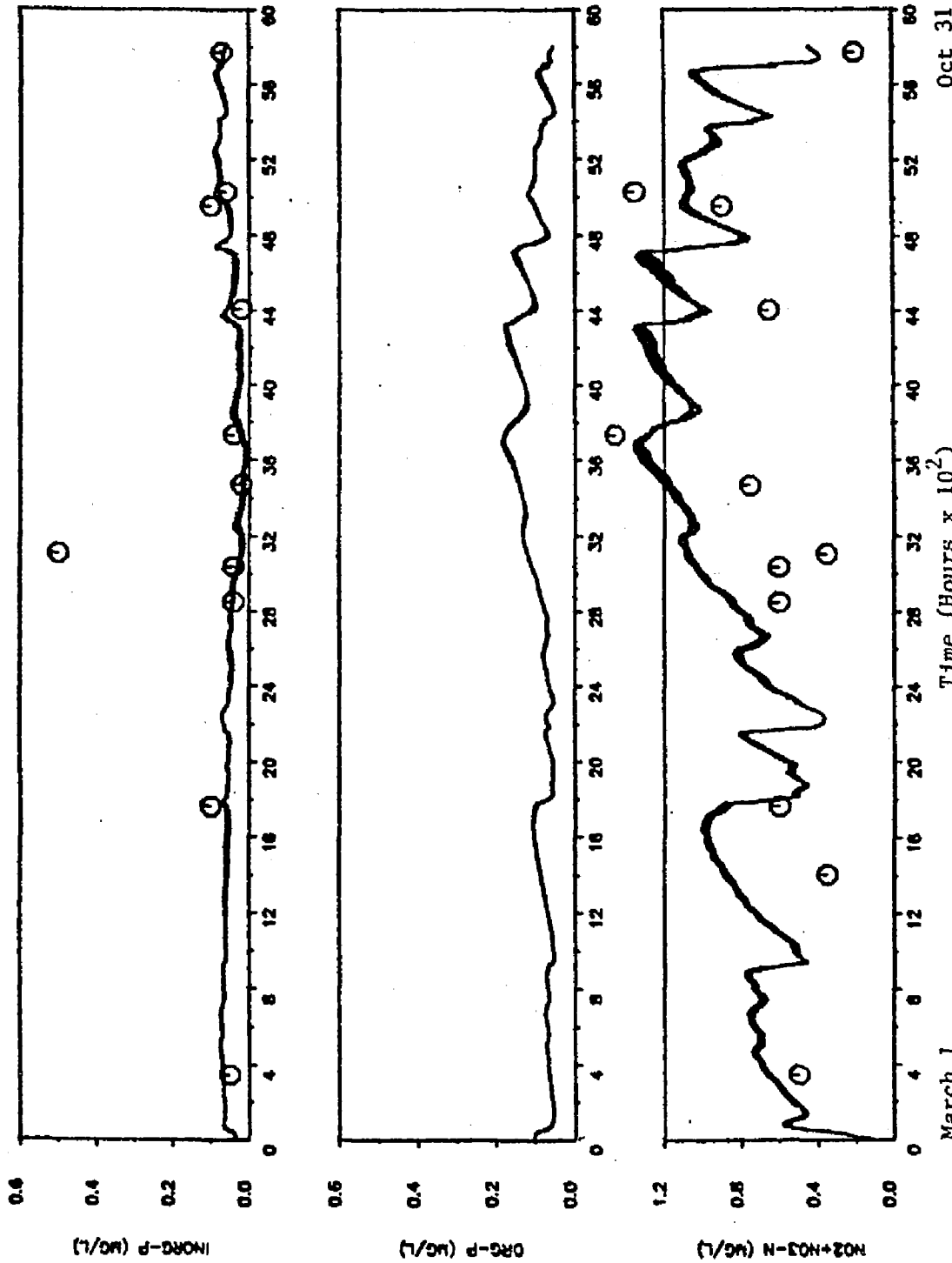
— computed; ○ observed.



March 1 Oct 31
Time (Hours x 10²)

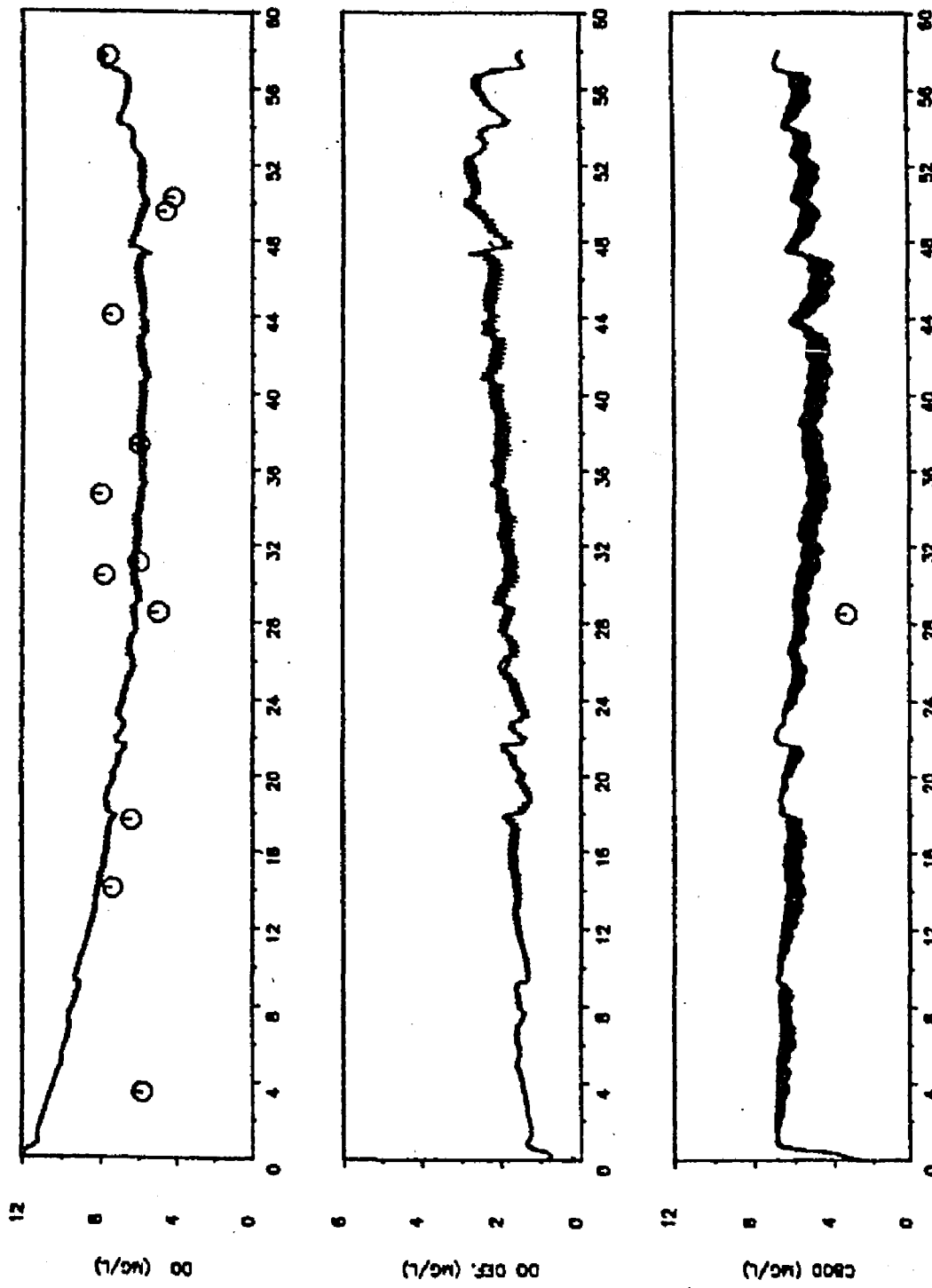
Figure 6.33 Computed and observed water quality constituents at node 26 in the James River.

— computed; ○ observed.



March 1
 Figure 6.33 (Cont'd) Computed and observed water quality constituents at node 26
 in the James River.
 Oct 31

— computed; ○ observed.



March 1 Oct 31
 Time (Hours x 10²)
 Figure 6.33 (Cont'd) Computed and observed water quality constituents at node 26
 In the James River.
 — computed; ○ observed.

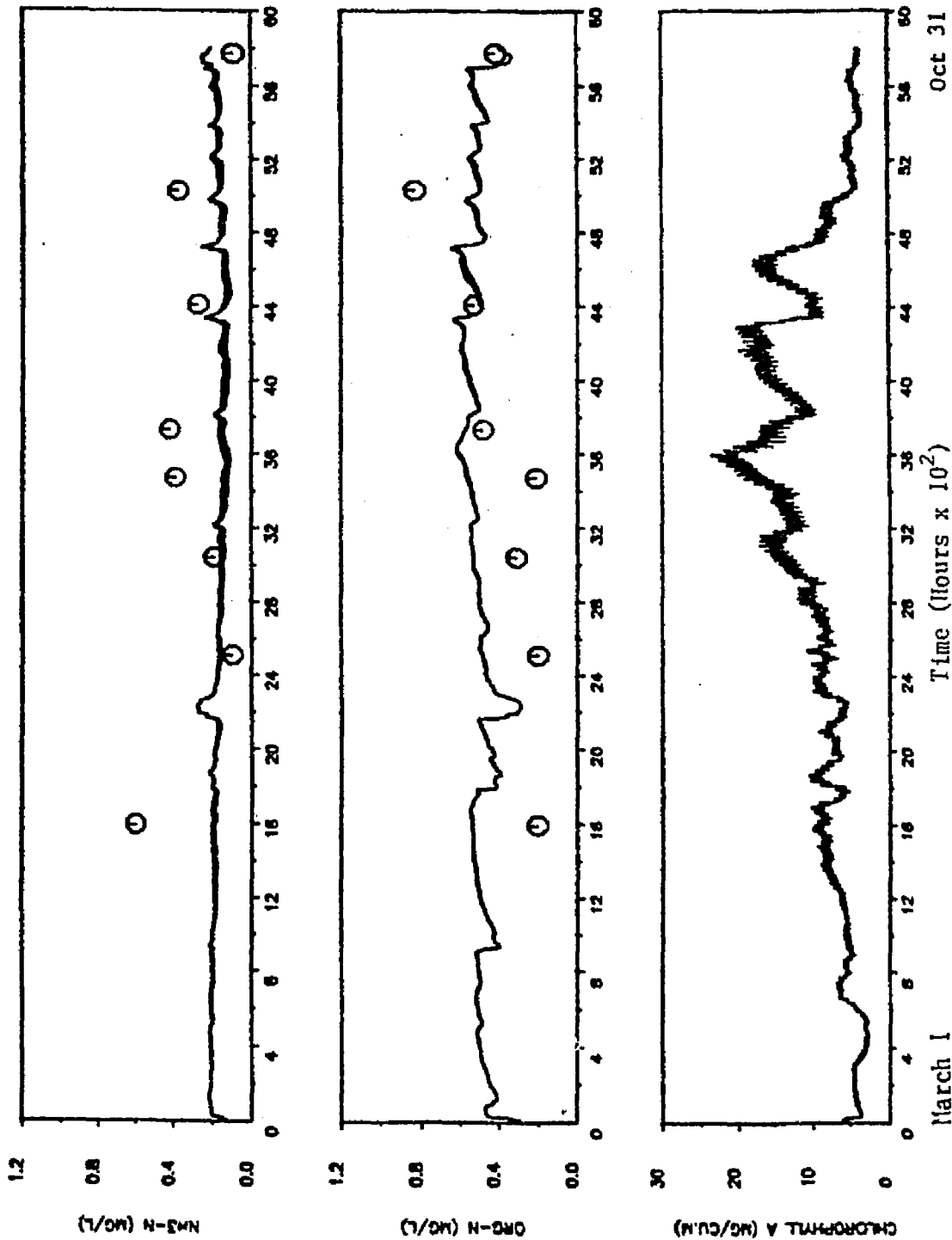
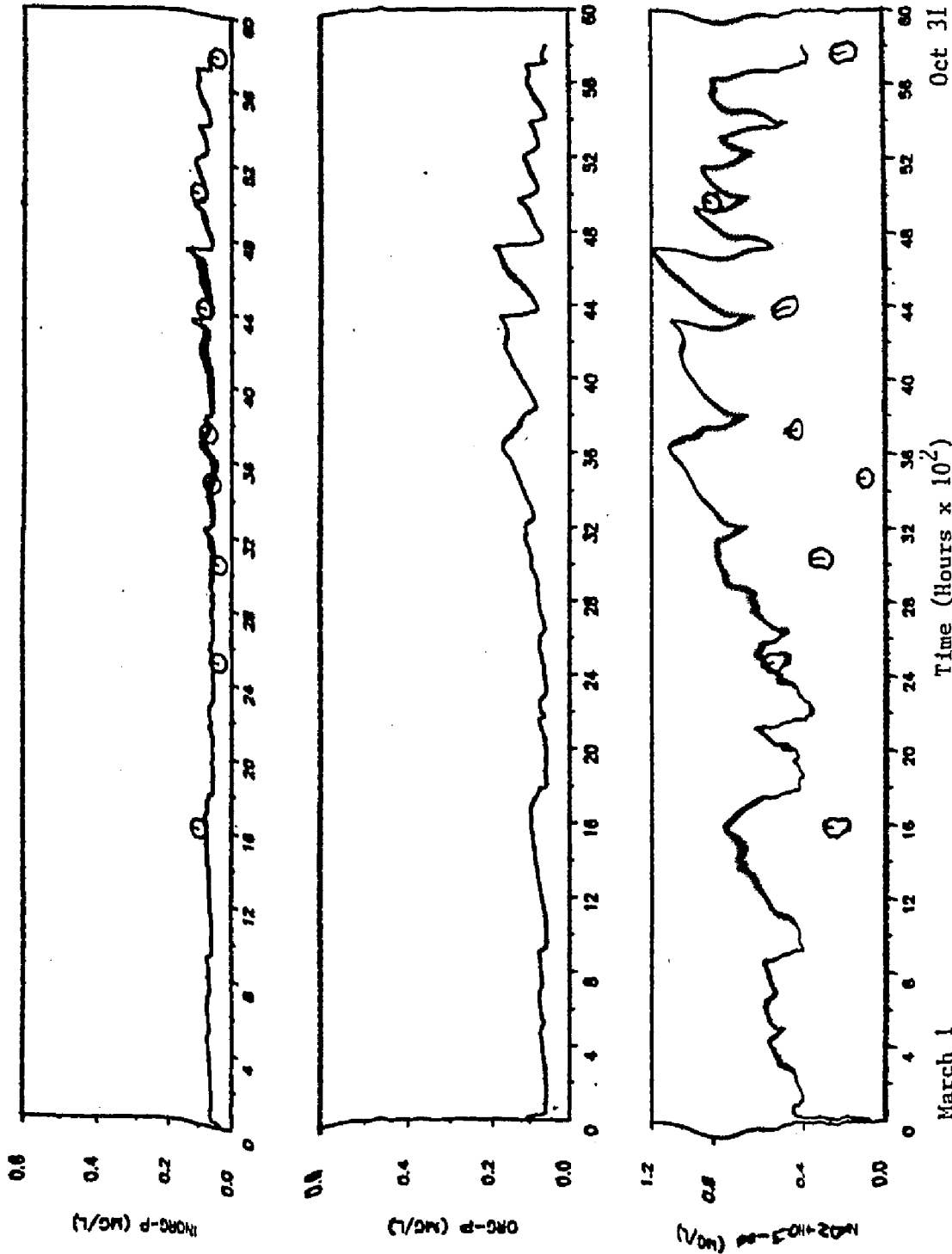
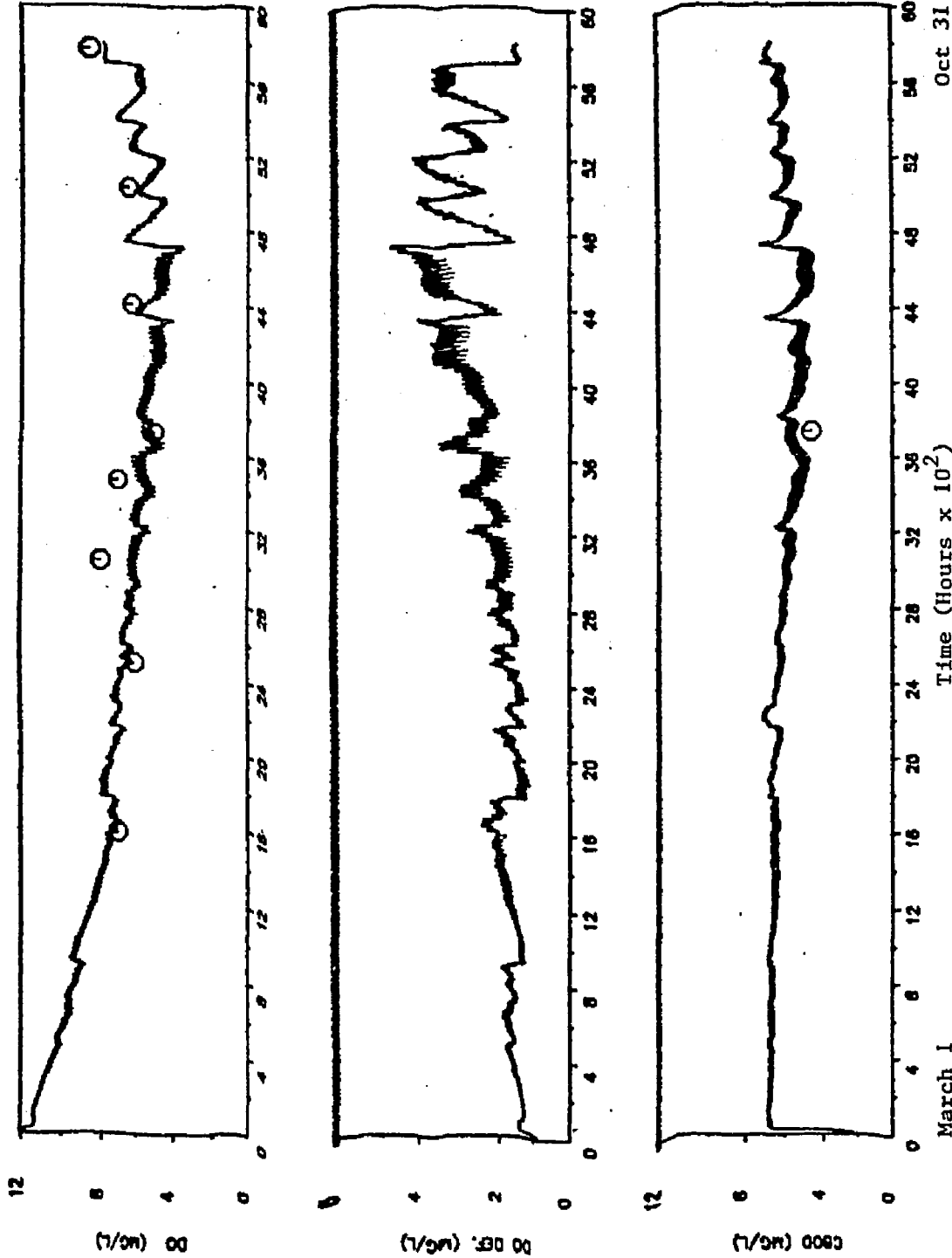


Figure 6.34 Computed and observed water quality constituents at node 32 in the James River.

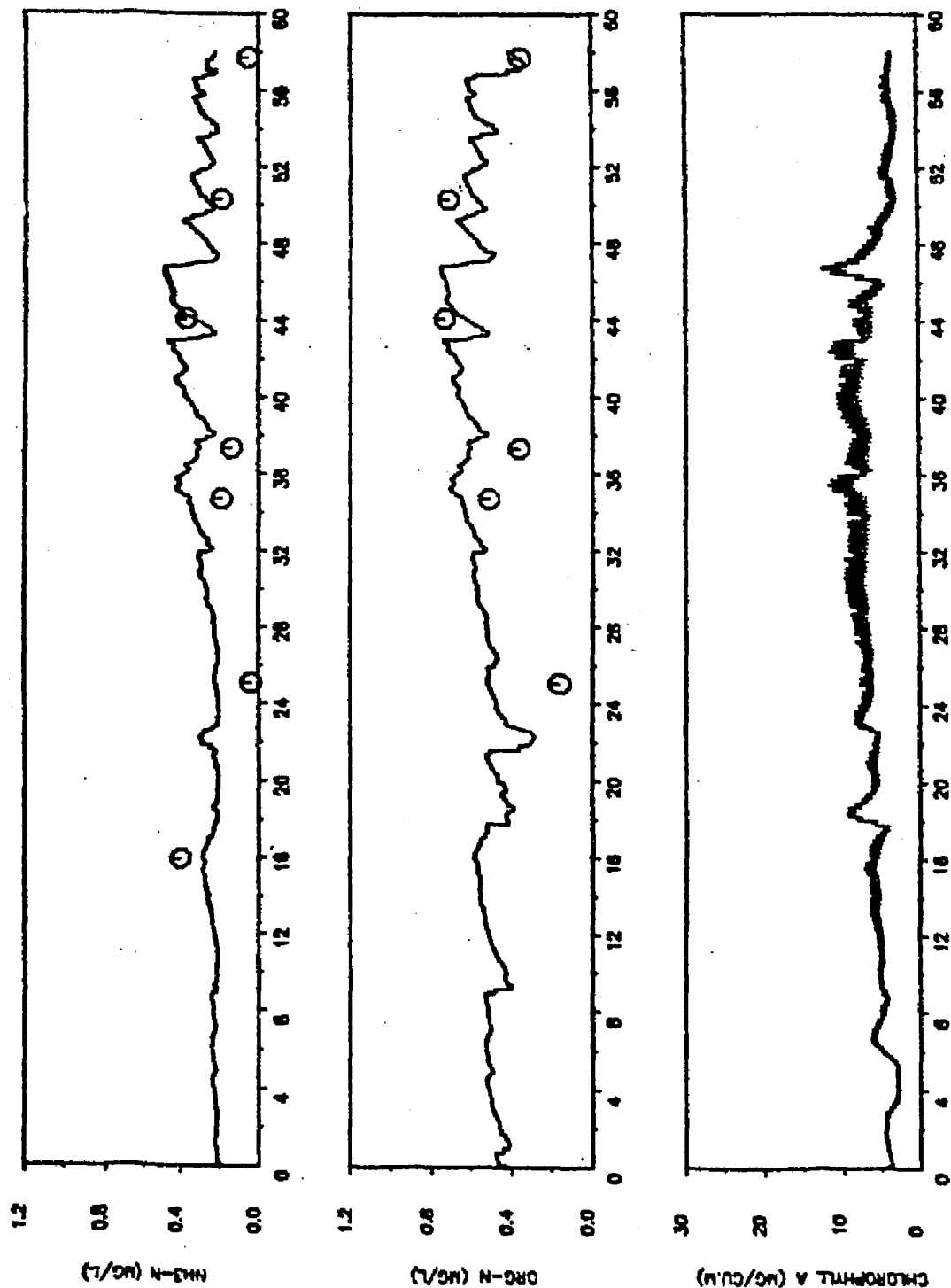


March 1 Oct 31
Figure 6.34 (Cont'd) Computed and observed water quality constituents at node 32 in the James River.

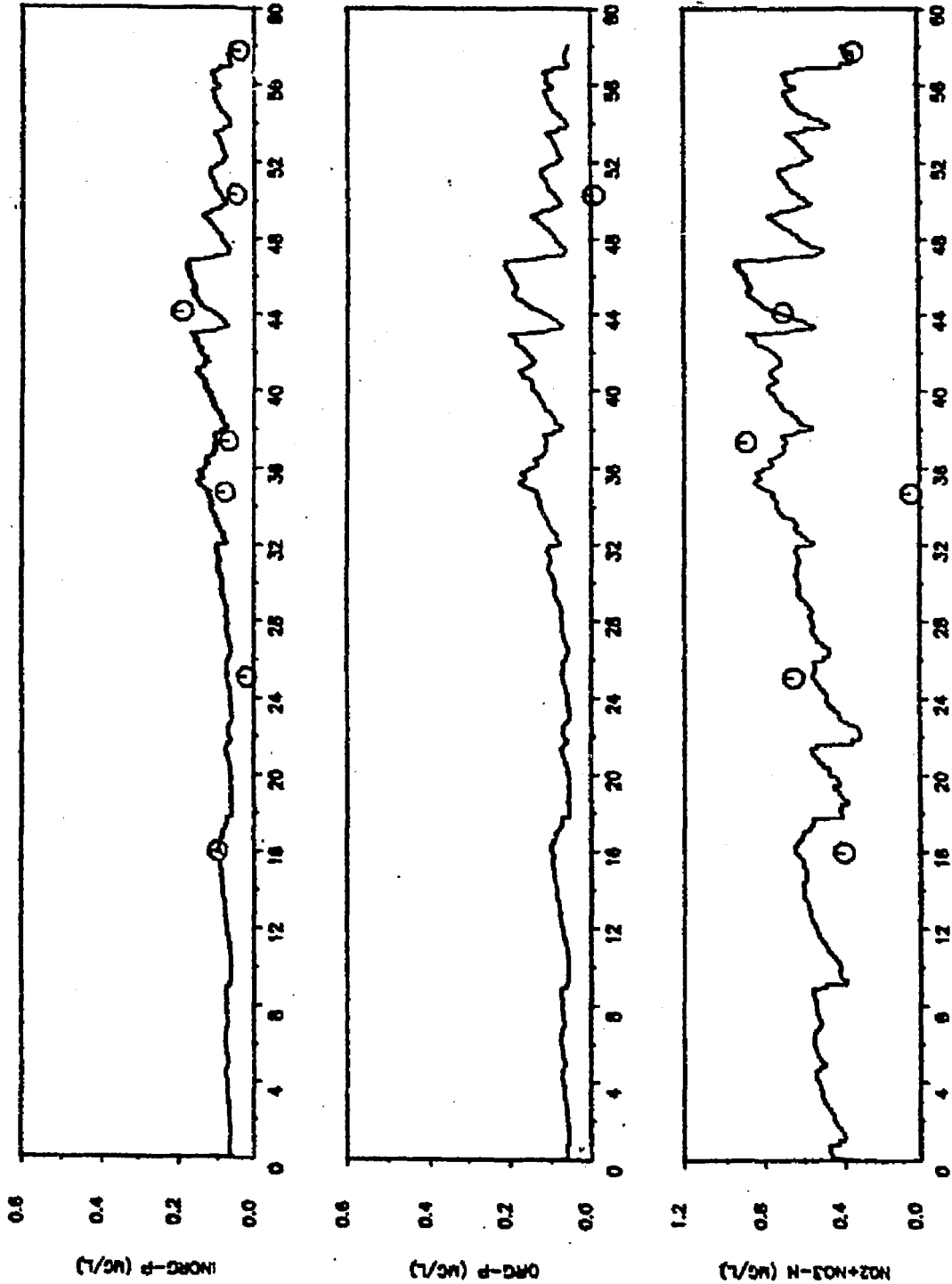
— computed; ○ observed.



March 1
 Oct 31
 Figure 6.34 (Cont'd) Computed and observed water quality constituents at node 32 in the James River.
 ——— computed; ○ observed.



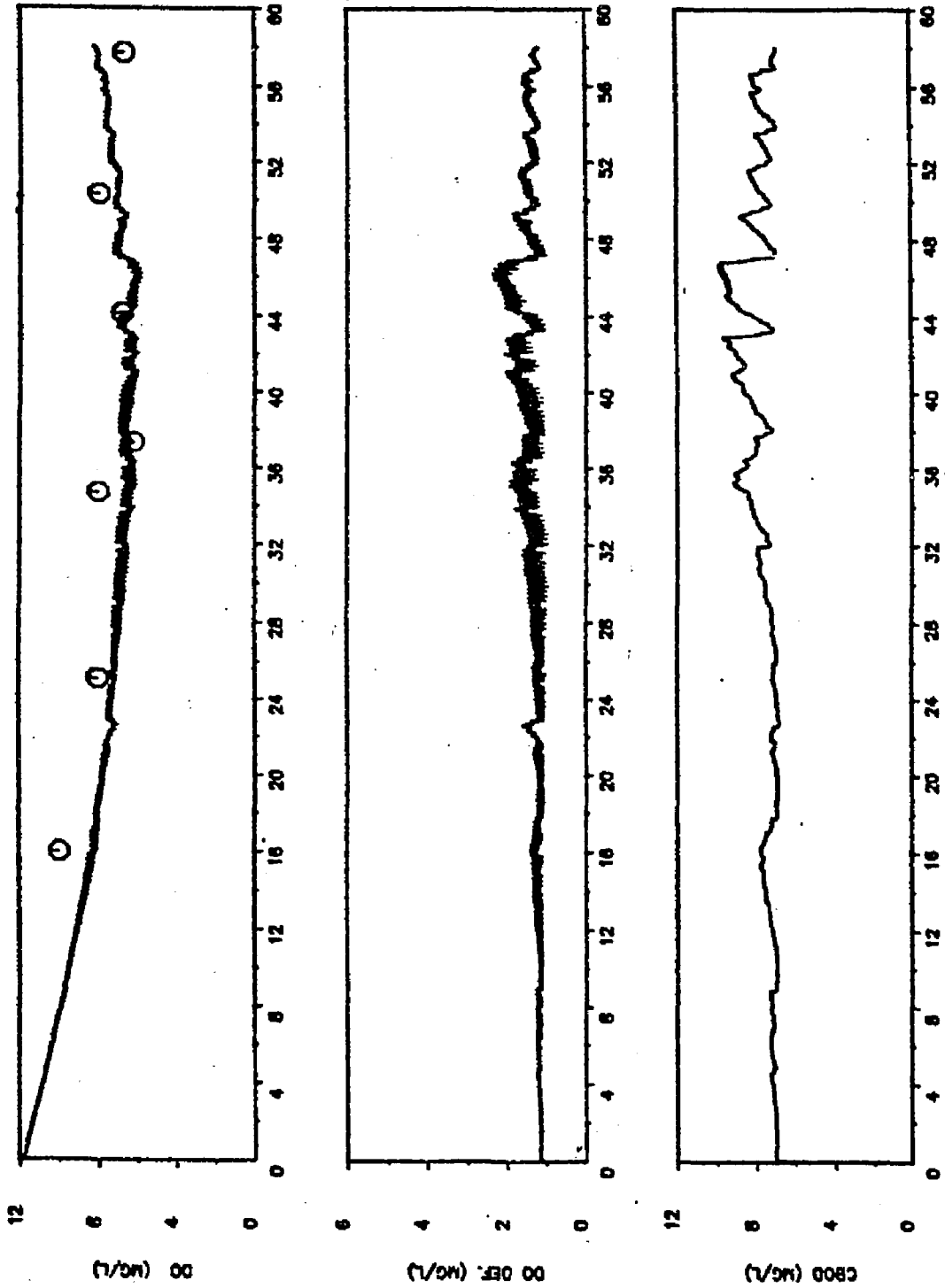
March 1 Oct 31
 Figure 6.35 Computed and observed water quality constituents at node 40
 in the James River.
 — computed; ○ observed.



March 1 Oct 31

Figure 6.35 (Cont'd) Computed and observed water quality constituents at node 40 in the James River.

— computed; ○ observed.



March 1
 Figure 6.35 (Cont'd) Computed and observed water quality constituents at node 40
 in the James River.
 Oct 31

Table 6.6 Calibration Parameters for the James River

Parameter	Symbol	Value	Unit
Dispersion coefficient	E	15-35	m ² /sec
Reaeration coefficient	k _g	10-30	
Coliform die off rate	not included in this study		
Phytoplankton optimum growth rate	k _g	0.121	1/day/ C
Extinction coefficient	k _e	1.0	1/m
Endogeneous respiration rate	k _r	0.004	1/day/ C
Zooplankton grazing rate	k _z	0.004	1/day/ C
Michaelis nitrogen constant	k _{mn}	0.018	mg/l
Michaelis phosphorous constant	k _{mp}	0.006	mg/l
Organic-N to NH ₃ -N hydrolysis rate	k ₂	0.0025	1/day/ C
Nitrogen chlorophyll ratio	r _n	0.01	mg/μg
NH ₃ to NO ₃ nitrification rate	k ₃	0.01	1/day/ C
Organic-P to inorganic-P conversion	k ₅	0.001	1/day/ C
Phosphorus chlorophyll ratio	r _p	0.003	mg/μg
CBOD oxidation rate	k ₇	0.1	1/day
Carbon chlorophyll ratio	r _c	0.05	mg/μg
Photosynthetic quotient	k _{op}	1.4	
Respiratory quotient	k _{or}	1.0	
Benthic oxygen demand	b _g	0.1-0.3	gm/m ² /day
Settling and escaping rates :			
Chlorophyll	k _{s1}	0.02-0.041/day	
Organic-N	k _{s2}	0.0-0.041/day	
Ammonia-N	k _{s3}	0.0-0.041/day	
NO ₂ -NO ₃ -N	k _{s4}	0.0-0.161/day	
Organic-P	k _{s5}	0.01-0.031/day	
Inorganic-P	k _{s6}	0.0-0.031/day	
CBOD	k _{s7}	0.0-0.251/day	
DO Deficit	k _{s8}	0.0-0.381/day	

7 NETWORK FORMULATION

In this chapter, the formulation of the network solution is described. With some modifications to the computer program, the water quality model developed in chapter 5 can be used to solve network problems.

The basic equation governing the water quality in an estuarine network is the same as that for a single channel (equation 3.13), but additional constraints are required at the junctions. At the junctions it is assumed that the concentrations of all the nodes connected to a junction are compatible. The compatibility condition at a junction j is expressed as

$$C_j^n = C_j \quad (7.1)$$

where

C_j is defined as the concentration at junction j and

C_j^n is the concentration of node n connected to j .

It is further assumed that at a junction, the mass flux is conserved, so that at any junction j

$$\sum Q_j^n C_j = 0 \quad (7.2)$$

where

Q_j^n = flow of node n into junction j .

The sign convention at the junction is defined such that positive flow is towards the junction. With these assumptions, the computer

program can be modified to handle channel networks.

The topology of the network can be described by a connectivity matrix; for example consider an arbitrary network of channels as shown in Figure 7.1.

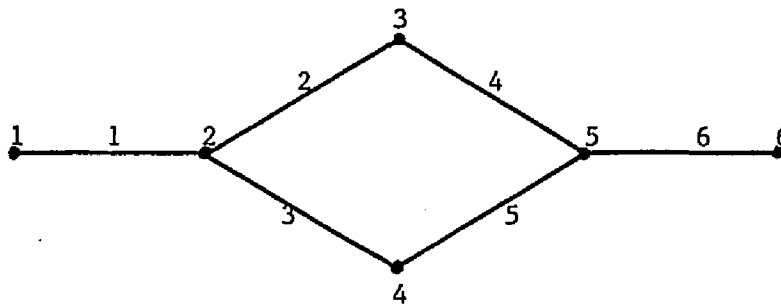


Figure 7.1 An arbitrary channel network.

Each element is designated by an element number, and each node is designated by a node number as shown. To describe how the elements are connected, a two-dimensional connectivity matrix is defined in Table 7.1.

Table 7.1 Connectivity Matrix

Element No.	Downstream Node No.	Upstream Node No.
1	1	2
2	2	3
3	2	4
4	3	5
5	4	5
6	5	6

The terms upstream and downstream are arbitrary, the sole purpose is to differentiate between the two nodes of an element.

Geometric properties are specified at the two ends of an element. For example, using the notation of subscripted variables in FORTRAN, the cross-sectional areas at the two ends of an element number L are $AREA(L,1)$ and $AREA(L,2)$ respectively. Other geometric properties are specified for the two ends in a similar fashion.

With these modifications, the element equations can be assembled in a similar way as described in chapter 4.

7.1 Verification of Network Model

Verification of models is usually carried out by comparing the calculated results with analytical solutions. However, since there is no analytical solution to network problems in general. Therefore in order to verify the network formulation, networks that are mathematically equivalent to a single channel have to be devised. In this study two such networks as shown in Figure 7.2 are used.

These two networks are mathematically equivalent to the problem as described in section 5.1, but they are represented in the computer program as network problems. After discretizing the networks, the two cases were run. The results of these two cases were found to be identical to the ones described in section 5.1. Therefore this gives assurance that the formulation of the network model is correct.

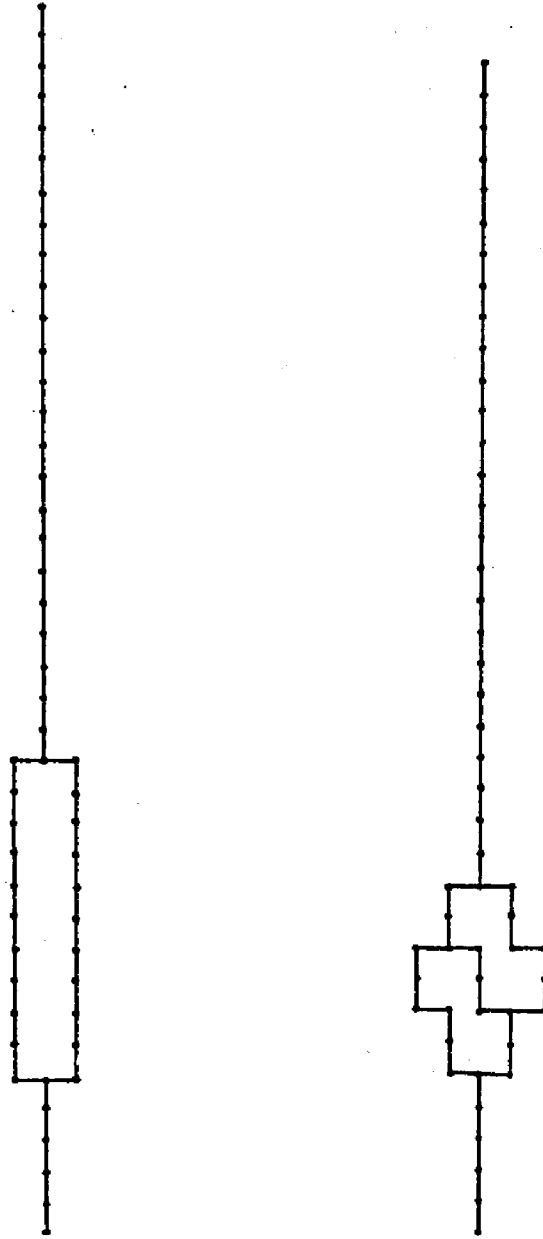


Figure 7.2 Two example channel networks used in the model.

8 THE APPLICATION TO APPOMATOX RIVER

This chapter outlines the application of the one dimensional water quality network model to the Appomatox River. The emphasis here is to demonstrate the use of the model, rather than a comprehensive study of the phytoplankton dynamics of the river. Figure 8.1 shows the lower portion of the Appomatox River which extends from the mouth at the city of Hopewell to the city of Petersburg. This portion of the river consists of two main channels and several smaller interconnecting channels, forming a very complicated network. This portion of the river is tidal but the water is fresh. The depth of the river varies from about 9 meters at the mouth to about 2 meters at Petersburg. The width of the river varies from about 700 meters at the mouth to about 60 meters at Petersburg. Cross-sectional areas vary from 1,500 square meters at the mouth to about 70 square meters at Petersburg. The mean tidal range is 0.79 meters at the mouth and 0.88 meters at Petersburg. There is a gauging station at Matoaca about 10 kilometers upstream from the study area. The average fresh water inflow at Matoaca in August 1977 is 4.72 cubic meters per second.

The model was calibrated using data from an intensive survey conducted on August 17, 1977. Due to the many uncertainties in the input waste loadings, it was decided to use tidal average conditions for calibration. The point source loadings used were average values of samples collected during the survey. The nonpoint source loadings were

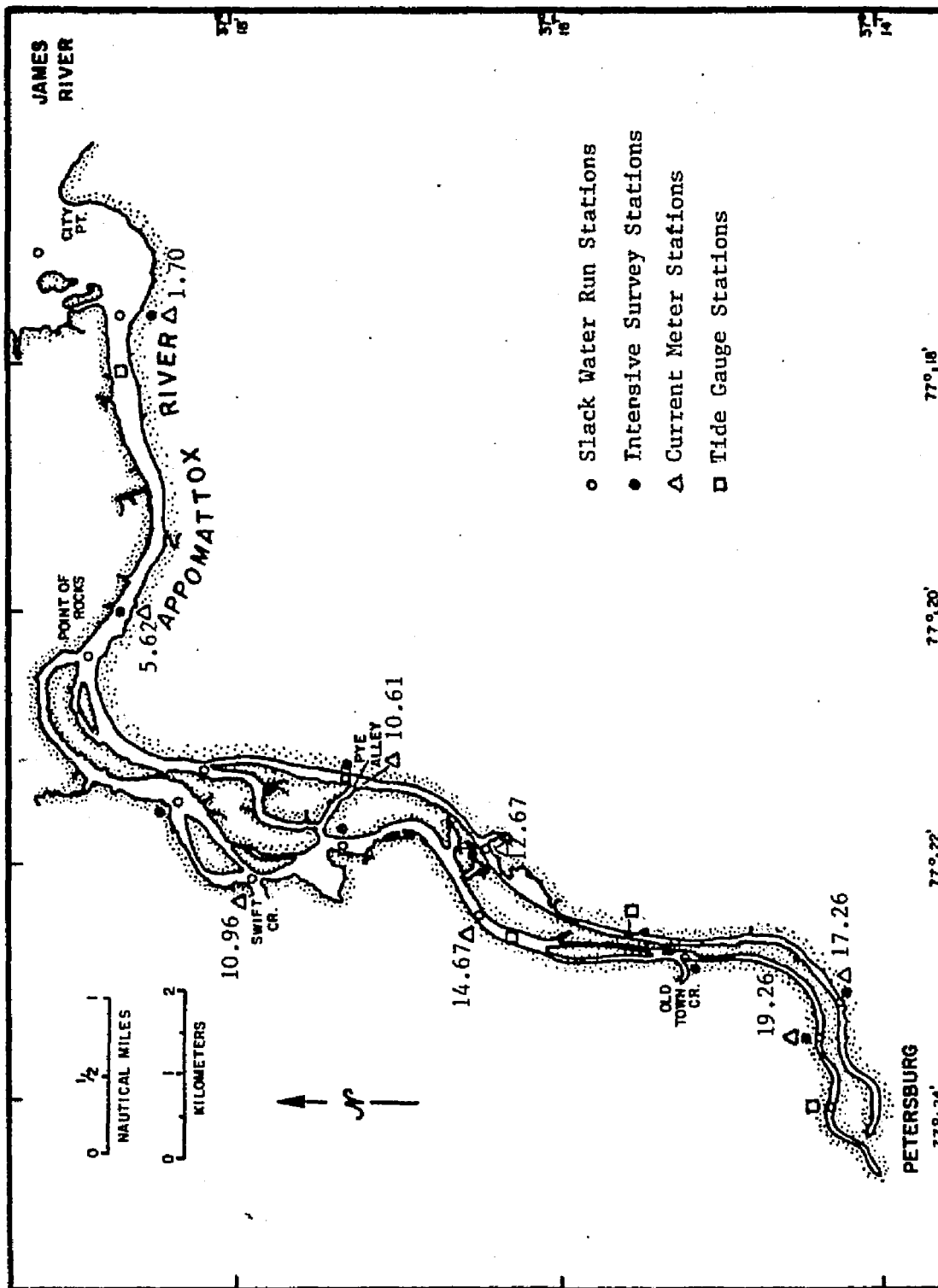


Figure 8.1 Location of sampling stations in the Appomattox River.

estimated based on the characteristics of the area. The boundary conditions and waste inputs were held constant throughout the calibration period. The model was run until a dynamic equilibrium was achieved and the average values of the last tidal cycle was then compared with the field data.

8.1 The Finite Element Network

Laying out a good network is essential for an efficient solution and requires experience from the analyst. The following are some guidelines for laying out the grid.

(a) Boundaries should be placed as far as possible away from the area of interest, since some inaccuracies are to be expected in the data used for the specification of the boundary conditions.

(b) A node must be placed at every junction, and there should be at least two elements within any branch.

(c) There should be more elements at locations where concentration gradients are expected to be large, for example near wastewater outfalls.

(d) Lengths of adjacent elements should change gradually.

Figure 8.2 shows the finite element network used to represent the Appomattox River in this study. A total of 41 elements and 38 nodes is used. The lengths of the elements varies from about 320 meters to 1,600 meters. The downstream boundary is at node 1, and there are two upstream boundary nodes, numbers 35 and 38.

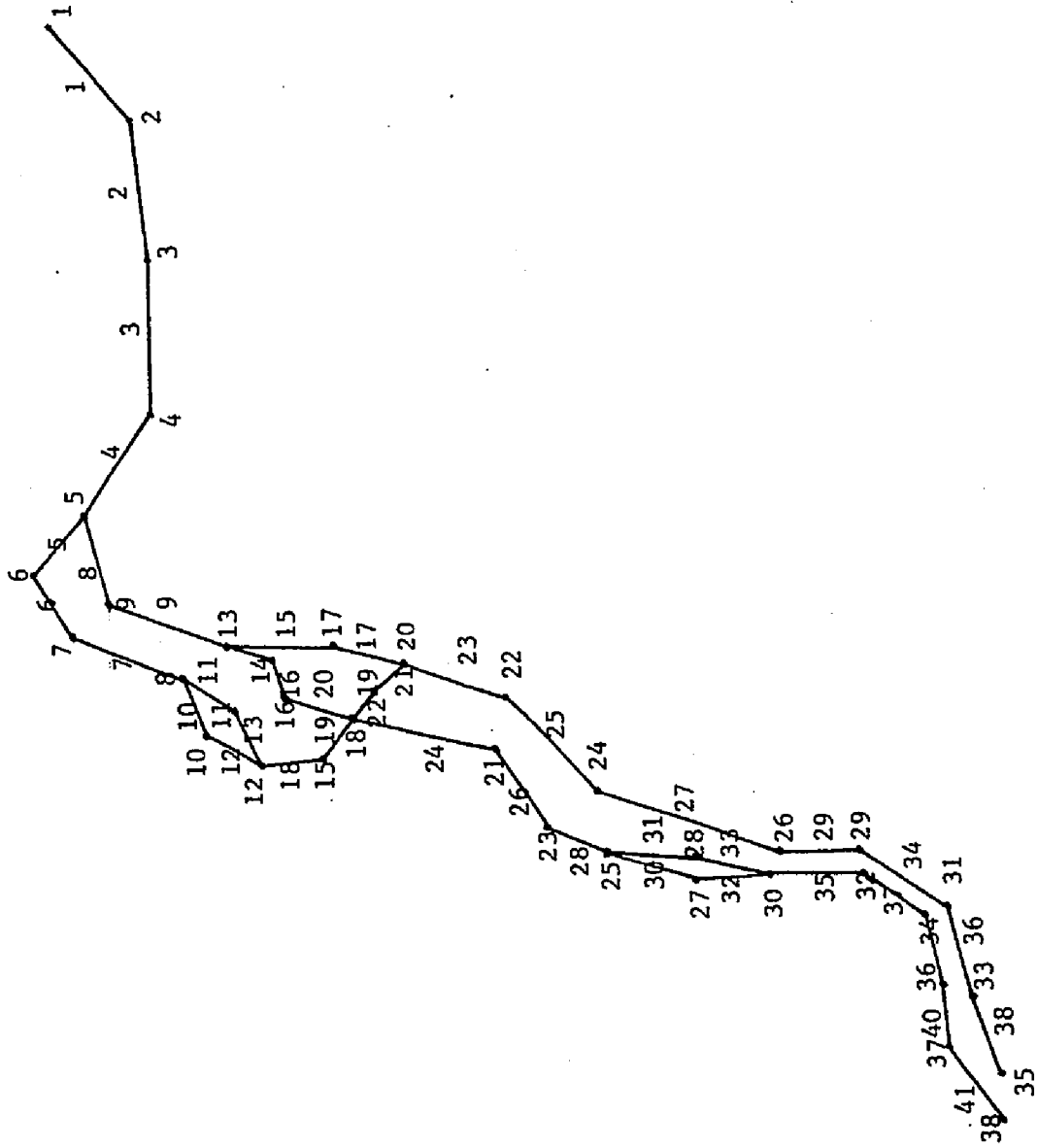


Figure 8.2 Model segments for the Appomattox River.

8.2 Water Quality Data

Two intensive water quality surveys were conducted in 1977, the first was on July 14-15, the second on August 16-17. There were eight intensive sampling stations (Figure 8.1). Samples at each station were collected at one hour intervals for 24 consecutive hours. At each station samples were taken at 1 meter below surface, mid-depth and at 1 meter above bottom when the water was deep; otherwise the samples were taken from mid-depth. The samples were analysed for the following constituents

- (1) chlorophyll 'a',
- (2) TKN,
- (3) ammonia nitrogen,
- (4) nitrate nitrogen,
- (5) nitrite nitrogen,
- (6) total phosphorous,
- (7) orthophosphorous,
- (8) CBOD5 and
- (9) DO.

In addition, Secchi disk visibility and temperature were also measured. Long term CBOD (30 days) were determined for a few samples for estimating the CBODU/CBOD5 ratio. When necessary, field data were converted to the model variables using the following assumptions

organic nitrogen = TKN - ammonia nitrogen,

inorganic phosphorous = orthophosphorous,

average CBODU/CBOD5 = 2.31 and

organic phosphorous = total phosphorous - orthophosphorous.

8.3 Fresh Water Inflow

There is a flow gauging station at Matoaca, approximately 10 kilometers upstream from Petersburg. The fresh water inflow values used in the model were estimated from the measurements at this station. For the purposes of simulating tidal average conditions, the average flow of August 1977 was used. The inflow into each model element was estimated by proportioning to the drainage area subtended by the element. The estimated fresh water inflows were 4.7 cubic meters per second for the most upstream element and 5.7 cubic meters per second for the most downstream element.

8.4 Point Sources

The locations of five point source discharges to the lower portion of the Appomatox River are shown in Figure 8.1. Table 8.1 is a listing of the waste discharges that were used as input data for the model calibration. These values were taken from the Virginia State Water Control Board reported monthly average discharges for August 1977 (unpublished data).

Table 8.1 Point Source Loadings for the Appomatox River (kg/day).

Ele No.	Flow (m ³ /sec)	Org-N	NH ₃ -N	NO ₂ -NO ₃ -N	Org-P	Inorg-P	CBOD
1	.356	1.7	1.7	.01	0.5	1.2	23.5
7	.010						123.1
15	.0059	3.67	4.18	0.03	0.83	2.13	56.8
35	.0027	2.80	2.80	0.02			28.0
39		29.96	3.15	250.08	0.94	185.55	214.4

8.5 Non-Point Sources

No non-point source data was available. However, since the magnitude of non-point sources is known to be quite large in general, sometimes even at an order of magnitude larger than the point sources, therefore an attempt was made to estimate the amount of these sources using data from adjacent rivers. The effects of these estimates can be best examined in the sensitivity analyses. Two types of non-point sources identified in the study area were the exports from the marsh areas that line the banks of the river and the urban runoffs from the cities of Hopewell and Petersburg.

Inputs From Marsh Areas: A large portion of the river is lined with marshes. The rate of nutrient exports is estimated using data from Glebe Gut, a fresh water marsh on the James River. Because of its proximity, it is assumed that the marshes on the the Appomatox River have similar characteristics. Sweeney (1978) measured the amount of CBOD5, ammonia nitrogen, and TKN exported to the James estuary from Glebe Gut. The nutrient export values on a kg/ha/day basis are shown in Table 8.2.

Table 8.2 Nutrient Export From Glebe Gut. After Sweeny (1978).
(kg/ha/day)

CBOD5	NH ₃ -N	TKN
0.139	-0.024	0.106

A negative sign means that there is a net import of nutrients to the marshes. The inputs to the Appomatox River were calculated by

multiplying the values in Table 8.2 with the corresponding marsh areas. The marsh areas in the Appomatox was planimetered from National Ocean Survey chart No. 12251. The estimated nutrient exports to the various elements in the model are shown in Table 8.3

Table 8.3 Estimated Nutrient Loadings From Marshes (kg/day).

Element No.	Marsh area (km ²)	CBOD5	NH ₃ -N	TKN
1	0.8	11.1	-1.9	8.5
2	0.2	2.8	-0.5	2.1
3	0.6	8.3	-1.4	0.6
4	0.3	4.1	-0.7	3.2
7	0.3	4.1	-0.7	3.2
8	0.2	2.8	-0.5	2.1
11	0.2	2.8	-0.5	2.1
13	0.1	1.4	-0.2	1.1
16	0.1	1.4	-0.2	1.1
24	0.1	1.4	-0.2	1.1
25	0.1	1.4	-0.2	1.1
27	0.1	1.4	-0.2	1.1
37	0.2	2.8	-0.5	2.1
36	0.1	1.4	-0.2	1.1
37	0.2	2.8	-0.5	2.1

Urban Runoffs : The estimate of urban runoffs is based on the data of Jaworski (1971). The values of nutrient loadings from an urban area on a kg/ha/day basis are given in Table 8.4.

Table 8.4 Estimated Nutrient Loadings from Urban Runoff (kg/ha/day)

Total-P	NO ₂ -NO ₃ -N	TKN	BOD5
0.0056	0.011	0.034	0.068

The surface area of the city of Hopewell immediately adjacent to the river that is assumed to drain into the river is estimated to be about 30 square kilometers. These loads were assumed to spread evenly into the lower portion of the river. The surface area of the city of Petersburg draining into the upper portion of the river is estimated to be about 20 square kilometers. These loads are assumed to spread evenly into the upper portion of the south branch of the river. The estimated urban contributions into the various elements are shown in Table 8.5.

Table 8.5 Estimated Nutrient Loadings from Urban Runoff (kg/day)

Element No.	Total-P	NO ₂ -NO ₃ -N	TKN	BOD5
1	4.2	8.3	25.5	51.0
2	4.2	8.3	25.5	51.0
3	4.2	8.3	25.2	51.0
4	4.2	8.3	25.2	51.0
34	3.7	7.3	22.7	45.3
36	3.7	7.3	22.7	45.3
38	3.7	7.3	22.7	45.3

The above two types of non-point sources were combined as the total non-point sources and converted into the forms required by the model. The resultant total non-point source loadings are shown in Table 8.6

Table 8.6 Estimated Total Nonpoint Source Loadings (kg/day).

Element	Org-N	NH ₃ -N	NO ₂ -NO ₃ -N	Org-P	Inorg-P	CBODU
1		15.3	8.3	3.8	0.4	143.4
2		16.7	8.3	3.8	0.4	124.3
3		15.8	8.3	3.8	0.4	137.0
4		16.5	8.3	3.8	0.4	127.3
7	3.2					9.5
8	2.1					6.5
11	2.1					3.2
13	1.1					3.2
16	1.1					3.2
24	1.1					3.2
25	1.1					3.2
27	1.1					3.2
34		15.4	7.3	3.3	0.4	104.6
36		15.2	7.3	3.3	0.4	107.8
37	2.1					6.5
38		15.4	7.3	3.3	0.4	104.6

8.6 Initial Conditions

In order to save computer time, the average intensive water quality data were used as initial conditions. Values at all nodal points in the model were estimated by interpolating between the values at sampling stations.

8.7 Boundary Conditions

The downstream boundary conditions used were the average intensive values collected during Aug 16-17, 1977. The values of organic phosphorous and inorganic phosphorous which were not measured during the intensive survey, were estimated from some grab samples taken during the survey. Upstream boundary conditions were estimated in a similar fashion. The values of the boundary nodes are given in Table 8.7.

Table 8.7 Boundary Concentrations.

Node No	Chlorophyll (ug/l)	Org-N (mg/l)	NH ₃ -N (mg/l)	NO ₂ -NO ₃ (mg/l)	Org-P (mg/l)	Inorg-P (mg/l)	CBOD (mg/l)	DO.DEF (mg/l)
1	28.57	0.81	0.19	0.21	0.1	0.01	7.2	3.67
35	1.62	1.32	0.38	0.27	0.1	0.01	0.5	4.16
38	1.62	0.23	0.10	0.66	0.1	0.01	0.5	4.16

8.8 Tidal Elevations and Tidal Currents

Tidal elevations and currents in the water quality model were calculated using sinusoidal functions. The tidal elevation at each node i in the model is calculated using equation:

$$\eta_i = b_i \sin \frac{2\pi}{T} (t - \theta_i + \gamma_i) \quad (8.1)$$

where

η_i = water surface above mean water level,

b_i = tidal amplitude,

θ_i = phase difference between tide at the mouth and node i ,

t = time, hr,

T = tidal period, 12.42 hr and

γ_i = phase difference between tidal current and tidal velocity, assumed constant.

The tidal amplitudes and frequencies are obtained from field measurements. Tidal elevations were measured at two separate occasions, June 27 - July 20, 1977 and August 8-18, 1977. Harmonic analysis of the tide records has shown that the semidiurnal component (M_2) accounts for more than 80% for the variations. Therefore it was decided to use the semidiurnal tide in the simulation. The measured tidal amplitudes at

stations 1.75, 14.46, 14.67 and 19.98 (see Figure 8.1) are shown in Table 8.8. Tides at all other locations are estimated assuming a linear variation of the tidal amplitude between stations.

Table 8.8 Mean Tidal Amplitudes.

Station	Date	Mean Amplitude (m)
1.75	6/27/77 - 7/20/77	0.488
1.75	8/09/77 - 8/18/77	0.378
14.46	8/09/77 - 8/18/77	0.424
14.67	6/29/77 - 7/17/77	0.421
20.58	8/11/77 - 8/18/77	0.381

The tidal velocities at each node in the model are calculated similarly using equation

$$U_i = a_i \sin \frac{2\pi(t - \theta_i)}{T} + U_{fi} \quad (8.2)$$

where

t = time (hour),

U_i = tidal velocity at node i (m/hr),

a_i = velocity amplitude of node i (m/hr),

U_{fi} = fresh water inflow velocity at node i (m/hr) :

$$U_{fi} = Q_{fi}/A_i$$

Q_{fi} = fresh water inflow from the drainage area upstream of the node i (m^3/hr) and

A_i = instantaneous cross-sectional area at the node i (m^2).

The cross-sectional area is calculated by:

$$A_i = A_{oi} + B_i \eta_i \quad (8.3)$$

where

A_i = cross-sectional area below mean tide level (m^2) and

B_i = top width at node i (m).

The amplitudes and frequencies of currents are obtained from field measurements. Currents were measured during two separate occasions; July 13-20 and August 11-18, 1977. The current amplitudes measured at stations 1.70, 5.60 and 10.61 are shown in Table 8.9. The amplitudes at other stations are calculated assuming a linear variation of amplitudes along the length of the river.

Table 8.9 Mean Current Amplitudes (m/sec).

Station	Jul 13-20,77	Aug 11-18,77
1.72	0.333	0.346
5.60	0.392	0.448
10.61	-	0.337

8.9 Calibration Results.

Calibration was carried out by adjusting the parameters in a trial and error manner. Starting with the initial conditions, the model was run until a dynamic equilibrium was achieved, the average values of the last tidal cycle was then compared with the field data. This type of calibration can only represent the average conditions. The extent to

which a model can be calibrated depends on the availability of field data. Ideally all the model parameters should be measured, however, due to the expenses involved, a complete set of measurements is seldom available and therefore in practice many parameter values are derived from reported literature values. In this study, all model parameters were derived from reported literature values. During the calibration process, all parameters were kept within the reported ranges. The use of literature values generally assures an order of magnitude accuracy for a parameter. A more rigorous analysis of phytoplankton dynamics is beyond the scope of this study.

The list of the calibrated parameters are presented in Table 8.10 and the plots of the model results together with the ranges of the field data are given in Figures 8.3 through 8.8. Model results in general agree well with the field data. The only exceptions are the values of nitrite-nitrate nitrogen at kilometer 17 on the north branch, and the values of organic nitrogen at kilometer 17 on the south branch. These could be due to the estimated waste loadings were too low.

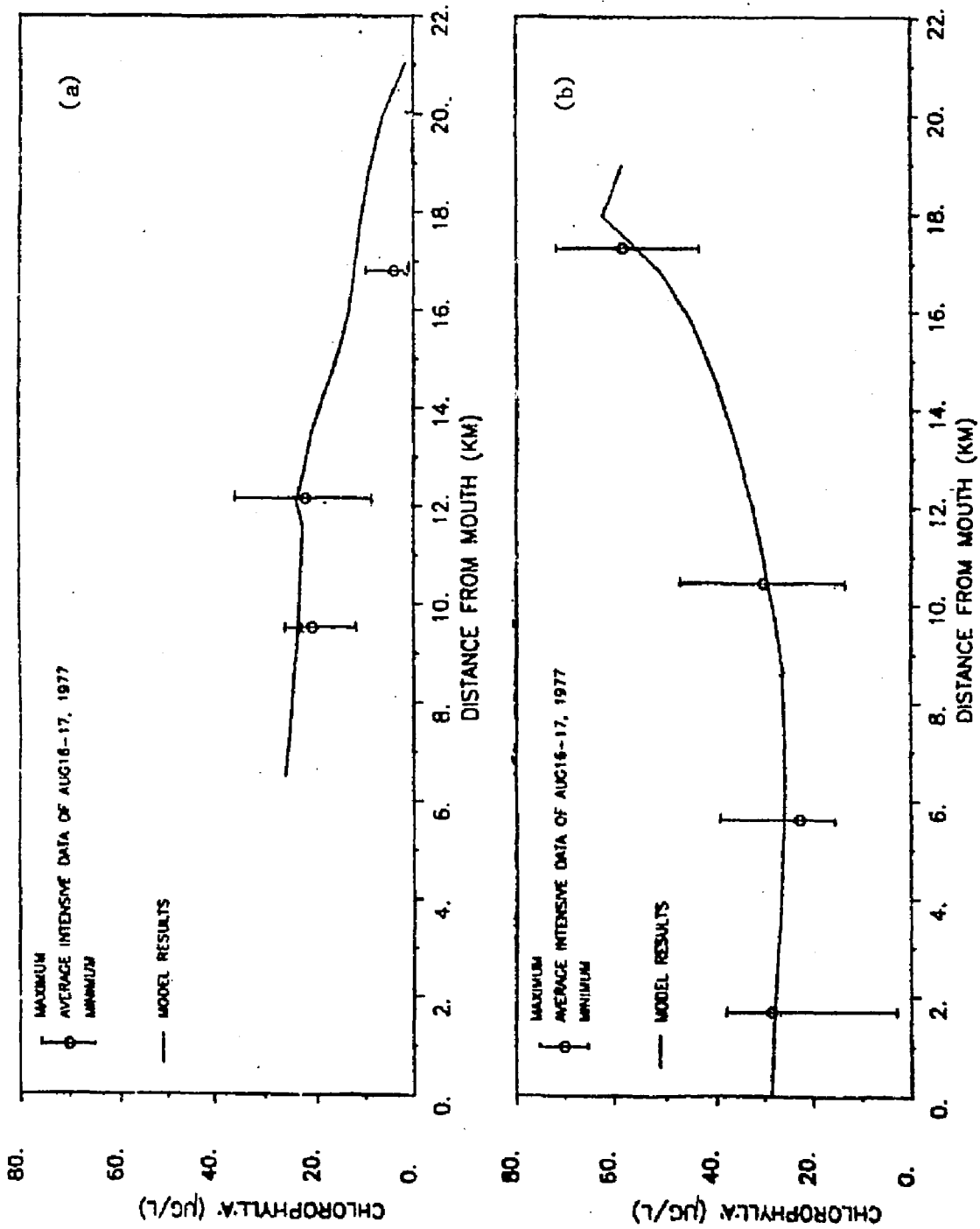


Figure 8.3 Computed vs observed Chlorophyll 'a' concentrations, (a) North branch, (b) South branch.

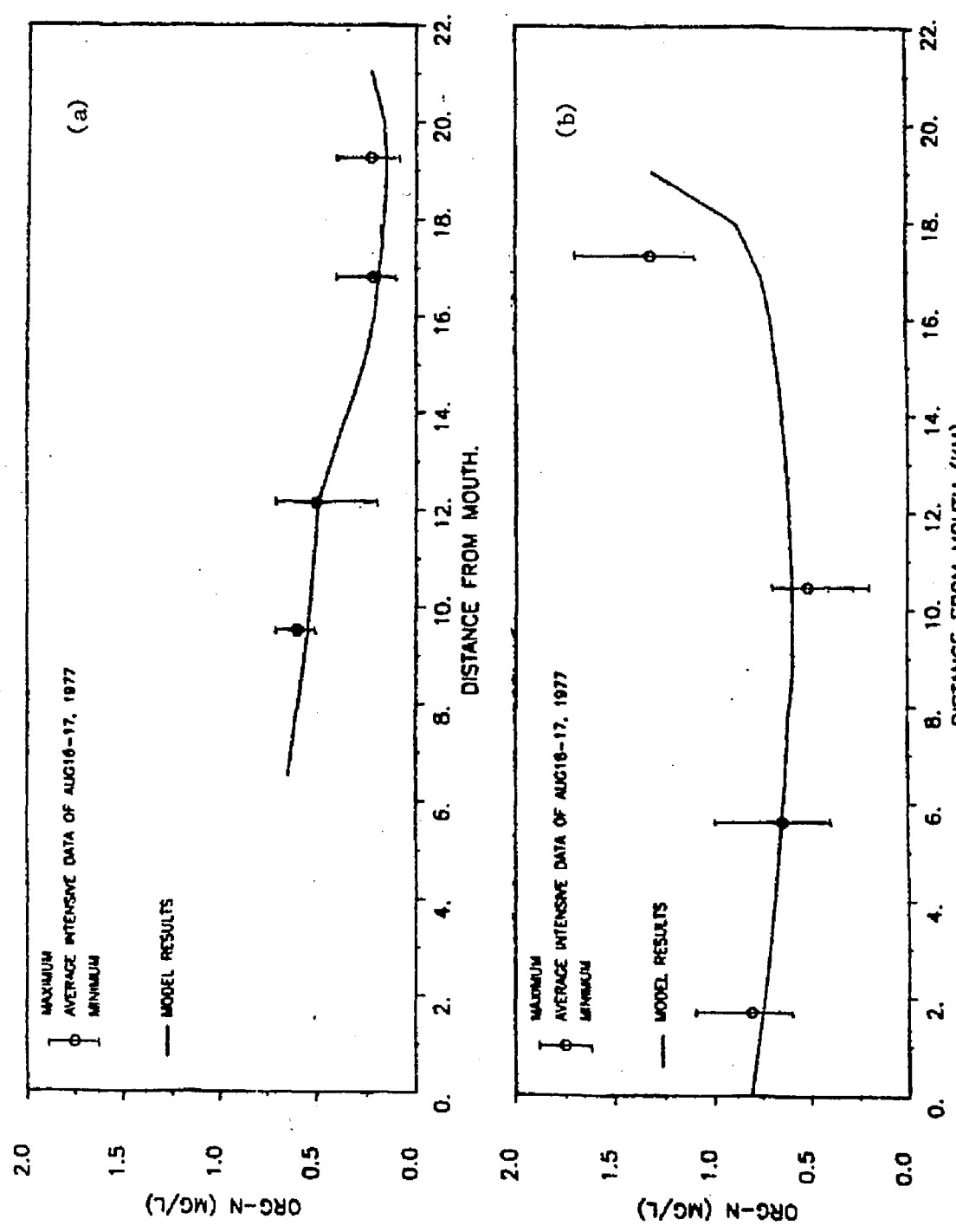


Figure 8.4 Computed vs observed Organic-N concentrations, (a) North branch, (b) South branch.

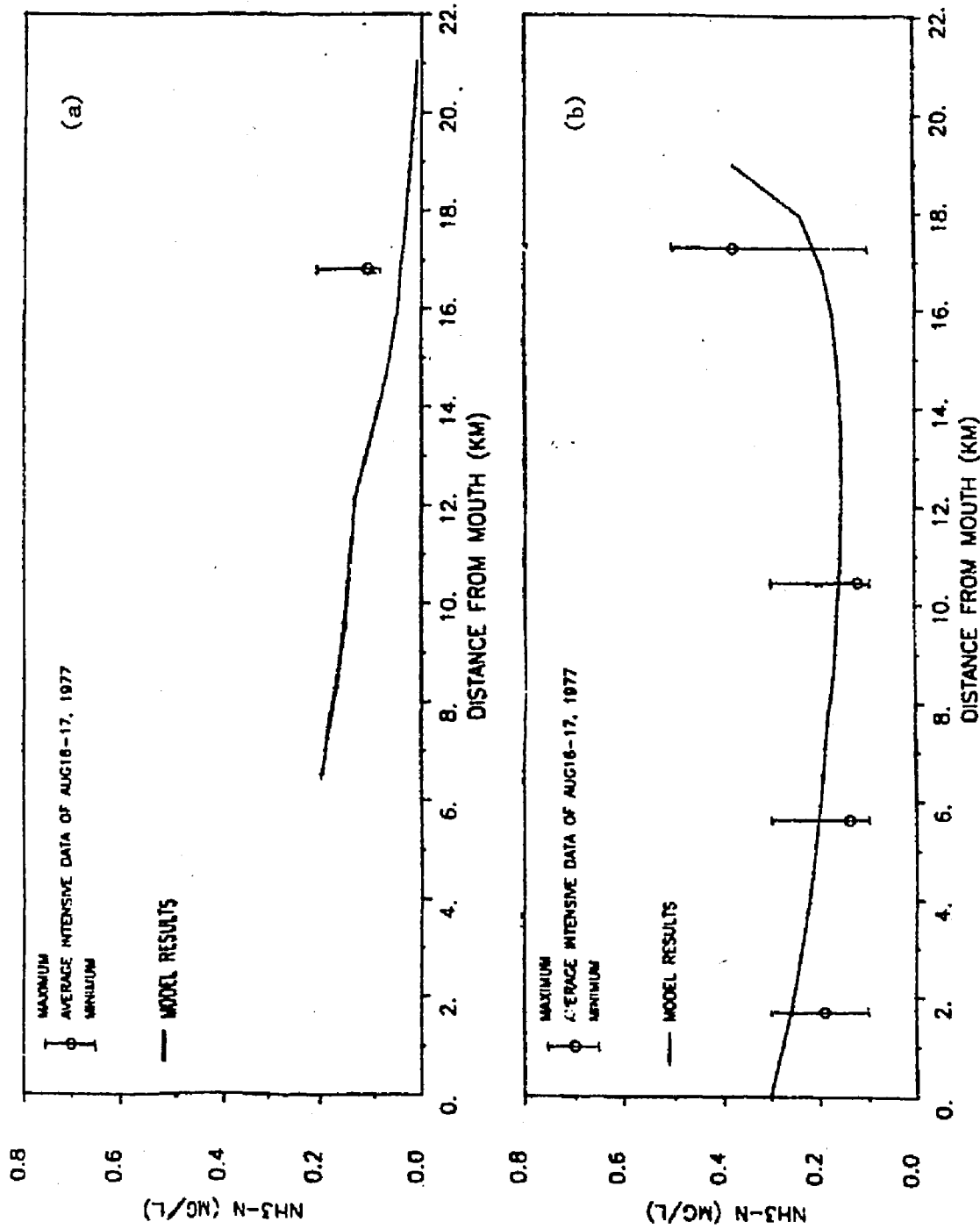


Figure 8.5 Computed vs observed Ammonia-N concentrations
 (a) North branch, (b) South branch.

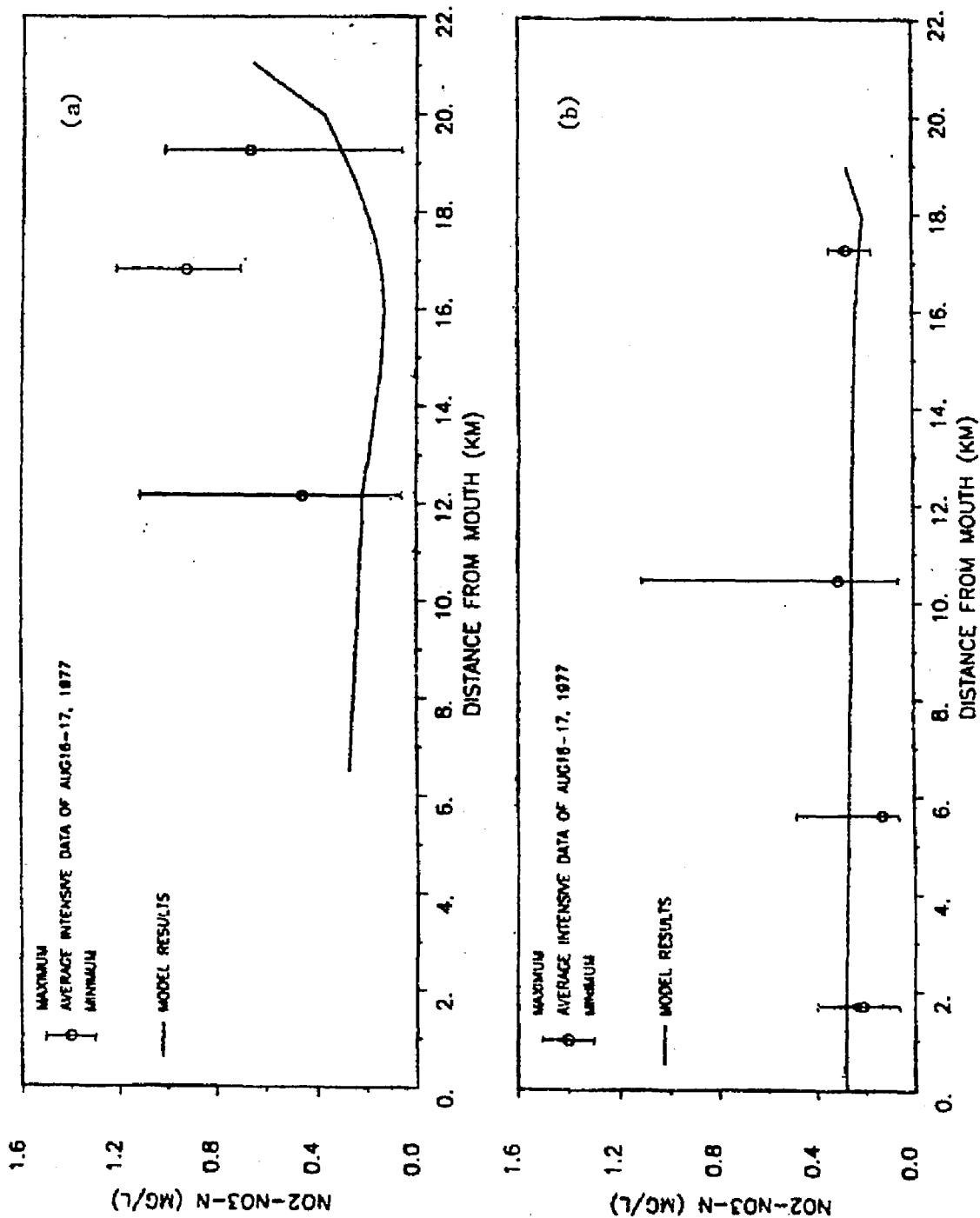


Figure 8.6 Computed vs observed Nitrite-Nitrate concentrations, (a) North branch, (b) South branch.

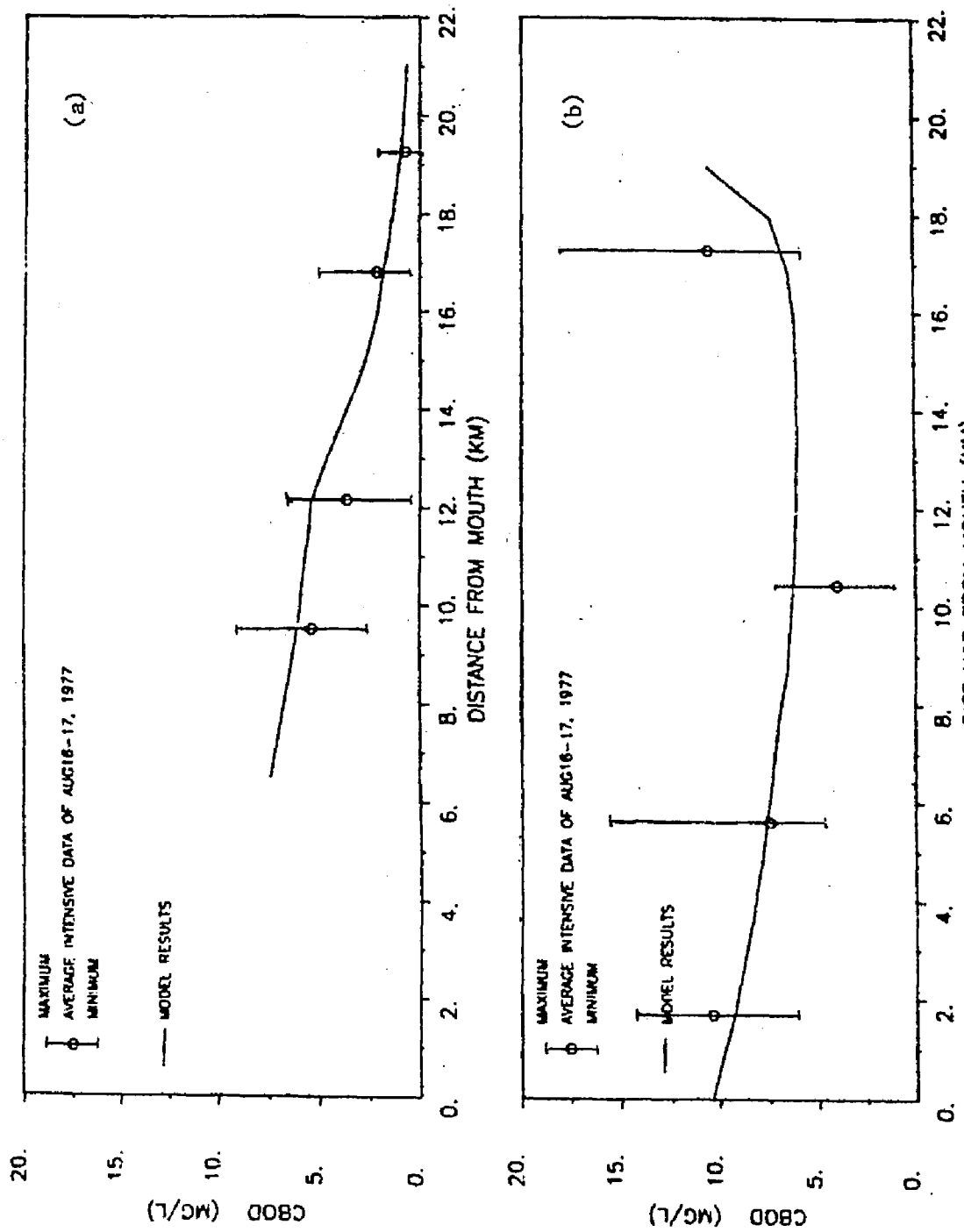


Figure 8.7 Computed vs observed CBOD concentrations, (a) North branch, (b) South branch.

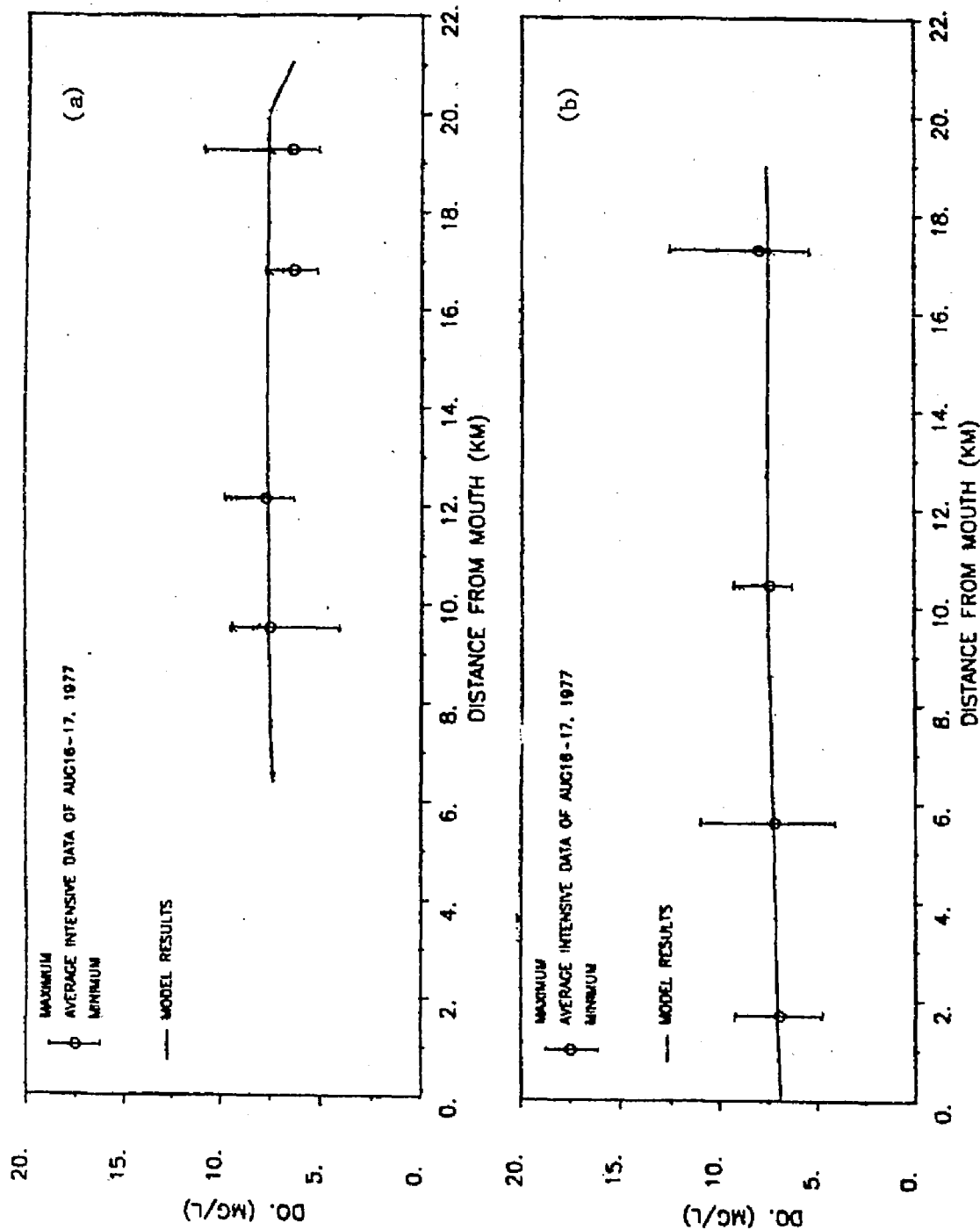


Figure 8.8 Computed vs observed DO concentrations, (a) North branch, (b) South branch.

Table 8.10 Water Quality Model Calibration Parameters.

Parameter	Symbol	Value	Unit
Dispersion coefficient	E	34	m ² /sec
Reaeration coefficient	k _g	10.8	
Coliform die off rate	not included in this study		
Phytoplankton optimum growth rate	k _g	0.5	1/day/ C
Extinction coefficient	k _e	0.4	1/m
Endogeneous respiration rate	k _r	0.005	1/day/ C
Zooplankton grazing rate	k _z	0.1	1/day
Michaelis nitrogen constant	k _{mn}	0.015	mg/l
Michaelis phosphorous constant	k _{mp}	0.005	mg/l
Organic-N to NH ₃ -N hydrolysis rate	k ₂	0.007	1/day/ C
Nitrogen chlorophyll ratio	r _n	0.01	mg/μg
NH ₃ to NO ₃ nitrification rate	k ₃	0.008	1/day/ C
Organic-P to inorganic-P conversion	k ₅	0.005	1/day/ C
Phosphorus chlorophyll ratio	r _p	0.001	mg/μg
CBOD oxidation rate	k ₇	0.5	1/day
Carbon chlorophyll ratio	r _c	0.05	mg/μg
Photosynthetic quotient	k _{op}	1.4	
Respiratory quotient	k _{or}	1.0	
Benthic oxygen demand	b _g	1.0	gm/m ² /day
Settling and escaping rates :			
Chlorophyll	k _{s1}	0.0	1/day
Organic-N	k _{s2}	0.1	1/day
Ammonia-N	k _{s3}	0.0	1/day
NO ₂ -NO ₃ -N	k _{s4}	0.0	1/day
Organic-P	k _{s5}	0.1	1/day
Inorganic-P	k _{s6}	0.0	1/day
CBOD	k _{s7}	0.0	1/day
DO Deficit	k _{s8}	0.0	1/day

9 EXPLICIT INTEGRATION

The time integrations used in the previous chapters are implicit methods. The implicit method is theoretically unconditionally stable. Therefore large integration time steps can be used. However, as the time step gets larger, the accuracy of the solution will suffer. The explicit integration method on the other hand is only conditional stable and the size of the integration time steps is more restricted. But the explicit formulation is simpler and requires less computer execution time. Therefore the explicit method offers an advantage when small integration time steps are required, either because of small grid sizes are used or higher accuracy is required.

In this chapter, the formulation using the explicit integration method is described.

9.1 Finite Element Formulation

Instead of using equation (3.10), the following form of the conservation of mass equation is used

$$\frac{\partial C}{\partial t} + U \frac{\partial C}{\partial x} = \frac{\partial}{\partial x} E \frac{\partial C}{\partial x} - \frac{Cq}{A} + S \quad (9.1)$$

where the symbols are as defined previously. The finite element formulation is similar to that described in chapter 4. Using the Galerkin weighted residual method yields

$$[K] \frac{d\{C\}}{dt} = \{F\} \quad (9.2)$$

where

$$[K] = \int_L \frac{\partial C}{\partial t} \delta C$$

$$\{F\} = \int_L \left\{ \left(U \frac{\partial C}{\partial x} - S + \frac{Cq}{A} \right) \delta C + E \frac{\partial C \partial \delta C}{\partial x \partial x} \right\} dx$$

The continuity and momentum equations are derived similarly.

9.2 Time Integration Using the Explicit Method

Using the explicit integration, equation (9.2) is written in the finite difference form as

$$[K] (\{C\}_{n+\frac{1}{2}} - \{C\}_{n-\frac{1}{2}}) = \Delta t \{F\} \quad (9.3)$$

Solving for $\{C\}_{n+\frac{1}{2}}$

$$\{C\}_{n+\frac{1}{2}} = [K]^{-1} (\Delta t \{F\} + [K] \{C\}_{n-\frac{1}{2}}) \quad (9.4)$$

The matrix $[K]$ in equation (9.4) is time invariant, therefore it is only necessary to assemble and invert it once thus making a large savings in computer execution time.

9.3 Model Verification

For comparison purposes, the test problems as described in sections 5.2 and 5.3 were run using this new formulation. Figure 9.1 shows the result of the model for a conservative substance using time steps of 9 and 4 seconds. Figure 9.2 shows the result of the model for a non-conservative substance also using the same time steps.

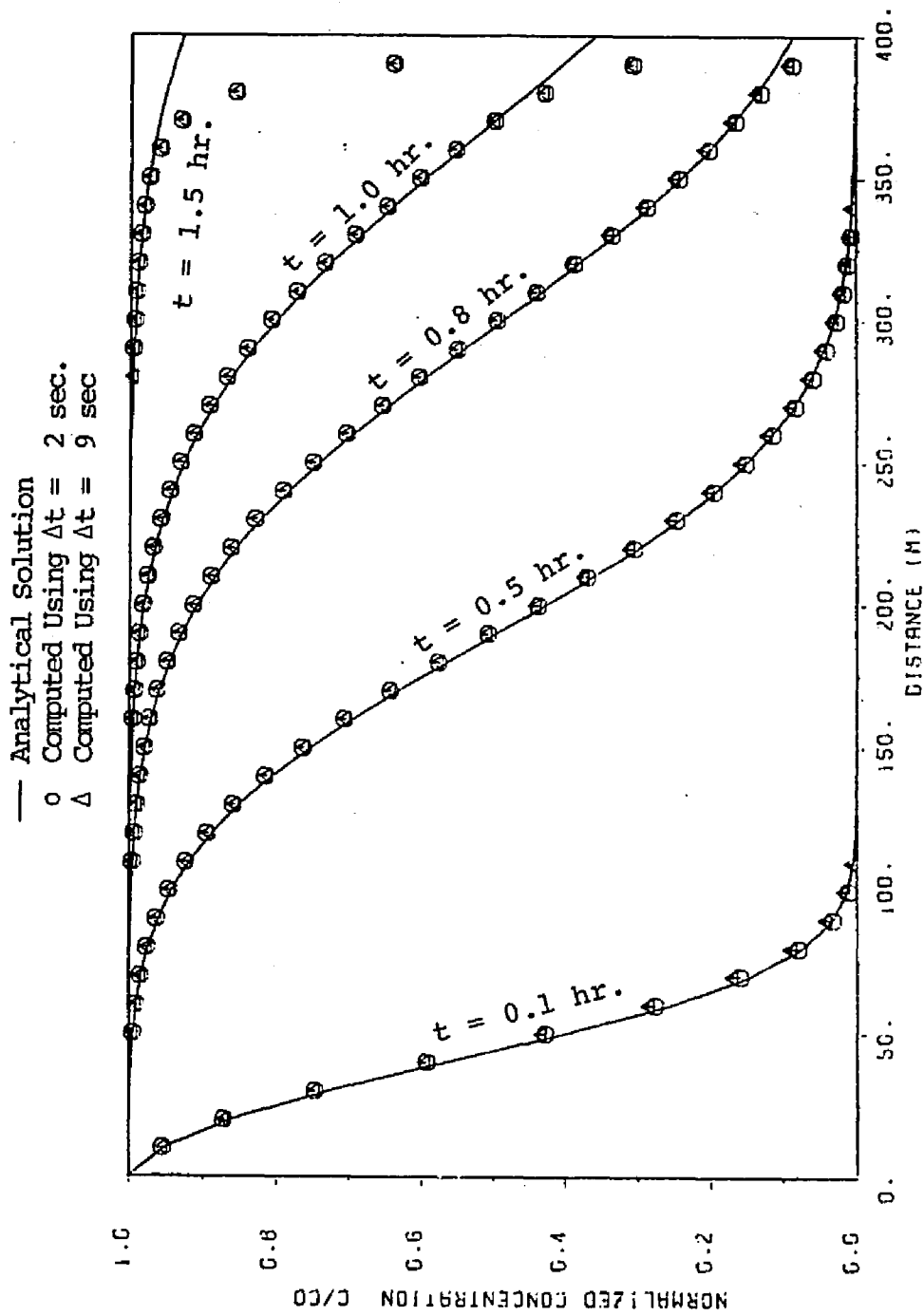


Figure 9.1 Comparison of explicit solutions to analytical solutions using no decay rate.

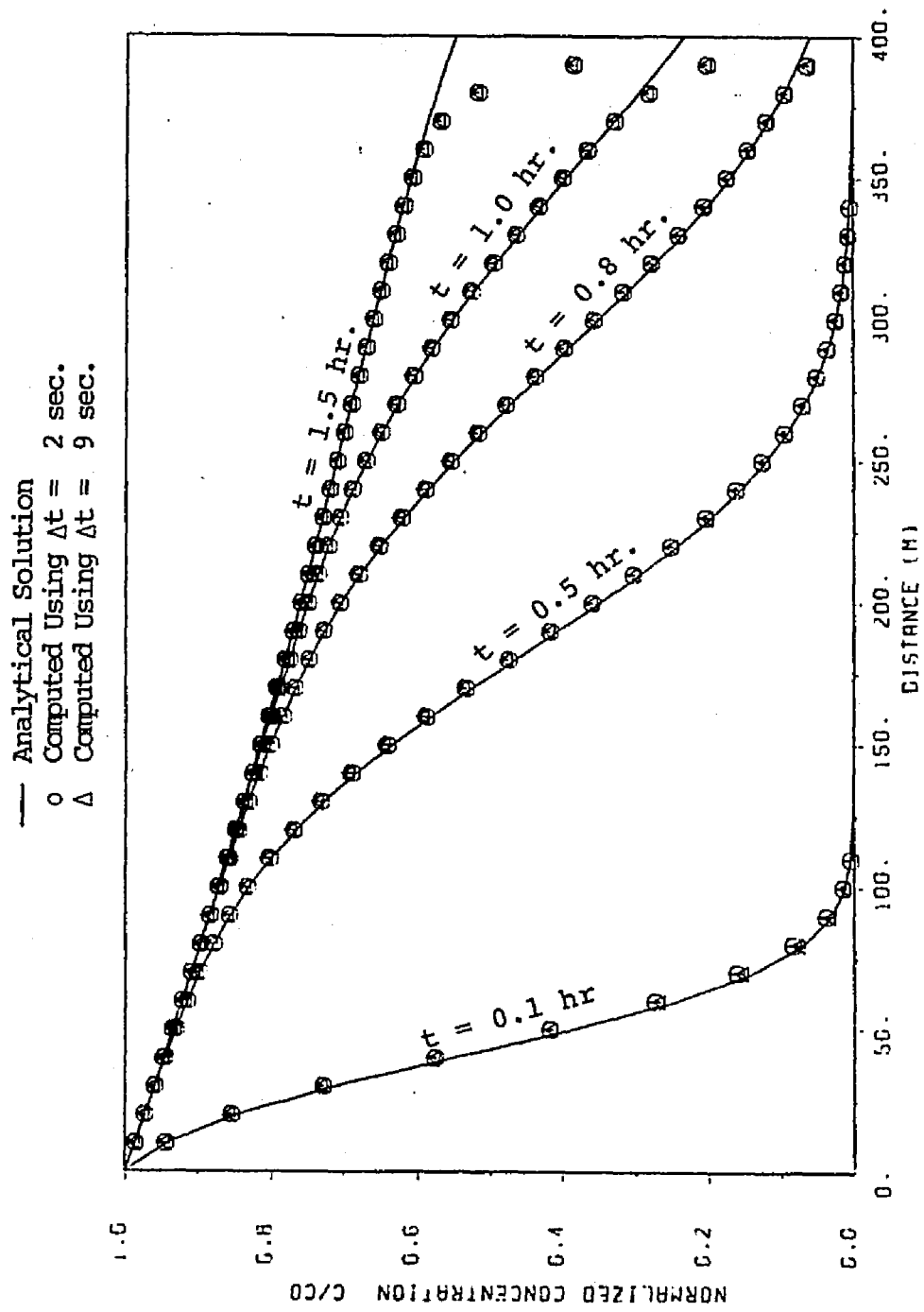


Figure 9.2 Comparison of explicit solutions to analytical solutions using decay rate = 0.5 per hour.

The integration is found to be stable for time steps at least up to 9 seconds. The execution time per time step is about 3 times faster than the implicit version. Therefore the explicit integration offers advantages when the situation allows for its use.

10 CONCLUDING REMARKS

A water quality model based on the principle of conservation of mass has been developed. The motivation for this study was to develop a network model that can be applied to the Appomatox River, since no model of this nature has been previously developed. For practical reasons, it was appropriate to develop a non-network model first. After this has been made operational, the model can then be extended to handle networks. In chapters 4, 5 and 6 the development of the non-network model was described, the extension to the network model was described in chapters 7 and 8.

Some of the features of the water quality model are that the downstream boundary condition is related to the state of the tidal flow; the upstream boundary condition can be specified either as a fixed concentration boundary or a flux boundary; temperature and solar radiation vary both spatially and temporally; the saturation growth rate of the phytoplankton is computed by the model based on light acclimation; the growth rate reduction due to nutrient limitations is expressed as a product of Michaelis-Menton expressions rather than a single limiting nutrient; either ammonia nitrogen or nitrate nitrogen can be specified as preferential uptake by phytoplankton.

It is anticipated as with all modeling activities that the models

presented in the present study will be expanded in the future to incorporate additional features. Therefore the computer programs have been written in a modular structure to facilitate future changes.

The application of the model to the James River has shown that the model can be used to make long term simulations economically. In the case of the Appomatox River the lack of field data made it necessary to simulate tidal average conditions.

From the experience gained during this study, the following is recommended for future research :

(1) The rate parameters used in this study were all obtained from literature values. Site specific measurement of some of the rate parameters is needed to add confidence to the calculations.

(2) Models require a large amount of data for both input and for calibration comparison. Therefore a sampling strategy should be developed for obtaining reliable inputs and data for calibration.

(3) At present comparison between the computed and the observed values are based on visual and graphical inspections. A meaningful statistic which will allow direct comparison of observed-predicted datasets should be developed.

(4) Sensitivity analysis should be conducted to determine the parameters to which the model response is most sensitive.

(5) The model should be used to simulate a different set of data for verification.

(6) When the model is used to make a simulation over several seasons, the question of seasonal change of phytoplankton species should be addressed. This can be investigated by adding a second phytoplankton species to the model.

APPENDIX

EVALUATION OF THE ELEMENT INTEGRALS

The integrals in equations (4.1), (4.2) and (4.4) are evaluated term by term. In this Appendix the superscript *e* is used to denote element properties and the symbol Σ is used to denote summation over all the elements. For brevity the symbols *dx* is omitted in all the integrals; and the superscript *e* is also omitted when not ambiguous.

The subscripts 1 and 2 are used to denote values at the two end nodes of an element (see Figure 4.1).

The integrals in equation (4.1) are

$$\begin{aligned} \int_L B \frac{\partial \eta}{\partial t} \delta \eta &= \Sigma \int_e B \frac{\partial \eta}{\partial t} \delta \eta \\ &= \Sigma \{\delta \eta\}^T \int_e \{N\} \{N\}^T \{B\} \{N\}^T \frac{\partial \{ \eta \}}{\partial t} \\ &= \Sigma \{\delta \eta\}^T [M_\eta^e] \frac{\partial \{ \eta \}}{\partial t} \end{aligned}$$

$$\begin{aligned} \int_L \frac{\partial Q}{\partial x} \delta \eta &= \Sigma \int_e \frac{\partial Q}{\partial x} \delta \eta \\ &= \Sigma \{\delta \eta\}^T \int_e \{N\} \frac{\partial \{N\}^T \{Q\}}{\partial x} \\ &= \Sigma \{\delta \eta\}^T [K_\eta^e] \{Q^e\} \end{aligned}$$

$$\begin{aligned} \int_L q \delta \eta &= \Sigma \int_e q^e \delta \eta \\ &= \Sigma \{\delta \eta\}^T \int_e \{N\} q^e \end{aligned}$$

$$= \Sigma \{\delta\eta\}^T \{F_\eta^e\}$$

where the matrices

$$\begin{aligned} [M_\eta^e] &= \int_e \{N\} \{N\}^T \{B\} \{N\}^T \\ &= \frac{L^e}{12} \begin{bmatrix} 3B_1 + B_2 & B_1 + B_2 \\ B_1 + B_2 & B_1 + 3B_2 \end{bmatrix} \end{aligned}$$

where $L^e = x_2 - x_1$ is the length of an element (see Figure 4.1).

$$\begin{aligned} [K_\eta^e] &= \int_e \{N\} \frac{\partial \{N\}^T}{\partial x} \\ &= \frac{1}{2} \begin{bmatrix} -1 & 1 \\ -1 & 1 \end{bmatrix} \end{aligned}$$

$$\begin{aligned} \{F_\eta^e\} &= \int_e \{N\} q^e \\ &= \frac{q^e L^e}{2} \begin{Bmatrix} 1 \\ 1 \end{Bmatrix} \end{aligned}$$

Equation (4.1) is reduced to

$$\{\delta\eta\}^T \left\{ [M_\eta^e] \frac{d\{\eta\}}{dt} + [K_\eta^e] \{Q\} - \{F_\eta^e\} \right\} = 0 \quad (A1)$$

Next we define the global vector arrays as follows

$$\{\delta\eta\} = \text{union of all } \{\delta\eta^e\}$$

$$\{\eta\} = \text{union of all } \{\eta^e\}$$

$$\{Q\} = \text{union of all } \{Q^e\}$$

Equation (A1) can be assembled into a single equation in matrix

form

$$\{\delta\eta\}^T \left\{ [M_\eta] \frac{d\{\eta\}}{dt} + [K_\eta] \{Q\} - \{F_\eta\} \right\} = 0 \quad (A2)$$

where the global matrices $[M_\eta]$, $[K_\eta]$ and $\{F_\eta\}$ are obtained from the assemblage of the element matrices. Since $\{\delta\eta\}$ is an arbitrary function, the terms within the brackets in equation (A2) must vanish, i.e

$$[M_\eta] \frac{d\{\eta\}}{dt} + [K_\eta] \{Q\} - \{F_\eta\} = 0 \quad (A3)$$

Evaluation of equation (4.2) for each element e

$$\begin{aligned} \int_e \frac{\partial Q}{\partial t} \delta Q &\approx \{\delta Q\}^T \int_e \{N\} \{N\}^T \frac{\partial \{Q\}}{\partial t} \\ &= \{\delta Q\}^T [M_Q^e] \frac{\partial \{Q\}}{\partial t} \\ \int_e \frac{\partial QU}{\partial x} \delta Q &\approx \int_e \left(U \frac{\partial Q}{\partial x} + Q \frac{\partial U}{\partial x} \right) \delta Q \\ &= \{\delta Q\}^T \int_e \left(\{N\} \{N\}^T \{U\} \frac{\partial \{N\}^T \{Q\}}{\partial x} + \{N\} \{N\}^T \{Q\} \frac{\partial \{N\}^T \{U\}}{\partial x} \right) \\ &= \{\delta Q\}^T [K_Q^e] \{Q^e\} \end{aligned}$$

where U is taken to be the velocity from the previous integration time step.

$$\begin{aligned} - \int_e \left(gA \frac{\partial \eta}{\partial x} + \frac{gQ|Q|}{AC^2 R_h} + gA \frac{d_c \partial \rho}{\rho \partial x} \right) \delta Q &\approx - \{\delta Q\}^T \int_e \left(g \{N\} \{N\}^T \{A\} \frac{\partial \{N\}^T \{\eta\}}{\partial x} \right. \\ &\quad \left. + f_1 \{N\} \{N\}^T \{Q\} + f_2 \{N\} \{N\}^T \{A\} \frac{\partial \{N\}^T \{\rho\}}{\partial x} \right) \\ &= \{\delta Q\}^T \{F_Q^e\} \end{aligned}$$

defining :

$$f_1 = \frac{g|\bar{Q}|}{AC_c^2 R_h}$$

$$f_2 = g \frac{\bar{d}_c}{\rho}$$

where the overbar denotes the average values of the two end nodes, for example $\bar{A} = (A_1 + A_2)/2$.

The matrices are

$$\begin{aligned} [M_Q^e] &= \int_e \{N\} \{N\}^T \\ &= \frac{L^e}{6} \begin{bmatrix} 2 & 1 \\ 1 & 2 \end{bmatrix} \end{aligned}$$

$$\begin{aligned} [K_Q^e] &= \int_e \{N\} \{N\}^T \{U\} \frac{\partial \{N\}^T}{\partial x} + \int_e \{N\} \frac{\partial \{N\}^T \{U\}}{\partial x} \{N\}^T \\ &= \frac{1}{6} \begin{bmatrix} -2U_1^- & U_2 & -2U_1^+ & U_2 \\ -U_1^- & 2U_2 & U_1^+ & 2U_2 \end{bmatrix} + \frac{1}{6} \begin{bmatrix} -2U_1^+ & 2U_2 & -U_1^+ & U_2 \\ -U_1^+ & U_2 & -2U_1^+ & 2U_2 \end{bmatrix} \end{aligned}$$

$$\begin{aligned} \{F_Q^e\} &= - \int_e (g \{N\} \{N\}^T \{A\} \frac{\partial \{N\}^T \{\eta\}}{\partial x} + f_1 \{N\} \{N\}^T \{Q\} + f_2 \{N\} \{N\}^T \{A\} \frac{\partial \{N\}^T \{\rho\}}{\partial x}) \\ &= - \frac{g}{6} \begin{bmatrix} -2A_1^- & A_2 & -2A_1^+ & A_2 \\ -A_1^- & 2A_2 & A_1^+ & 2A_2 \end{bmatrix} \{\eta^e\} - \frac{f_1 L^e}{6} \begin{bmatrix} 2 & 1 \\ 1 & 2 \end{bmatrix} \{Q^e\} \\ &\quad - f_2 \begin{bmatrix} -2A_1^- & A_2 & -2A_1^+ & A_2 \\ -A_1^- & 2A_2 & A_1^+ & 2A_2 \end{bmatrix} \{\rho^e\} \end{aligned}$$

Substituting all the integrals into equation (4.2) and performing the global assembly of all the elements, the resultant equation can be expressed in matrix form as

$$[M_Q] \frac{d\{Q\}}{dt} + [K_Q] \{Q\} - \{F_Q\} = 0$$

Where $[M_Q]$, $[K_Q]$ and $\{F_Q\}$ are obtained from the global assembly of all the elements in the domain L.

Evaluation of equation (4.4) for each element e

$$\begin{aligned} \int_e A \frac{\partial C}{\partial t} \delta C &\approx \{\delta C\}^T \int_e \{N\} \{N\}^T \{A\} \frac{\partial \{N\}^T \{C\}}{\partial t} \\ &= \{\delta C\}^T [M_C^e] \frac{\partial \{C\}}{\partial t} \\ \int_e (Q \frac{\partial C}{\partial x} + k_s AC + Cq) \delta C + \int_e AE \frac{\partial C \partial \delta C}{\partial x \partial x} &\approx \{\delta C\}^T \int_e (\{N\} \{N\}^T \{Q\} \frac{\partial \{N\}^T \{C\}}{\partial x} \\ &+ k_s \{N\} \{N\}^T \{A\} \{N\}^T \{C\} + q^e \{N\} \{N\}^T \{C\} + E^e \{N\}^T \{A\} \frac{\partial \{N\}^T \{C\}}{\partial x} \frac{\partial \{N\}}{\partial x}) \\ &= \{\delta C\}^T [K_C^e] \{C^e\} \end{aligned}$$

$$\begin{aligned} \int_e W \delta C &= \{\delta C\}^T \int_e \{N\} W^e \\ &= \{\delta C\}^T [F_C^e] \end{aligned}$$

where the matrices

$$\begin{aligned} [M_C^e] &= \int_e \{N\} \{N\}^T \{A\} \{N\}^T \\ &= \frac{L^e}{12} \begin{bmatrix} 3A_1 + A_2 & A_1 + A_2 \\ A_1 + A_2 & A_1 + 3A_2 \end{bmatrix} \\ [K_C^e] &= \int_e (\{N\} \{N\}^T \{Q\} \frac{\partial \{N\}^T}{\partial x} + k_s \{N\} \{N\}^T \{A\} \{N\}^T + q^e \{N\} \{N\}^T \{C\} \\ &+ E^e \{N\}^T \{A\} \frac{\partial \{N\}^T}{\partial x} \frac{\partial \{N\}}{\partial x}) \end{aligned}$$

$$\begin{aligned}
&= \frac{1}{6} \begin{bmatrix} -2Q_1^- & Q_2 & -2Q_1^+ & Q_2 \\ -Q_1^- & 2Q_2 & Q_1^+ & 2Q_2 \end{bmatrix} + \frac{k_s L^e}{12} \begin{bmatrix} 3A_1^+ & A_2 & A_1^+ & A_2 \\ A_1^+ & A_2 & A_1^+ & 3A_2 \end{bmatrix} \\
&\quad + \frac{qL^e}{6} \begin{bmatrix} 2 & 1 \\ 1 & 2 \end{bmatrix} + \frac{E^e A}{L^e} \begin{bmatrix} 1 & -1 \\ -1 & 1 \end{bmatrix}
\end{aligned}$$

$$\begin{aligned}
[F_C^e] &= \int_e \{N\} w^e \\
&= \frac{w^e L^e}{2} \begin{Bmatrix} 1 \\ 1 \end{Bmatrix}
\end{aligned}$$

Substituting all the integrals into equation (4.4) and performing the global assemblage, again the resultant equation can be written in matrix form as

$$[M_C] \frac{d\{C\}}{dt} + [K_C] \{C\} - \{F_C\} = 0$$

where the matrices $[M_C]$, $[K_C]$ and $\{F_C\}$ are obtained from the assemblage of all the elements in the domain L .

REFERENCES

- Chen H.S., et al., 1979. A Two-Dimensional Hydrodynamic and Biochemical Water Quality Model and its Application to the Lower James River. Special Rep. No. 183, Va. Inst. of Mar. Sci.
- Chen, C.W., 1970. "Concepts and Utilities of Ecologic Model." JSED, ASCE, Vol. 96, No. SA5 (October).
- Chow, C.Y., 1979. An Introduction to Computational Fluid Mechanics. John Wiley and Sons.
- Christodoulou, G.C. and Connor, J.J., 1976. Mathematical Modeling of Dispersion in Stratified Waters. Technical Rep. No. 219, Ralph M. Parsons Laboratory for Water Resources and Hydrodynamics, Dept. of Civil Eng., MIT, Cambridge, Mass.
- Colijn, F., 1982. "Light Absorption in the Waters of the Ems-Dollard Estuary and its Consequences for the Growth of Phytoplankton and Microphytobenthos." Netherlands Journal of Sea Research, 15(2) : 196-216.
- Daily, J.E. and Harleman, D.R.F., 1972. Numerical Model for the Prediction of Transient Water Quality in Estuary Networks. Report No. 158, Ralph M. Parsons Laboratory for Water Resources and Hydrodynamics, Dept. of Civil Eng., MIT, Cambridge, Mass.
- DiToro, D.M., D.J. O'Connor and R.V. Thomann, 1970. A dynamic model of phytoplankton populations in natural waters. Env. Eng. and Sci. Prog., Manhattan College, Bronx, N.Y.
- DiToro, D.M., Thomann, R.V., O'connor, D.J., and Mancini, J.L., 1977. "Estuarine Phytoplankton Biomass Models - Verification Analysis and Preliminary Applications." The Sea, Vol. 6, John Wiley and Sons.
- Dobbins, W.E., 1964. "BOD and oxygen relationships in streams." Proc. ASCE, 95, No. HY4 (July).
- Feigner, K.D. and Harris, H.S., 1970. Documentation Report, FWQA Dynamic Estuary Model. U.S. Dept. of Interior, FWQA (July).

- Fleming, R.H., 1939. "The Control of Diatom Populations by Grazing." J. Cons. Perm. Expl. Mer. 14.
- Gresho, P.M. and Lee, R.L., 1981. "Don't Suppress the Wiggles - They are Telling you Something !." Computer and Fluids, Vol. 9, No. 2, p. 223-254 (June).
- Guide, V. and O. Villa, Jr., 1972. Chesapeake Bay Nutrient Input Study. Technical Rep. 47, EPA, Region III, Annapolis Field Office (September).
- Gunaratnum, D.J. and Parkins, F.E., 1970. Numerical Solution of Unsteady Flows in Open Channels. Technical Rep. No. 127, Hydrolab, Dept. of Civil Eng., MIT (July).
- Haas, L.W., 1977. "The Effect of the Spring-Neap Tidal Cycle on the Vertical Salinity Structure of the James, York and Rappahannock Rivers, Virginia, U.S.A.." Estuarine and Coastal Marine Sci., Vol. 5, p. 485-496.
- Harleman, D.R.F., 1971. "One-Dimensional Models." In Estuarine Modelling: An Assessment. Tracor, Inc.
- Harleman, D.R.F. and C.H. Lee, 1969. The Computation of Tides and Currents in Estuaries and Canals. Tech. Bull. No. 16, Committee on Tidal Hydraulics, Corp. of Eng., U.S. Army.
- Huebner, K.H., 1975. The Finite Element Method for Engineers. John Wiley and Sons.
- Hyer, P.V., A.Y. Kuo, and B.J. Neilson, 1977. Water Quality Models of Back and Pogooson Rivers, Virginia. Special Rep. No. 144, Va. Inst. of Mar. Sci.
- Jaworski, N.A., et al., 1971. A Water Resource Water Supply Study of the Potomac Estuary. Tech. Rep. 35, Ches. Tech. Sup. Lab. EPA, Annapolis, Md.
- Kremer, J.N. and S.W. Nixon, 1978. A Coastal Marine Ecosystem - Simulation and Analysis. Springer-Verlag, Germany.
- Kuo, A.Y., P.V. Hyer and C.S. Fang, 1979. Manual of Water Quality Models for Virginia Estuaries. Special Rep. No. 214, Va. Inst. of Mar. Sci.
- Lee, C.H. and Harleman, D.R.F., 1971. One-Dimensional Real-Time Model for Estuarine Water Quality Prediction. Ralph M. Parsons Laboratory, MIT (January).
- Lotka, A.J., 1925. Elements of Physical Biology. Williams and Wilkins.

- Najarian, T.O. and Harleman, D.R.F., 1975. A Nitrogen Cycle Water Quality Model for Estuaries. Tech. Rep. No. 204, Ralph M. Parsons Laboratory for Water Resources and Hydrodynamics, Dept. of Civil Eng., MIT, Cambridge, Mass.
- Neilson, B.J. and L. Eugene Cronin, 1981. Estuaries and Nutrients. Human Press, Clifton, New Jersey.
- O'Connor, D.J., 1966. "An analysis of the dissolved oxygen distribution in the East River." J. WPCF, 38, No. 11 (November).
- O'Connor, D.J., 1960. "Oxygen Balance of an Estuary." J. of the Sanit. Eng. Div., ASCE, Vol. 86, No. SA3, Proc. Paper 2477 (May).
- O'Connor, D.J., 1967. "The Temporal and Spatial Distribution of Dissolved Oxygen in Streams." Water Resources Res., Vol. 3, p. 65-79.
- O'Connor, D.J., and DiToro, D.M., 1970. "Phytosynthesis and Oxygen Balance in Streams." Proc. J. Sanit. Eng. Div., ASCE, Vol. 96, No. SA2, p. 547-571.
- Riley, G.A., 1946. "Factors Controlling Phytoplankton Populations on Georges's Bank." J. Mar. Res., 6, 54-73.
- Riley, G.A., 1956. "Oceanography of Long Island Sound 1952-54. II. Physical Oceanography." Bull. Bing. Ocean. Coll. 15, 15-46.
- Roache, P.J., 1972. Computational Fluid Dynamics. Hermosa Publishers, Albuquerque, N.M.
- Steel, J.H., 1972. "Environmental Control of Photosynthesis in the Sea." Limnol. Oceanography, 7, 137-150.
- Streeter, H.W. and E.B. Phelps, 1925. A study of the pollution and natural purification of the Ohio River. U.S. Public Health Service, Public Health Bull. 146.
- Sweeney, J.T., 1980. Measurement and Analysis of Tidal Marsh Fluxes of Oxygen Demanding Materials. Masters Thesis, Va. Inst. of Mar. Sci.
- Sverdrup, H.W., Johnson, M.W. and Fleming, R.H., 1942. The Oceans. Prentice Hall Inc., Englewood Cliffs, N.J., p. 82.
- Taylor, G.I., 1954. "The dispersion of matter in turbulent flow through a pipe." Proc. Roy. Soc. London (A), 223 (May).
- Thomann, R.V., 1963. "Mathematical Model for Dissolved Oxygen." J. Sanit. Eng. Div., Proc. ASCE, 83, SA5 (October).

- Thomann, R.V., DiToro, D.M. and O'connor, D.J., 1974. "Preliminary Model of Potomac Estuary Phytoplankton." JEED, ASCE, Vol. 100, No. EE2 (June).
- Tracor, Inc., 1971. Estuarine Modeling : An Assessment. EPA 1607DZV 02/71.
- Volterra, V., 1926. "Variations and Fluctuations of the Number of Individuals in Animal Species Living Together." Animal Ecology. New York, McGraw-Hill.
- Wang, H.P., 1977. "Multi-leveled Finite Element Hydrodynamic Model of Block Island Sound." Finite Element in Water Resources, edited by W.G. Gray, G.F. Pinder and C.A. Brebbia, Pentech, London.
- Wang, John D. and Jerome J. Connor, 1975. Mathematical Modelling of Near Coastal Circulation. Rep. No. 200, Ralph M. Parson Laboratory, MIT (April).
- Zienkiewicz, O.C., 1977. The Finite Element Method. 3rd ed., McGraw-Hill Book Company (UK).

VITA

Yothin Unkulvasapaul

Born in Yala, Thailand on August 26, 1947. Attended Triam Udom High School in Bangkok. Obtained a Bachelor of Engineering in Civil Engineering from the University of New South Wales Australia (1972). Obtained a Master of Engineering in Environmental Engineering from Asian Institute of Technology, Bangkok (1976). Entered post-graduate studies at the College of William and Mary, School of Marine Science in September, 1978. Graduate Assistant, Department of Physical Oceanography and Hydraulics, School of Marine Science until June 1982. Presently Marine Scientist B, Department of Physical Oceanography and Hydraulics, School of Marine Science.